UNIVERSIDAD DE INVESTIGACIÓN DE TECNOLOGÍA EXPERIMENTAL YACHAY

Escuela de Ciencias Químicas e Ingeniería

TÍTULO: Oxidative dehydrogenation of macrocyclic ligands coordinated to nickel and copper

Trabajo de integración curricular presentado como requisito para la obtención del título de Químico

Autor:

Masapanta Yugcha Nelson Estorgio

Tutor:

Ph.D. Saucedo Vázquez Juan Pablo

Urcuquí, junio 2021

SECRETARÍA GENERAL
(Vicerrectorado Académico/Cancillería)
ESCUELA DE CIENCIAS QUÍMICAS E INGENIERÍA
CARRERA DE QUÍMICA
ACTA DE DEFENSA No. UITEY-CHE-2021-00018-AD

A los 29 días del mes de junio de 2021, a las 10:00 horas, de manera virtual mediante videoconferencia, y ante el Tribunal Calificador, integrado por los docentes:

Presidente Tribunal de Defensa	Dra. HIDALGO BONILLA, SANDRA PATRICIA , Ph.D.
Miembro No Tutor	Dr. OROPEZA OREA, RUTH FIDELINA , Ph.D.
Tutor	Dr. SAUCEDO VAZQUEZ, JUAN PABLO , Ph.D.

El(la) señor(ita) estudiante **MASAPANTA YUGCHA, NELSON ESTORGIO**, con cédula de identidad No. **0503398992**, de la **ESCUELA DE CIENCIAS QUÍMICAS E INGENIERÍA**, de la Carrera de **QUÍMICA**, aprobada por el Consejo de Educación Superior (CES), mediante Resolución **RPC-SO-39-No.456-2014**, realiza a través de videoconferencia, la sustentación de su trabajo de titulación denominado: **OXIDATIVE DEHYDROGENATION OF MACROCYCLIC LIGANDS COORDINATED TO NIKEL AND COPPER**, previa a la obtención del título de **QUÍMICO/A**.

El citado trabajo de titulación, fue debidamente aprobado por el(los) docente(s):

Tutor	Dr. SAUCEDO VAZQUEZ, JUAN PABLO , Ph.D.

Y recibió las observaciones de los otros miembros del Tribunal Calificador, las mismas que han sido incorporadas por el(la) estudiante.

Previamente cumplidos los requisitos legales y reglamentarios, el trabajo de titulación fue sustentado por el(la) estudiante y examinado por los miembros del Tribunal Calificador. Escuchada la sustentación del trabajo de titulación a través de videoconferencia, que integró la exposición de el(la) estudiante sobre el contenido de la misma y las preguntas formuladas por los miembros del Tribunal, se califica la sustentación del trabajo de titulación con las siguientes calificaciones:
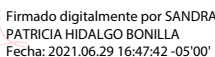
Tipo	Docente	Calificación
Miembro Tribunal De Defensa	Dr. OROPEZA OREA, RUTH FIDELINA , Ph.D.	10,0
Tutor	Dr. SAUCEDO VAZQUEZ, JUAN PABLO , Ph.D.	10,0
Presidente Tribunal De Defensa	Dra. HIDALGO BONILLA, SANDRA PATRICIA , Ph.D.	10,0

Lo que da un promedio de: **10 (Diez punto Cero)**, sobre 10 (diez), equivalente a: **APROBADO**

Para constancia de lo actuado, firman los miembros del Tribunal Calificador, el/la estudiante y el/la secretario ad-hoc.
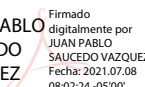
Certifico que *en cumplimiento del Decreto Ejecutivo 1017 de 16 de marzo de 2020, la defensa de trabajo de titulación (o examen de grado modalidad teórico práctica) se realizó vía virtual, por lo que las firmas de los miembros del Tribunal de Defensa de Grado, constan en forma digital.*

MASAPANTA YUGCHA, NELSON ESTORGIO
Estudiante

SANDRA PATRICIA HIDALGO BONILLA
Firmado digitalmente por SANDRA PATRICIA HIDALGO BONILLA
Fecha: 2021.06.29 16:47:42 -05'00'

Dra. HIDALGO BONILLA, SANDRA PATRICIA , Ph.D.
Presidente Tribunal de Defensa

JUAN PABLO SAUCEDO VAZQUEZ
Firmado digitalmente por JUAN PABLO SAUCEDO VAZQUEZ
Fecha: 2021.07.08 08:02:24 -05'00'

Dr. SAUCEDO VAZQUEZ, JUAN PABLO , Ph.D.
Tutor

AUTORÍA

Yo, **NELSON ESTORGIO MASAPANTA YUGCHA**, con cédula de identidad 0503398992, declaro que las ideas, juicios, valoraciones, interpretaciones, consultas bibliográficas, definiciones y conceptualizaciones expuestas en el presente trabajo; así cómo, los procedimientos y herramientas utilizadas en la investigación, son de absoluta responsabilidad de el/la autora (a) del trabajo de integración curricular. Así mismo, me acojo a los reglamentos internos de la Universidad de Investigación de Tecnología Experimental Yachay.

Urcuquí, junio 2021.

_____

Nelson Estorgio Masapanta Yugcha

C.I. 0503398992

AUTORIZACIÓN DE PUBLICACIÓN

Yo, **NELSON ESTORGIO MASAPANTA YUGCHA,** con cédula de identidad 0503398992, cedo a la Universidad de Tecnología Experimental Yachay, los derechos de publicación de la presente obra, sin que deba haber un reconocimiento económico por este concepto. Declaro además que el texto del presente trabajo de titulación no podrá ser cedido a ninguna empresa editorial para su publicación u otros fines, sin contar previamente con la autorización escrita de la Universidad.

Asimismo, autorizo a la Universidad que realice la digitalización y publicación de este trabajo de integración curricular en el repositorio virtual, de conformidad a lo dispuesto en el Art. 144 de la Ley Orgánica de Educación Superior

Urcuquí, junio 2021.

Nelson Estorgio Masapanta Yugcha
C.I. 0503398992

Dedicatory

Dedicated to:

To God for giving me one more day of life, a wonderful family and the opportunity to learn from great teachers at Yachay Tech University.

To my parents Manuel and Rosa for their example in hard, constant and intelligent work. For being present and guiding me in every moment of my life.

To my brothers Angel and Manuel for trusting me.

To my friends from the house T2-7 in YT.

To my friends Paul Maldonado, Franco Roman, Erick Ortega and others in YT.

<div align="right">Nelson Estorgio Masapanta Yugcha</div>

Acknowledgements

"Hardships often prepare ordinary people for an extraordinary destiny"   CS Lewis

"The greatest enemy of knowledge is not ignorance it's the illusion of knowledge"

Stephen Hawking

 "The world breaks everyone and afterward many are stronger in the broken places"

Ernest Hemingway

I would like to thank to all the people that helped me during this research project and my college career.

To Juan Pablo Saucedo to be a great person, a guide and support in the development of this research work.

To Lola de Lima, Manuel Caetano, Thibault Terencio and Daniela Navas for their help in the laboratory during the experimental phase.

To the members of the jury Msc. Ruth Oropeza and PhD Sandra Hidalgo for helping me improve the quality of this work with their revisions and corrections.

To Yachay Tech University to be the "alma mater" in my chemistry career.

To all the teachers who taught me to love science and shared me their knowledge during the last five years.

Nelson Estorgio Masapanta Yugcha

Resumen

La funcionalización de aminas convirtiéndolas en derivados más reactivos como nitrilos, amidas, nitrocompuestos entre otros, le confiere una riqueza en la reactividad química a dichos compuestos. Particularmente los compuestos que contienen nitrilos cumplen funciones importantes en diferentes campos, por ejemplo en la medicina en la síntesis de fármacos como el vildagliptin (antibiótico), periciazine (antiséptico), citalopram (antidepressant) entre otros; en la industria hay nitrilos en compuestos como el cianoacrilato de metilo (adhesivo), acrilonitrilo (monómero), etc. En la academia existe nitrilos como intermediarios para la síntesis de diferentes grupos funcionales como ácidos carboxílicos, amidas, aldehídos, etc., sin embargo, las rutas sintéticas que son utilizadas para la obtención de dichos derivados no son las mejores en cuanto a rendimientos, selectividad o los subproductos son tóxicos. Estos son factores importantes que han limitado el desarrollo de más compuestos con nitrilos. En este sentido, encontrar un método de síntesis con bajo impacto ambiental y de alta plusvalía desde el punto de vista químico es importante.

En el presente proyecto de tesis se usó la reacción de deshidrogenación oxidativa de ligantes amínicos macrocíclicos coordinados a níquel y cobre en la búsqueda de síntesis de compuestos que contienen iminas o incluso nitrilos. Como estrategia para promover la obtención de nitrilos, se testeo la reacción en pH básicos. Adicionalmente, se realizó un estudio cinético de algunas de las reacciones mencionadas anteriormente. La reactividad de $[Fe(DMSO)_6]$ $(NO_3)_3$ con el ligante polinitrogenado *picdien* se usó como modelo ya que la obtención de derivados imínicos del picdien ha sido reportada previamente[1].

La caracterización de los productos obtenidos se realizó por espectroscopía Uv-vis, susceptibilidad magnética, espectroscopía infrarrojo, entre otros. En el caso de estudio del presente trabajo, la reacción modelo entre hierro con el ligante picdien, los resultados de Uv-vis demuestran que se produjo la reacción de deshidrogenación oxidativa ya que el espectro del producto final presenta las bandas características para un compuesto de Fe(II) low spin. En el caso del estudio de la reactividad de cobre con el ligante picdien se demostró la coordinación del metal con el ligante pero no se obtuvo evidencia de la oxidación del mismo. Por otro lado, en el caso del estudio de la reactividad de cobre con el ligante picdien no se observó con claridad la formación de un doble enlace en el espectro IR. En el caso de la

reactividad de Cu y Ni con el ligante amínico macrocíclico HMTA se encontraron señales de nitrilos en el IR cuando la reacción es llevada a cabo a pH 14 y pH>14 respectivamente lo cual da evidencia de la oxidación del ligante. Finalmente, en los estudios cinéticos se ha encontrado que la constante de velocidad de los complejos de niquel son menores que los complejos de cobre (Cu-HMTA > Ni-HMTA, Cu-Picdien > Ni-Picdien).

Palabras claves:

Deshidrogenación oxidativa, funcionalización de aminas, pH básicos, picdien, HMTA, Cu, Ni.

Abstract

The functionalization of amines, turning them into more reactive derivatives such as nitriles, amides, nitro-compounds, among others. Nitrile-containing compounds have relevant applications in different fields such as medicine in the synthesis of drugs such as vildagliptin (antibiotic), periciazine (antiseptic), citalopram (antidepressant) among others; in industry there are nitriles in compounds such as methyl cyanoacrylate (adhesive), acrylonitrile (monomer), etc. In academia exists nitriles as intermediates for the synthesis of different functional groups such as carboxylic acids, amides, aldehydes, etc., however, the synthetic routes that are used to obtain such derivatives are not the best in terms of yields, selectivity or by-products are toxic; these are important factors that have limited the development of more nitrile compounds. In this sense, developing of a synthetic method with low environmental impact and high added value from the chemical point of view is of vital importance.

In this thesis project, the oxidative dehydrogenation reaction of macrocyclic amine ligands coordinated to nickel and copper was used in the search for alternatives to the synthesis of compounds containing imines or even nitriles. As a strategy to promote the obtaining of nitriles derivatives, the reaction was tested in pH basics. Additionally, a kinetic study of some of the reactions mentioned above was carried out. The reactivity of [Fe (DMSO)$_6$](NO$_3$)$_3$ with the polynitrogenated ligand pydien was used as a model since the reactivity towards obtaining the oxidative dehydrogenation products is well documented[1].

The characterization of the products obtained was carried out by Uv-vis spectroscopy, magnetic susceptibility, and infrared spectroscopy, among others. In the case of the study of our model reaction between iron with the pydien ligand, the Uv-vis results show that the oxidative dehydrogenation reaction occurred since the spectrum of the final product presents the characteristic bands for an Fe(II) low spin compound. In the case of the study of copper reactivity with pydien, the coordination of the metal with the ligand was demonstrated, but no evidence of oxidation was obtained. On the other hand, in the case of copper reactivity with the pydien ligand, the formation of a double bond in the IR spectrum is not clearly observed. Finally, in the case of the reactivity of Cu and Ni with the macrocyclic amine HMTA we found signs of nitriles in the IR spectra when the reaction was carried out under

basic conditions (pH 14), this result gives evidence of the oxidation of the ligand. The kinetic studies shows that the rate constant of the complexes of nickel are less than the complexes of copper (Cu-pydien> Ni-pydien while Cu-HMTA> Ni-HMTA).

Key words:

Oxidative dehydrogenation, amine functionalization, basic pH, pydien, HMTA, Cu, Ni.

ABBREVIATIONS

List of abbreviations

OD: Oxidative dehydrogenation

HMTA: Hexamethylenetetramine

MW: Molecular Weight

m.p.: melting point

b.p.: boiling point

s: solubility

ρ: Density

Uv-vis: Ultraviolet – Visible Spectroscopy

IR: Infrared Spectroscopy

DMSO: Dimethyl Sulfoxide

LS: Low spin

HS: High spin

BM: Bohr Magneton

INDEX

LIST OF FIGURES

List of tables

CHAPTER I

1.0 GENERAL CONSIDERATIONS ABOUT COORDINATION CHEMISTRY

Inorganic chemistry has a branch that is responsible for the study of coordination complexes called coordination chemistry. This branch studies the chemical behavior between the transition metals with a ligand. Commonly in coordination chemistry, the union between the central metal ions with the ligand is called a complex compound through the coordinated covalent bond.[2] Where the ligand gives up a pair of no bounded free electrons to form the bond (M $\leftarrow$: L (D)) (Fig. 1). The ligand is a neutral or charged molecule (negative or positive) with a set of atoms that can exist independently of the metal ion. According to Lewis in most cases the ligands act as Lewis bases (electron donors) while the metal ion acts as Lewis acids (electron acceptors). In some cases the ligands donate more than one pair of electrons to the metal ion. On the other hand, an important characteristic in coordination complexes is the coordination number of the metal ion. This is equivalent to the number of donor atoms bonded to the central metal ion. Thus, the coordination numbers equal to 2, 3, 4, 5, 6 represent a geometry of the metal complex that are linear, trigonal planar, tetrahedral or square plane, trigonal bipyramid and octahedral, respectively.[3]
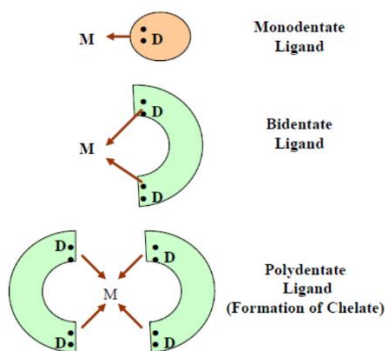
Figure 1. Coordination bond between a metal (Lewis acid) and a ligand (Lewis base).[4]

1.1 COPPER AND NICKEL IN COORDINATION COMPOUNDS

Among the transition metals, copper has an atomic number twenty-five. This element can be found with an average of 68, 0.003, and 0.7, 1.0 ppm in the Earth's crust, in sea water, in the sun and in the human body respectively. This metal is widely used due to its great qualities such as ductility, high thermal and electrical conductivity, resistance to corrosion, etc.

Copper is an essential metal in human nutrition in small amounts, since it can be toxic to health if there are large amounts.[5]

Despite copper stabilizes only two oxidation states, it has been used for multiple applications such as catalysis, pigments for paints, glass, as superconductors, etc. On the other hand, the demand for copper alloys has grown quite a bit because the alloy material shows improved physical and chemical characteristics.[6] The crystalline atomic model of copper is a cubic structure centered on the faces. The characteristic color of copper is due to the wavelengths (blue and green) that are adsorbed and allows the excitation of the electrons from the valence band (full of electrons) to the conduction band s-p (Fig. 2).[5]
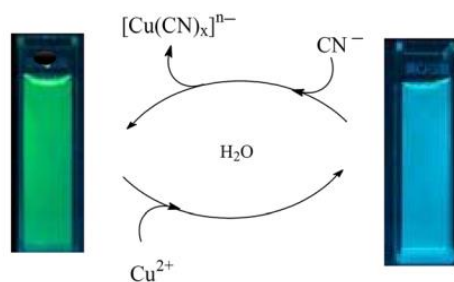
Figure 2. Two characteristic colors of copper in different compounds.[7]

Copper has the ability to acquire four oxidation states ($+1$, $+2$, $+3$, 0), being copper(II) the most stable oxidation state.[5] Copper(II) ion is classified as a hard acid, thus the ligands that coordinate perfectly with them are ligands that contain nitrogen, oxygen, chlorides and sulfur as donors.[8] On the other hand, copper(I) ion is a soft acid that prefers to bind with softer ligands (halides) to form homoleptic complexes as for example $[Cu(CN)_2]^-$, $[CuCl_2]^-$, $[CuCl_3]^-$.[9,10] Copper(III) can be detected in biological systems by multinuclear copper systems because they activate O_2.[11]

Few decades ago, copper has received great attention because it is cheap, abundant in the nature and is a trace essential metal in the metabolism of animal and plants cells.[12] Copper presents some properties such as antibacterial and antiviral and is used to eliminate pathogens that causes some issues to the people.[13] Also, copper nanoparticles and copper have some applications as catalysts, electrocatalysis, photocatalysis and gas-phase catalysis.[14]

Nickel is the twenty-second most abundant element on the earth's crust. Naturally, its

abundance is distributed in isotopes such as ^{58}Ni 68.27%, ^{60}Ni 26.10%, ^{61}Ni 1.13%, ^{62}Ni 3.59%, and ^{64}Ni 0.91%. Nickel has a face-centered cubic structure and exhibits ferromagnetic characteristics. Nickel coordination chemistry is quite extensive with mono and polydentate ligands. The best known oxidation states of nickel range from 0 to +IV, being nickel(I) and nickel(II) commonly found in organometallic compounds while nickel(IV) is stabilized by ligands that contain oxime, amino acid and amides in its structure.[15]

Nickel(0) has a highly covalent bond with π-acceptor ligands (i.e. PR_3, CO, alkenes, N_2, and CN^-) because its electron configuration is d^9. Nickel(0) is a chemical species rich in free electrons in its outer shell orbital allowing it to bond strongly with the π-acceptor orbital of ligands[15] for instances nickel tetra carbonyl forms organometallic complexes with a tetrahedral geometry, its bonds are linear (Ni-C-O) with one σ bond and other π bond[16] (Fig. 3). It also forms adducts with O_2, CO_2, CS_2, and SO_2 forming a square plane configuration. Generally, Nickel(0) (a diamagnetic element) is oxidized to Nickel(II) by the oxidative addition reaction. This allows the formation of an octahedral geometry for Nickel(II).[15]
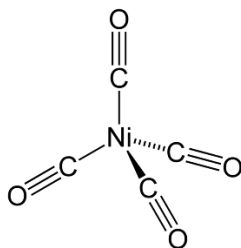
Figure 3. Tetrahedral geometry of Ni(CO)₄.

Nickel(I) is rare but it can be stabilized with nitrogen donor macrocycles, and tripodal phosphorous systems. Nickel(I) has a d^9 electronic configuration with an unpaired electron in its valence shell showing paramagnetic behavior. They typically show varied stereochemistry from 3-ligand coordinate complexes (sterically hindered) to 5-ligand coordinate complexes and in electron transfer reactions Ni^+ is a radical intermediate between Ni^0 and Ni^{2+}.[15]

1.2 OXIDATIVE DEHYDROGENATION

Oxidative dehydrogenation (OD) between nitrogenous ligands (polyamines) and the metal center have been studied extensively for decades. This reaction has three important characteristics: first is the loss 2 electrons and 2 protons, second is the formation of double bond formation type imine and third is the dismutation reaction in which one molecule is reduced while the other molecule is oxidized (Fig. 4). These reactions are dependent on the nature of the metal ion and the ligand.[17]
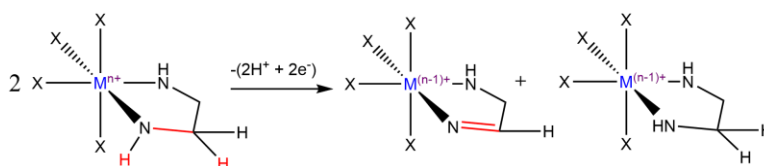
Figure 4. General scheme of oxidative dehydrogenation reactions.[18]

Curtis *et al.* reported the oxidation of macrocyclic ligands coordinated to iron(II) in milder oxidizing conditions. On the other hand, the same conditions was proved for the copper(II) and nickel(II) complexes but they required the strong conditions to produce oxidation the macrocycle.[19,20] So, Curtis had reported the formation of a nickel tetraaza macrocycle complex and the OD of amines in various metals such as Co, Fe, Cu, etc.[17] In this sense, Enrique and co-workers[21] had carried out an analysis of the influence of pH on the OD of the bis(N-methylimidazole) trieneiron(III) complex. Thus, at pH 5-6 there is an instable change the oxidation state of the metal while at pH 7-9 there is a complete dehydrogenation reaction with add $[Fe(CN)_6]^{3-}$ and more OH^-. So, there is a change in the oxidation state of

iron +3 to +2 at 25°C. As seen in the Fig. 5.
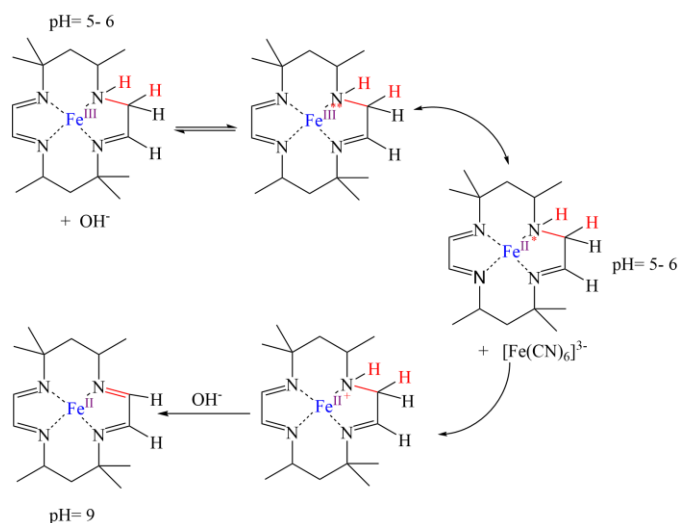
Figure 5. Oxidative dehydrogenation in iron complex.[21]

Likewise, Saucedo and co-workers[22] reported the OD of an iron(III)-amine complex with 1,9-bis(2'-pyridyl)-5-[(ethoxy-2''-pyridyl)methyl]-2,5,8-triazanonane) to an iron(II)-imine complex (1,9-bis(2'-pyridyl)-5-[(ethoxy-2''-pyridyl)-methyl]-2,5,8-triazanon-1-ene. This reaction was performed under neutral or basic conditions while under acidic conditions there was no structural changes of the compound. In this synthesis, a redox reaction occurs where Fe(III) center was reduced to an oxidation state Fe(II). Additionally, the reaction is influenced by the presence of molecular oxygen in the reaction (Fig. 6).
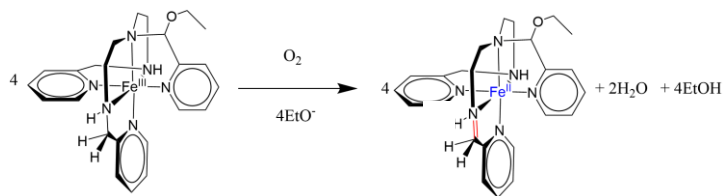
Figure 6. OD reaction of iron(III)-amine to iron(II)-imine complex.[22]

Thus, the transition metals have an important role in the oxidation of organic ligands as for example in the coordination in alcohols allowing the formation of aldehydes and ketones.[18] other examples of OD have been reported for iron, copper, and other metals. In an article published by Victor Ugalde *et al.*[1] they reported OD between the ligand pydien[23](L_2=1,9-

bis(2'-pyridyl)-2,5,8-triazanonane; Fig. 7a) with iron (III) which produced a compound containing imine in its structure and an increase in the denticity of the ligand from 5 to 6 (L4=1,9-bis(2'-pyridyl)-5-[(ethoxy-2''-pyridyl)methyl]-2,5,8-triazanon-1-ene) Fig.7b. The product is kinetically and thermodynamically stable.[1] In last two cases, there was OD reaction for iron complexes are favored under neutral or basic conditions.
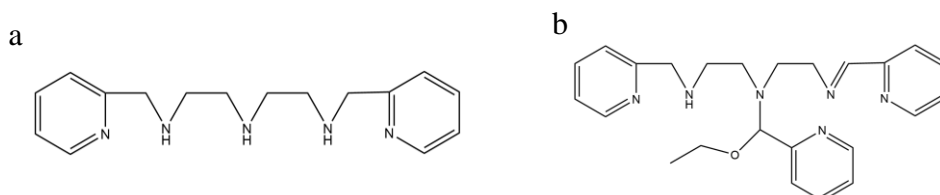
Figure 7. Structure of ligand a) L2(Pydien)[23] b) L4.[18]

In the case of copper, Alexander and co-workers[24] showed the OD reaction of copper chloride dihydrate with 5-(pyridine-2-yl-methyl)-2-thioxo-4-imidazolidinones (L) promoting the formation of a di-nuclear copper (II) complex. In this reaction, the first step (OD) was produced in the absence of oxygen, while in step 2, oxygen was involved producing a redox reaction on copper $Cu^{1+}/Cu^{+1.5}$. Due to the interaction of copper with oxygen, reactive oxygen species (ROS) type derivatives were produced (Fig. 8).
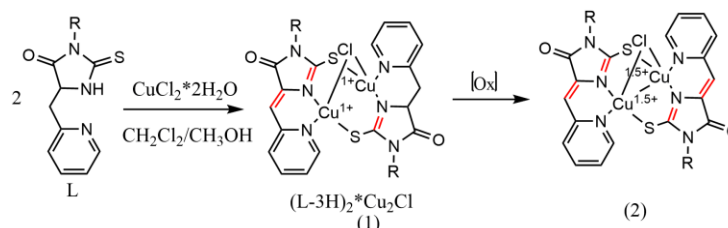
Figure 8. Formation of bonds (C=C and C=N) via OD.[24]

Polyamines are nitrogen compounds important in the OD study because polyamines are strong bases with high affinity for the proton and can form complexes at room temperature.[25] As we mentioned earlier, OD allows the formation of a double bond and it happens because the metal ion oxidizes to an unstable state, then to achieve its stability and is reduced while hydrogenation consists in the formation of single bonds with the help of external agents where the central metal do not play an important role. This can be seen in Fig. 9 where the right path represents the oxidative dehydrogenation of the cyclam ligand by the ionic nickel

metal, while in the opposite path we have the hydrogenation of the [Ni(cyclam)]$^{2+}$ complex.[26]
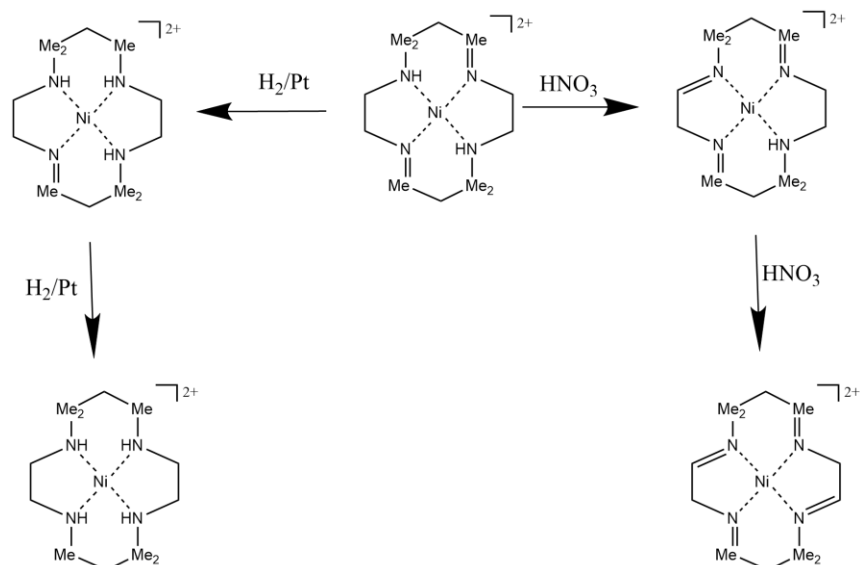
Figure 9. Process of oxidative dehydrogenation and reductive hydrogenation of the nickel (II) complex.[26]

On the other hand, the reactions of the same ligand (cyclam) with different metals form double bonds in different places of the macrocyclic compound. This is observed in the case of the reaction of the cyclam with iron(II) and nickel(II) (Fig. 10).[26]
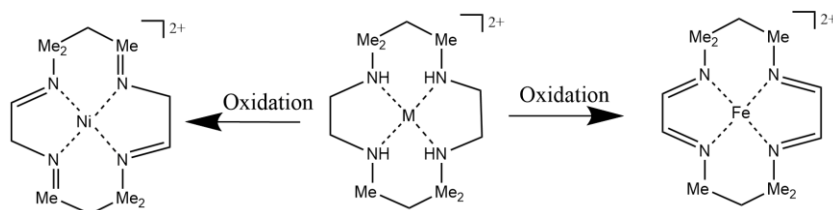
Figure 10. Oxidation depend to metal-ion in polyamines.[27]

1.3 OXIDATIVE DEHYDROGENATION IN NITRILE SYNTHESIS

Nitriles and amines are functional groups required industrially in pharmaceuticals, dyes, pesticides and polymers. In organic chemistry nitriles are used as intermediates for the synthesis of other organic compounds (Fig. 11) and some drugs that contain nitriles in their structure such as milrinone, encracapone, odanacatib are used for the treatment of diseases as insufficiency cardiac, inhibitor in Parkindon's and osteoporosis respectively. While other compounds as acetonitrile, benzonitrile and propionitrile are used as solvents[28]. And methyl cyanoacrylate used as adhesive, etc (Fig. 12).[29]
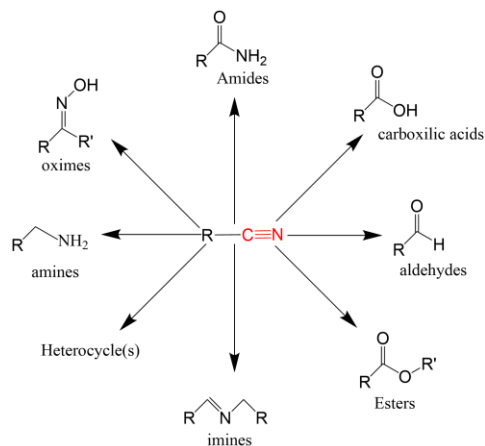
Figure 11. Nitriles convert to others functional groups.[28]

Traditional methods for the synthesis of nitrile compounds such as, ammoxidation, Sandmeyer, Rosenmund-von Braun, dehydration of aldoximes and amides are catalyzed reactions that are not friendly to the environment because it uses toxic substances; moreover, they have low selectivity, and requires special reaction conditions. Also, these syntheses are not economically viable and have been tirelessly researched by scientists.[30]
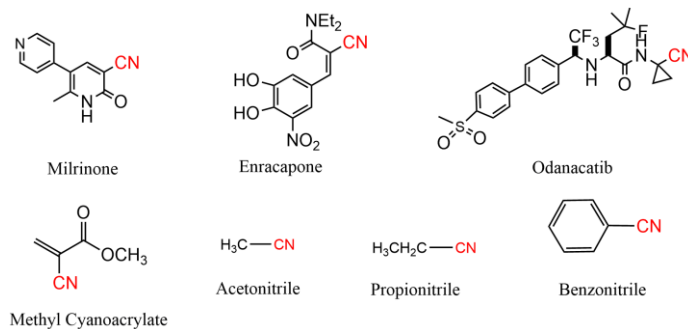
Figure 12. Organic compounds contain nitrile group.[31]

Currently, the OD of amines shows efficient results since this reaction does not require hydrogen acceptors, which produces molecular hydrogen as a by-product. An interesting example of this method uses ruthenium complexes that catalyze the OD of secondary amines to imines. Examples of such catalyst are $RuH_2(CO)(PPh_3)_3$, Shvo's catalytic system and Ru(II)-NNC, while for primary amines to nitriles the ruthenium pyrazole/KOBu system is used.[32] Another type of important components in catalysis is the use of additives (acids and inorganic salts) that activate the substrate for the generation or regeneration of catalytic activity.[32]

1.4 OXIDATIVE DEHYDROGENATION FROM ALCOHOLS TO IMINES AND NITRILES IN COPPER, NICKEL, IRIDIUM AND IRON COMPLEXES

Despite most OD reactions of amine ligands leads to the formation of imines, there are other OD reactions in which the formation of nitriles have been reported. In the late 1980s, Yamasaki *et al.*[33] reports that nickel with $K_2S_2O_8$ form an oxidizing compound in the OD of allylic alcohols to unsaturated carbonyls. This method is called catalytic oxidation of nickel peroxide and is used to obtain nitriles. The reaction is carried out in a basic medium to favor the formation of a catalytically active $NiOH_2$ compound. In this synthesis they have used benzylamine to obtain benzylnitrile with a 93% yield, while the OD of 2-phenylethan-1-amine to a nitrile compound the yield was 97% (Fig. 13).
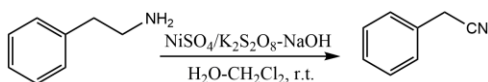
Figure 13. Dehydrogenation of benzyl amine to benzyl nitrile.[33]

An alternative for obtaining nitriles from primary amines is proposed by Wesley and Maurice.[34] In this process they used iridium as a metal active for the dehydrogenation and tert-butylene as an oxidizing agent. This reaction produced > 95% yield to obtain isobutyronitrile from isobutyl amine (Fig. 14a).
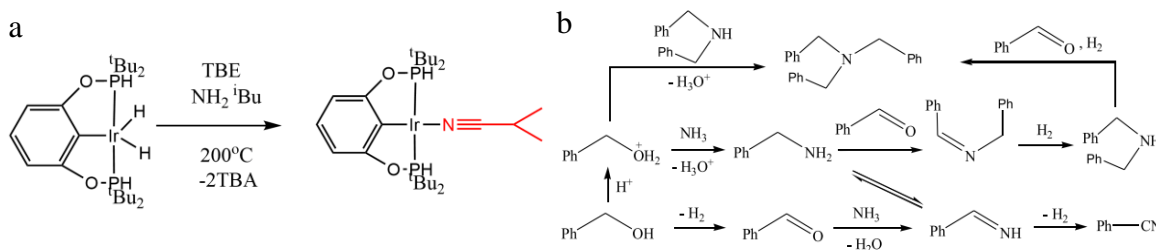
Figure 14. Reaction via for the formation a) isobutyronitrile,[34] *b) benzonitrile.*[35]

Years later a new form of synthesis in the conversion of benzyl alcohol to nitrile, Yuecheng Zhang and co-workers[35] used a Cu/SiO_2 catalyst and HCN or CuCN achieving a 98% yield in the synthesis. The synthetic route is based on the formation of alcohol in aldehyde and later it is dehydrogenated in the presence of copper. In this case, the proportion of copper used showed greater efficiency at 10.3%. If the amount exceeded, the catalytic power of the metal decreased and formed benzene and methylbenzene. In addition, they have carried out

tests with $Cu_{10.1}/TiO_2$, $Cu_{10.3}/ZrO_2$ but their yields were not favorable, while the doping between $Ni_{10.2}/SiO_2$ and $Cr_{10.2}/SiO_2$ showed poor acidity. On the other hand, the $Cu_{10.3}/SiO_2$ catalyst performed best at 340 °C with selectivity to benzyl alcohol of 97%, the catalyst tends to decrease its effectiveness after 32 hours of use but calcination of the catalyst at 550 °C regenerates it (Fig. 14b). These result show that some changes improve nitrile synthesis but do not reduce limited conditions (temperature, byproducts and etc). In this sense, Yunzhu wang *et al.*[36] in their article "Oxidant free conversion of alcohols to nitriles over Ni-based catalysts" mention that the synthesis of nitriles in nickel/aluminum oxide is more accessible. Because the Ni/Al_2O_3 catalyst has a durability of 90% after 48 hours of use and can effectively convert alcohols to nitriles regardless of the carbon chain. The general reaction begins with the transformation of the alcohol to aldehyde while the ammonia gas enters the reactor at 230 °C, the reaction between the aldehyde and the ammonia occurs on the surface of the aluminum to produce an imine. This imine is trapped on the nickel surface and dehydrogenation occurs to form nitrile. Nickel joined to aluminum had showed to be highly reactive to imines and produced a yield between 86 - 95% with a selectivity of 93-99%. They described the reaction way as dehydrogenation-imination-dehydrogenation (Fig. 15) and point out that it had allowed OD of alcohols and generate good yields in the synthesis of nitriles.
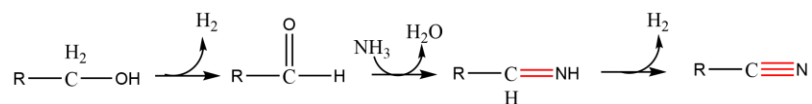
Figure 15. Scheme of conversion of alcohols to nitriles.[36]

Additionally, a study on the atomic dispersion of a metal complex (MX_4) (M = Fe, Co, Ni, etc., X = C, N) in a carbon framework has attracted a lot of attention for catalytic activity but due to the lack of effectiveness it had stalled this method. However, Hong-Hui *et al.*[37] have used boron as a heteroatom (uncoordinated) to enhance the catalytic process on the carbon framework and reduces the energy barrier for the oxidation of amines. This favors the generation of nitriles and prevents the formation of imines. The use of ammonia gas with oxygen are crucial for promoting the generation of nitriles and not imines. Under these conditions they carried out the complete conversion of benzylamine to benzylnitrile (Fig.

16). The results demonstrate that the non-coordination boron shapes the selective and catalytic activity at the iron sites.
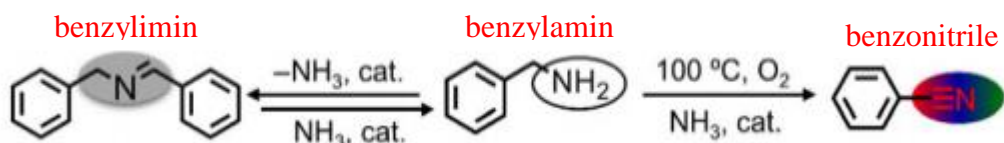
Figure 16. Catalytic performance of Fe active centers to form nitriles.[37]

CHAPTER II

2.0 PROBLEM STATEMENT & HYPOTHESIS

Currently, nitriles, amines and other functionalized derivatives of amines have received great attention due to their versatility and use in pharmaceutical products, in the development of biological materials and their high performance in polymeric materials. However, the methods used commonly to synthesize this derivatives (Sandmeyer, Rosemund-von Braun, nucleophilic substitution of cyanides by alkyl and aryl halides) use toxic or harmful starting materials, produce large amounts of toxic waste and require extreme conditions. In this sense, we propose the study and development of a more environmentally friendly synthesis of imines and nitriles. In order to have a deeper understanding of the dehydrogenation reaction, we use the well documented reaction of iron(III) with the pentadentate ligand pydien. On the other hand, once we develop an experimental protocol with our model reaction, we performed the study of the reactivity of a commercial macrocyclic ligand hexamethylenetetramine (HMTA) against copper and nickel. In this context, we use copper because it has been used the dehydrogenation of amines and alcohols[38,39] due to their remarkable redox properties. Likewise, we used nickel because of its low cost and because it is an active metal in several redox reactions coupled with hydrogen transfer.[40]

2.0 OBJETIVES

2.1 GENERAL OBJECTIVE

The main objective of this work is to study the oxidative dehydrogenation in macrocyclic ligands for the formation of imines and nitriles promoted by copper (II) and nickel (II).

2.2 SPECIFIC OBJECTIVES

− Synthesize macrocyclic complexes of copper (II) and nickel (II).
− Evaluate the conversion of bond simple of C-N to imines and nitriles.
− The study of chemical kinetics to know the reaction rate of metal complexes.
− Influence of pH changes on the formation of nitriles.
− Characterize the reaction products between macrocyclic ligands and the metallic ion with spectroscopic techniques: Uv-vis spectroscopic, IR spectroscopy, magnetic properties, and melting point.

CHAPTER III

3.0 EXPERIMENTAL PART

Next the synthesis will be presented of the metallic macrocyclic complexes of copper and nickel but before the experimental process of the synthesis of a macrocyclic iron complex will appear that was used as a model. Then the synthesized compounds are characterized with the conventional analytical techniques described in subsection 3.2. The compounds synthesized in the solid state product of the chemical reactions were subjected to spectroscopic analysis as IR, Uv-vis spectroscopy and magnetic susceptibility in the solid state while the solutions were analyzed by Uv-vis spectroscopy. Also some reactions are subjected to a kinetic study to measure their speed in the chemical reaction and find equations or mechanisms that describe it. The monitoring of the reactions are carried out by Uv-vis spectrophotometer.

3.1 REAGENTS USED

The reagents used in this work are presented in subsection 3.1.1 with their respective characteristics and quality with information and manufacturer data.

3.1.1 SOLIDS AND LIQUIDS

[Fe(DMSO)$_6$](NO$_3$)$_3$-yellow-green solid, MW: 710g/mol, s: H_2O

Iron(III) Nitrate Nonahydrate (Fe(NO$_3$)$_3$·9H$_2$O)-pale violet crystals, hygroscopic, MW:403.999 g/mol, m.p.: 47 °C, b.p.: 125 °C, ρ: 1.6429 g/cm^3, s: alcohol, acetone , pure 99%, brand: SIGMA-ALDRICH.

Lithium hydroxide (LiOH)-white solid, MW: 23.95 g/mol, m.p.: 462 °C, b.p.: 924 °C, ρ: 1.46 g/cm^3, s: H_2O.

Trichlorohydrate 1.9-bis(2´pyridyl)-2,5,8-triazaanonane (C$_{16}$N$_5$H$_{26}$Cl$_3$)-white powder, MW:394.359 g/mol, s: H_2O.

Sodium tetraphenylborate ((C$_6$H$_5$)$_4$BNa)-white solid, MW: 342.216 g/mol, m.p.: >310 °C, s: water

Nickel(II) chloride hexahydrate (Cl$_2$Ni·6H$_2$O)-green crystals, hygroscopic MW:237.69 g/mol, m.p.:140 °C, ρ: 1.92 g/cm^3 , pure 98%, brand: SIGMA-ALDRICH, s: H_2O.

Cupric sulfate pentahydrate (CuSO$_4$·5H$_2$O)-blue crystals, MW: 249.685 g/mol, m.p.: 110 °C, b.p.: decomposes, ρ: 2.286 g/cm^3, s: methanol, pure 99%, brand: SIGMA-ALDRICH.

Hexamethylenetetramine (C$_6$H$_{12}$N$_4$)-white solid, MW: 140.19 g/mol, m.p.:280 °C, b.p.: 246.7 °C, ρ: 1.33 g/cm^3 , pure 99%, brand: SIGMA-ALDRICH, s: H$_2$O.

Sodium ethoxide (C$_2$H$_5$ONa)-white to yellowish powder, hygroscopic, MW: 68.02 g/mol, m.p.: 300 °C, b.p.: 72.6 °C, ρ: 0.88 g/cm^3, s: ethanol, methanol, pure 99%, brand: SIGMA-ALDRICH.

Ethanol (C$_2$H$_5$OH)-liquid colorless, volatile, MW: 46.07 g/mol, m.p.:-114 °C, b.p.: 78 °C, ρ: 0.789 g/cm^3, s: water, pure 99.9%, brand: SIGMA-ALDRICH.

TertButanol (C$_4$H$_{10}$), MW: 74.123 g/mol, m.p.: 25 °C, b.p.: 83 °C, ρ: 0.78 g/cm^3, pure 99.9%, brand: SIGMA-ALDRICH. Room temperature is solid.

3.1.3 Materials and reagents for the neutralization of ligand

50 mL glass beaker, a glass bottle, a large holed rubber stopper, large Pasteur pipette, 30cm of a hose, a large 60 mL jar, 0.14 g of zinc, 1 mL of concentrated hydrochloric acid, a small cap, a para film tape, a 50 mL beaker, 5 mL of concentrated sulfuric acid, 1 g of sodium chloride.

3.2 LIST OF TECHNIQUES USED

- Infrared Absorption Spectra (brand: Agilent, model: Cary 630)
- UV-Vis Spectrophotometer (brand:Analytik Jena , model: SPECORD S 600)
- UV/Vis/NIR Spectrophotometer (brand:PerkinElmer , model: LAMBDA 1050+)
- Magnetic Susceptibility (Gouy method) (brand: Sherwood , model: Mk 1)
- Melting Point Measurements (brand: Electrothermal, model: IA9000 Series)

3.3 SYNTHESIS OF RAW MATERIALS

3.3.1 Synthesis of the [Fe(DMSO)$_6$](NO$_3$)$_3$ complex

The [Fe(DMSO) $_6$](NO$_3$)$_3$ complex was synthesized according to the procedure described in the literature.[41] In the 30 ml of DMSO, (1 g, 0.0025 mol) Iron(III) Nitrate Nonahydrate was added. The reaction was carried out on a water bath at 75 °C for one hour. Afterwards, the

reaction changed from a reddish-brown color to a yellow-green color (Fig. 17). This indicated the end of the reaction. The reaction was cooled at room temperature, then it was vacuum filtered to get a greenish yellow crystalline solid with yield 85% (Table 2).

Figure 17. Raw material [Fe (DMSO) $_6$] (NO$_3$)$_3$.

3.3.2 Synthesis of pydien(L$_2$ = 1,9-bis(2'-pyridyl)-2,5,8-triazanonane)·3HCl

This synthesis was carried out following the procedure described by Ugalde *et al.*[1] with some changes. In a round flask 2-pyridinecarboxaldehyde (0.210 mol) and diethylenetriamine (0.105 mol) were added in a ratio of 2:1, respectively. To this reaction, 25 mL of ethanol was added. The procedure was carried out in a reflux system at a temperature of 78 °C and constant stirring for 3 h. To this reaction 35.5 mL of glacial acetic acid was added to maintain an acidic pH at approximately 4.5 to promote the condensation of the Schiff base. During the reaction, color changes were observed starting from light green, light yellow to light orange (Fig. 18). This reaction was followed by thin layer chromatography (TLC) tests using a mixture of methanol, chloroform and hexane in a ratio of 1:5:3 as eluent. At the beginning of the reaction two spots corresponding to the aldehyde and the amine were observed on the TLC plate. The color change in the reaction was important in determining the completion of the reaction as it changed from transparent to orange. To confirm the completion of the reaction we follow with the TLC until the disappearance of an aldehyde spot. Fig. 18 describes the chemical equation of the reaction.

3.3.3 Neutralization process of ligand

3.3.3.1 Glass chamber with solution

In order to perform the reduction of the Schiff base obtained in the condensation (Fig. 18), the heterogeneous catalytic reduction method was used, which palladium on activated carbon (10% Pd) as catalyst under the presence of gaseous hydrogen. The solution obtained in the section 3.3.2 was added together with the activated carbon (Pd/C) in the container containing the dark orange solution.

3.3.3.2 Generation of hydrogen gas

In order to generate the hydrogen gas a catalytic reduction is necessary so, the syringe method reported by Mattson was used.[42] For this, the jar was disassembled and inserted the small cap into the syringe, put 14 g (0.2141 mol) of zinc on the cap, insert the plunger into the syringe, and seal the cap with the para film. 1 mL (0.0307 mol) of hydrochloric acid was absorbed with the syringe and cover it with the sealed cap (Fig. 19a). Then, it was immersed 2 cm of the syringe in water and adjust the syringe slowly until the acid comes into contact with the zinc. So, gas began to appear inside the syringe generating a displacement of the plunger outwards due to the pressure of the gas. When the reaction has consumed all the zinc metal, the lid was slowly removed into the water. Then, the plunger was pressed until a bubble appeared inside the water so that a little of the excess acid comes out of the syringe and pull it and allow enter a little water into the syringe so that the hydrochloric acid is diluted. Ready, 52.340 mL of H_g was generated (Fig. 19b).
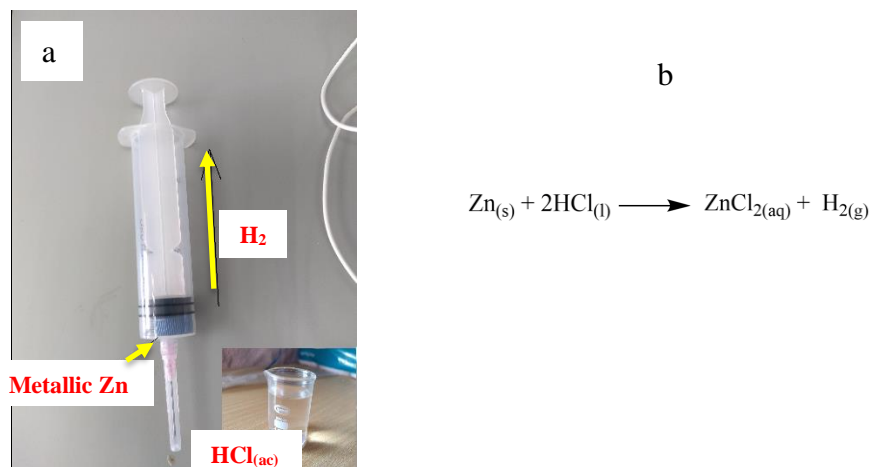
Figure 19. a) Syringe of hydrogen gas. b) Scheme of chemical equation for gas formation.

3.3.3.3 Introduction of the gas to the glass chamber

One end of a hose was adjusted to syringe and the other end to the Pasteur pipette (embedded in the container containing the solution) (Fig. 20a). The syringe was tilted so that the liquid is not at the end of the hose. Then, plunger was pressed so that all the gas passes through the hose to the container while in the solution appeared bubbles and shake it the container so that the reaction takes place. The hose was pressed to remove the syringe. The introduction of the gas was made by 4 times with a constant wiggle. The mixture was filtered to separate the activated carbon from the liquid solution and the solution changed color (yellow). Fig. 20b describes the chemical equation of the catalytic reaction of pydi-imine to pydien.
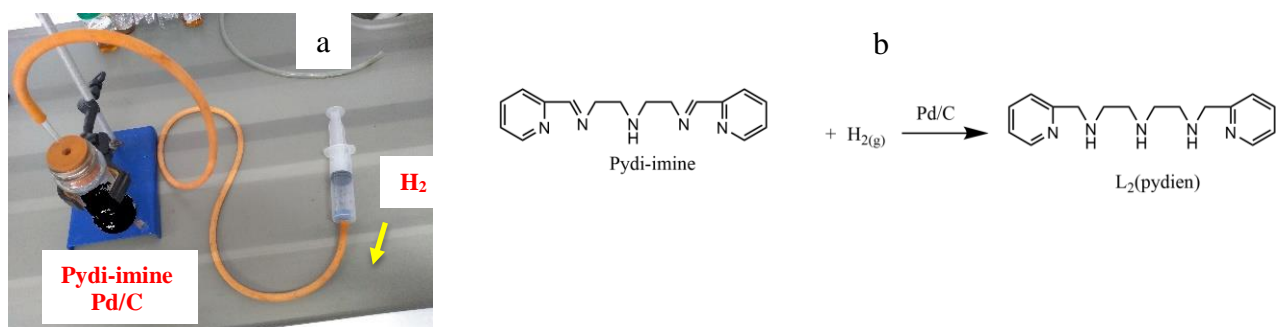
Figure 20. a) Transfer of H_2 (gas) to the imine reaction mixture. b) Reaction scheme for catalytic hydrogenation of Schiff's base and formation of L_2.

3.3.3.4 Procedure for the generation of gaseous hydrochloric acid in the solution

Once, the ligand is in the amine form is necessary to pass to form the tri-hydrochloride derivative since this hydrochloride is a stable solid and easy to manipulate it. The mixture obtained from the previous procedure was put in the glass chamber used in the previous

procedure. To generate gaseous HCl, 1 g (0.0171 mol) of sodium chloride was put in a glass chamber and introduce 5 mL (0.0933 mol) of sulfuric acid covering quickly with a stopper, 415 mL of HCl gas were generated (Fig. 21b) and bubbled to the ligand with the other end of the hose the formation of a white precipitate was observed indicating that the reaction was carried out successfully (Fig. 21a). At the end, the reaction was filtered under vacuum and obtain the pydien·3HCl. Then, in the Fig. 21c is the reaction between pydien and HCl gas with yield 20%.
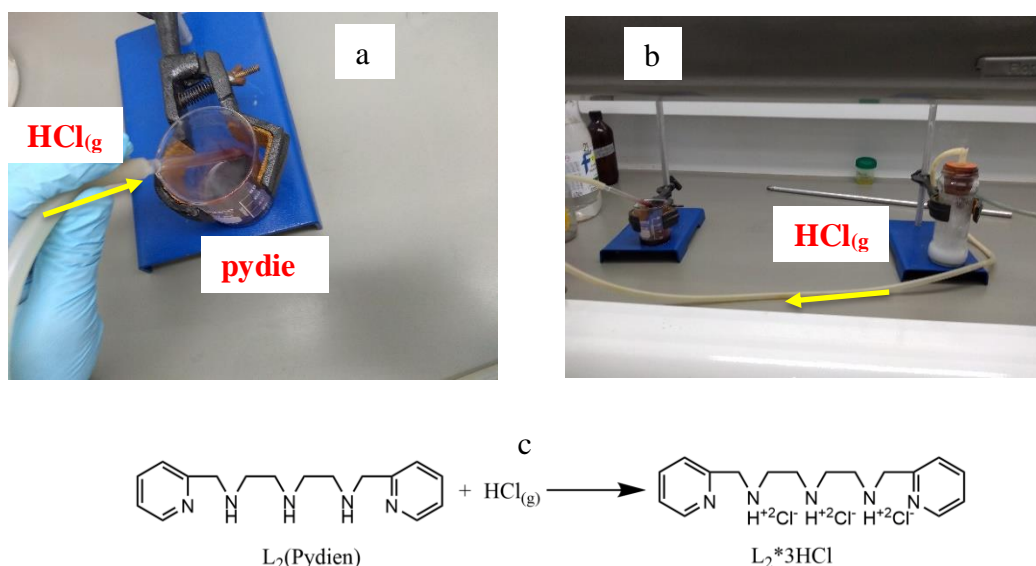
Figure 21. a) Precipitation of pydien in HCl gas b) Generation and transfer of gaseous hydrochloric acid c) Reaction scheme.

3.3.2 Reaction of Fe(III) with a hexadentate derivative of pydien in ethanol

The study of the reactivity of Fe(III) with L_2·3HCl was performed following the next procedure: In a 50 mL round bottle, 277 mg (0.704 mmol) of lithium hydroxide and 51 mg (2.1 mmol) of pydien were mixed with 30 ml of ethanol. The reaction was placed in a reflux system at 75 °C (in a water bath) with a constant stirred until the reaction is neutralized, that is, until the mixture is clear about 1.5 hours. Then, 75.4 mg (0.704 mmol) 2-Pyridinecarboxaldehyde was added to the reaction and the reaction turns brownish-yellow. The reaction was monitored by TLC until the disappearance of 2-pyridinecarboxaldehyde spot. Then, 500 mg (0.704 mmol) of $[Fe(DMSO)_6](NO_3)_3$ were added to the reaction mixture and the solution turns deep purple; 12 hours of reaction were allowed for all the components of the reaction to react completely. It carried out to slow stirrer with low temperature, after

that mixture reaction was reached at room temperature and cooled until 5 °C. Then, a few drops at 5 °C of the sodium tetraphenylborate in ethanol was added to obtain the sodium tetraphenylborate salt of the complex. Finally, the solution was vacuum filtered obtaining a solid with a 52% yield (Table 2) (Fig. 22a, b).
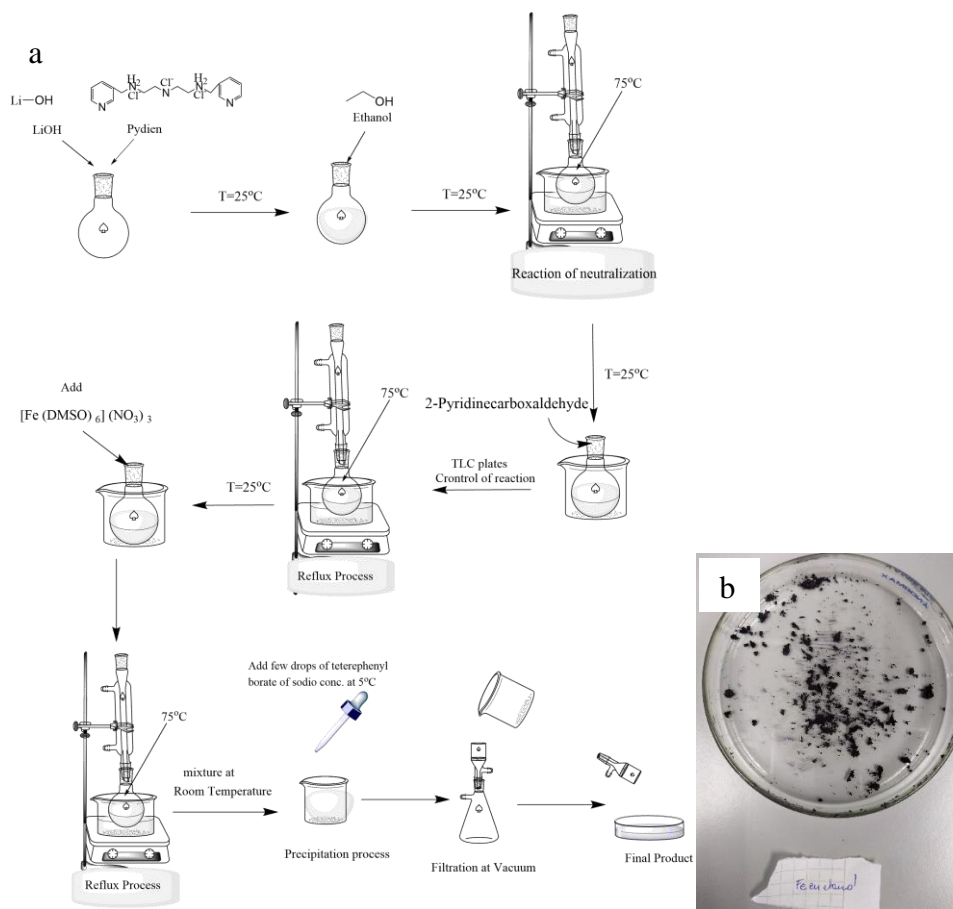
Figure 22. a) Reaction process of Fe complex in ethanol. b) Final product [Fe(II)·L₄]²⁺in ethanol.

3.3.3 Reaction of Fe(III) with a hexadentate derivative of pydien in tert-buthanol

To study the performance of Fe(III) with $L_2 \cdot 3HCl$ in tert-butanol, the same procedure above was followed with the same amounts of reagents. However, in this case there are the following changes: the change of solvent (tert-butanol) influenced the neutralization time from 1 to 4 hours. Another important change was in the dissolution temperature due to melting point of the solvent is 24 °C. The reactions must be carried out at a temperature ≥ 24 °C. Taking into account all these aspects, a solid product was dark purple (Fig. 23a) with a yield of 32% (Table 2).

3.3.4 Reaction of Ni(II) with an hexadentate derivative of pydien in tert-butanol

The study of the reactivity of Ni(II) with $L_2\cdot3HCl$ was performed following the procedure of section 3.3.2. In this synthesis, 110.8 g (4.62 mmol) of lithium hydroxide, 607.2 mg (1.5 mmol) of ligand, 164.9 mg (1.54 mmol) of 2-Pyridinecarboxaldehyde and 0.2g (1.54mmol) of $NiCl_2$ anhydride in 25 mL of tert-butanol was used. However, in this reaction was not necessary tetraphenylborate and leave the mixture at room temperature for the solvent to evaporate. After two weeks some of the volume of the mixture had disappeared and a crystal within the solution had formed (Fig. 23b). Despite this change, the reaction yield was poor but this result was a good sign because in previous reactions nothing of final product was obtained when tetraphenylborate was added in the solution.

Considering the performance obtained, in the next synthesis had modifications to the procedure and proposed the following synthetic route: In a 50 ml round bottle 594 mg (2.4 mmol) of lithium hydroxide and 326 mg (0.827 mmol) of $L_2\cdot3HCl$ were mixed with 30 ml of tert-butanol. The reaction was placed in a reflux system at 75 °C (in a water bath) with a constant stirred until the reaction is neutralized, that is, until the mixture is clear about 5 hours. Then, 200 mg (0.827 mmol) of nickel(II) chloride hexahydrate were added to the reaction mixture and the solution changed color from green to orange until it was purple; 12 hours of reaction were allowed for all the components of the reaction to react completely. So, the reaction mixture was left 12 hours at room temperature to evaporate the solvent and form the solid compound, which was vacuum filter. The compound is a light purple crystalline solid (Fig. 23c) with a yield of 51.65% (Table 2).

3.3.5 Reaction of Cu(II) with a hexadentate derivative of pydien in tert-butanol

The study of the reactivity of Cu(II) with $L_2\cdot3HCl$ was prepared with the procedure described in the previous section 3.3.2. The synthesis was carried out with the following amounts of reagents 201.6 mg (1.5 mmol) of copper chloride, 109.3 mg (4.5 mmol) lithium hydroxide, 160.6 mg (1.5 mol) of 2-pyridylcarboxylaldehyde in 20 mL of tert-butanol. Due to the chemical characteristics of solvent described in section 3.3.3. Dissolved tetraphenylborate in tert-butanol at 30 °C was slowly added to the reaction mixture to promote the formation

of the copper metal complex. However, due to the short time in the laboratory, the synthesis could not be completed. In the Fig. 23d is showed how the copper complex looked up to this point.
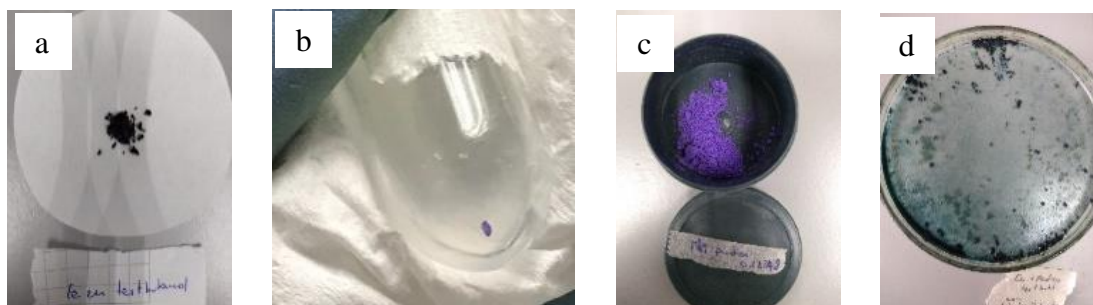
Figure 23. Final product of the reaction between L₆ with a) Fe(III), b) Ni(II), c)Ni(II) and d) Cu(II).

3.4 SYNTHESIS OF COMPLEXES WITH THE MACROCYCLIC LIGAND HMTA

3.4.1 Reaction of Cu(II) with HMTA in ethanol

The study of the reactivity of Cu(II) with HMTA was following with the next procedure:

In a 50 ml round bottle, 500 mg (2 mmol) copper sulfate pentahydrate and 281mg (2 mmol) of HMTA with 20 mL of ethanol. This synthesis was placed in a reflux system (in a water bath at 85 °C) with a constant stirred until the reaction is neutralized, that is, until the mixture is clear about 3 hours. Afterwards, the reaction was brought to room temperature and is filtered under vacuum (Fig. 24a). The complex synthesized is a solid compound of color vivid green (Fig. 24b) with a yield 95% (Table 2).
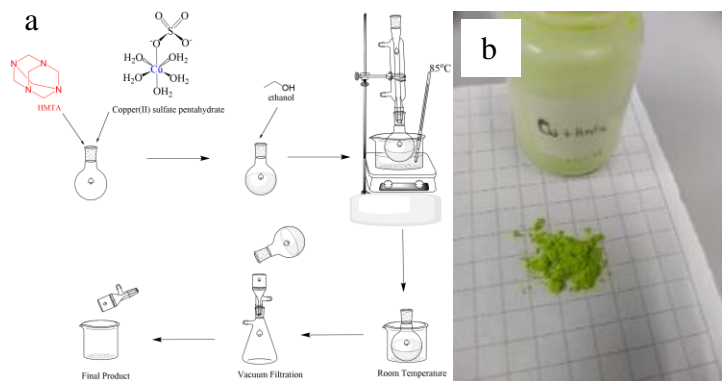
Figure 24. a) Procedure of synthesis Cu(II)-HMTA. b) Final product of Cu(II)-HMTA.

3.4.2 Influence of pH on the reaction

3.4.2.1 Reaction of HMTA with copper (II) at pH 9, 13 and 14

The reaction of HMTA with cupric sulfate was also carried out at different values of pH 9,

13 and 14 with the addition of sodium ethoxide since the influence of pH on the dehydrogenation reaction have been reported before.[43-46] To obtain pH 9, 0.032 g of sodium ethoxide was added at the beginning of the aforementioned reaction. At this pH value we obtained a green compound. To reach pH 13, 0.065 g of sodium ethoxide was added. At this pH value the compound was more deep green, for pH 14, an (0.08 g) of sodium ethoxide was added and we obtained a blacker green product. Finally at pH > 14 with excess > 0.08 g of sodium ethoxide was added in solution for obtain a black compound (Fig 25, Table 3).
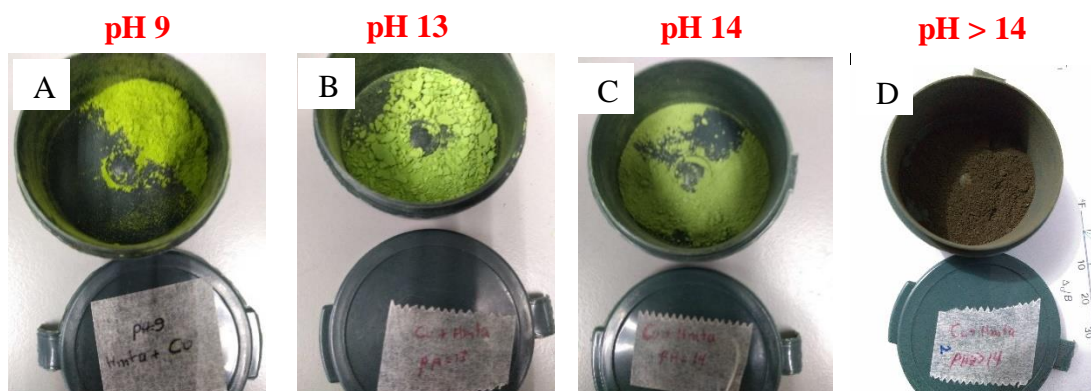
Figure 25. Complex of Cu(II)·HMTA at a) pH 9, b) pH13 c) pH 14 and d) pH>14.

3.4.3 Reaction of Ni(II) with HMTA in ethanol

To study the reactivity of Ni(II) with HMTA we follow the procedure described in the previous section 3.4.1. In the reaction the amounts of raw materials were 500 mg (2.1 mmol) nickel(II) chloride hexahydrate, 294.8 mg (2.1 mol) of HMTA and 20 mL ethanol at pH 7. The final product is a pale green solid compound (Fig. 26) and the reaction has a yield of 79% (Table 2).

Figure 26. Reaction product between Ni(II) and HMTA.

3.4.4 Influence of pH on the reaction

3.4.4.1 Reaction of HMTA with Nickel(II) to pH 10, 12, 14, >>14

To increase the pH from 7 to 10, 12, 14, >14 and >>14 of the synthesis described in section 3.4.1, 0.036 g, 0.054 g, 0.065 g, 0.09 g and 0.1 g of sodium ethoxide were added in each case. A pale green reaction product were obtained at pH 7, a greenish-yellow product was obtained at pH 10, green at pH 12, light green at pH 14, whitish brown at pH>14 and pH>>14 is black. This result at simple view we can say the basic pH change the physical properties of the product. So, it can be notice in the Fig. 26, 27 and Table 3.
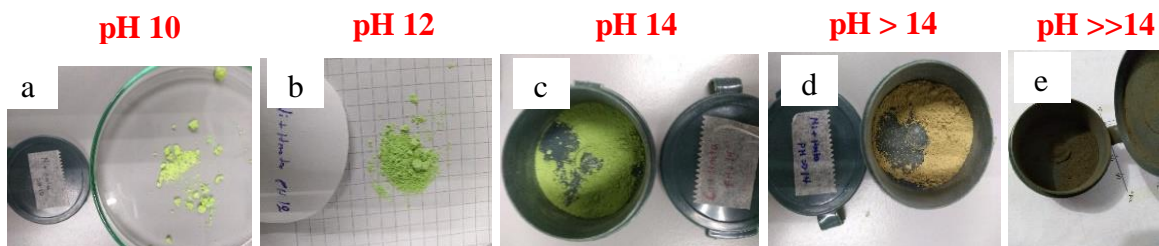
Figure 27. Ni(II)-HMTA at a) pH10, b) pH12, c) pH14, d) pH>14, e) pH>>14.

3.5 PREPARATION OF REAGENTS FOR THE MEASUREMENT OF CHEMICAL KINETICS

3.5.1 Kinetic of the reaction of a hexadentate derivative of pydien with $[Fe(DMSO)_6](NO_3)_3$

0.4 mg (0.001 mmol) of pydien·3HCl with 0.06 mg (0.003 mmol) lithium hydroxide were added to a small test tube. The test tubes were covered and place it in the oven at 35 °C with constant stirring for 12 hours to neutralize the ligand. Next, 0.11 mg (0.001 mmol) of 2-pyridinecarboxaldehyde was added and put in the Uv-vis cell the solution together with 0.710 mg (0.001 mmol) of $[Fe(DMSO)_6](NO_3)_3$.

3.5.2 Kinetic of the reaction of a hexadentate derivative of pydien with Cu(II) and Ni(II)

The solutions were prepared with the previous procedure but the iron compound was changed for 0.134 mg (0.001 mmol) $CuCl_2$ and 0.237 mg (0.001 mmol) $NiCl_2 \cdot 6H_2O$, respectively.

3.5.4 Kinetic of the reaction of HMTA with $CuSO_4 \cdot 5H_2O$

For the measurement of chemical kinetics, 2.4 mg (0.01 mmol) of copper sulfate pentahydrate with 1 mL of ethanol was added in a small test tube. In another test tube, 1.42 mg (0.01 mmol) of HMTA was added with 1 mL of ethanol. Both test tubes were heated to the boiling point of the solvent to dissolve the solid reagents. A dilution of 100 microliters

of copper sulfate dissolved with 900 microliters of ethanol (0.001067 M) was made and the same procedure was carried out with HMTA (0.001125 M). Finally, these solutions were added to the quartz cuvette and placed in the diode array Uv-vis equipment to follow the progress of the reaction.

3.4.3.2 Kinetic of the reaction of HMTA with $NiCl_2 \cdot 6H_2O$

For the kinetic measurement in this reaction, it was carried out with the same previous procedure but in this case with 2.376 mg (0.001 mmol) of nickel chloride pentahydrate and 1.42 mg (0.001 mmol) of HMTA in ethanol were used.

CHAPTER IV

4.0 RESULTS AND DISCUSSION

The analysis of the results and the discussion of this work are presented in the following two sections. In section 4.1 begin by describing the spectroscopic characteristics of raw materials to compare them with the main reaction products. The reaction of pydien with iron in ethanol was analyzed in order to use it as a model reaction of OD to compare in the reaction of pydien with copper and nickel in tert-butanol or methanol. In section 4.2, HMTA is the main study ligand and its behavior at basic pH levels. In both sections IR and Uv-vis spectroscopic characterization, magnetic measurements and in some cases a kinetic study of the reactions were carried out.

4.1 CHARACTERIZATION OF THE MAIN PRODUCT OF THE REACTION BETWEEN IRON(III) AND PYDIEN DERIVATE IN TERT-BUTANOL

For the successful identification of the OD product of our model reaction it is necessary to determine the characteristics of the raw material and the final product of the synthesis, for this reason the most important details of the spectroscopic characterization, magnetic susceptibility, melting point of $[Fe(DMSO)_6](NO_3)_3$ and $[Fe(III)L_6]^{2+}$ are presented below, note that from here to ahead the notation L_4 to identify the hexadentate derivative observed when iron(III) reacts with L_2 (Fig. 28).
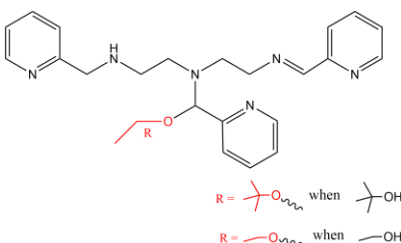
Figure 28. Structure of L_4 (9-bis (2'-piridil)-5-[tert-butoxy-2''-pridil) metil]-2,5,8-triazanon-1-eno) ligand derivate from L_2 after oxidative dehydrogenation reaction with $[Fe(DMSO)_6](NO_3)_3$. Performed in ethanol[1].

4.1.1 Characterization of the raw materials

4.1.1.1 $[Fe(DMSO)_6](NO_3)_3$.- According to the synthesis described in section 3.3.1, the compound obtained was greenish-yellow crystalline with a yield of 85% (Table 2). The complex is paramagnetic with a magnetic moment 5.73 BM (Table 1), which is in agreement

with the literature[47] showing that we have an Fe^{3+} high spin species in this complex. This compound has a melting point of 216 °C (Table 2). The crystal structure has been determined before by X-ray spectrometry[48] from which an octahedral geometry with bond interactions between oxygen and iron was determined.

4.1.1.1.1 IR characterization of $[Fe(DMSO)_6](NO_3)_3$

From the IR spectrum of $[Fe(DMSO)_6](NO_3)_3$ was performed the next assignation: in the ideal spectral we find a signal at 2996 cm^{-1} and the signal is assigned to the vibrational mode of the $-CH_3$ group. In the spectral there are two signal first to 1043 cm^{-1} and 827 cm^{-1}, which are vibrational modes for the NO_3^- while one medium signal at 1043 cm^{-1} correspond to SO group (Fig. 29).[49]
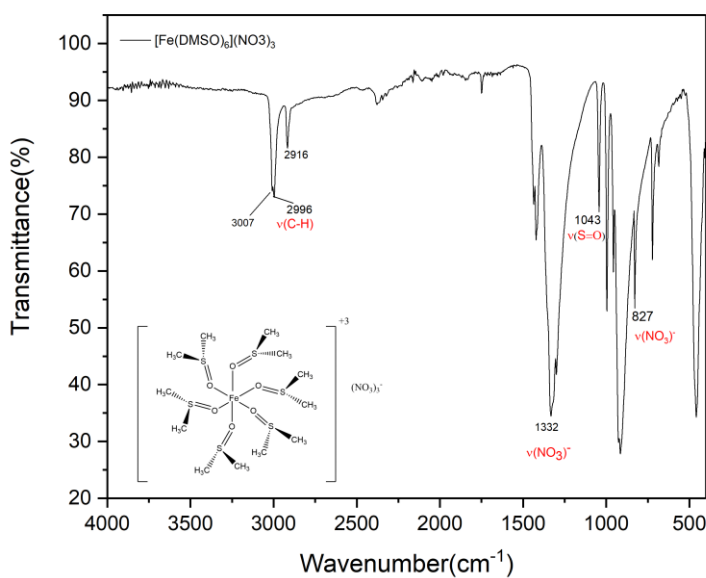
Figure 29. IR spectra of $[Fe(DMSO)_6](NO_3)_3$.

4.1.1.1.2 Electron absorption spectroscopy

In Fig. 30 there is the Uv-vis spectrum of the Fe(III) complex. Since iron has a 3+ oxidation state, then it is a d^5 species. For a d^5 species there are two possibilities for the spin state of iron, the first one is the case with five unpaired electrons in which ligands of the first part of the chemical series (π donor) provokes a weak crystal field splitting. On the other hand, in the second possibility there is only one unpaired electron in T_{2g} orbitals due to the strong crystal field splitting caused by the coordination of ligands of the final part of the

27

spectrochemical series (π acceptors). From the magnetic susceptibility studies in the previous section determined $\mu_{eff} = 5.8$ BM (Table 1) which indicate the presence of a d^5 high spin species. Analysis of the electronic spectrum in Fig. 30 shows no d-d electronic transitions in visible region, so this is an evidence of a d^5 high spin species since there is a $^6A_{1g}$ ground state for this species and there are not sextuplet excited states present according to Tanabe-Sugano diagram (Annex 1). This result is in agreement with that obtained by magnetic measurements.[50,1]
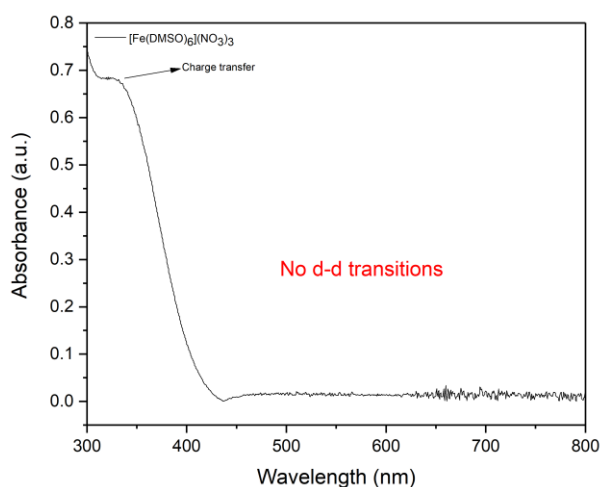
Figure 30. Uv-vis spectra of [Fe(DMSO)$_6$](NO$_3$)$_3$.

4.1.1.2 pydien·3HCl. - The compound obtained is a white solid soluble in water, DMSO, acetonitrile and slightly soluble in methanol and ethanol. The formula of the neutralized compound is $C_{16}N_5H_{26}Cl_3$. The yield of the synthesis was 20% and m.p. of 205 °C (Table 2).

4.1.1.2.1 IR characterization of L$_2$ (pydien·3HCl)

According to the IR spectrum there are signals in a range of 2381-2653 cm^{-1}, which are characteristic vibrational bands of N-H. A signal at 2939 cm^{-1} is correspond to vibrational stretch band to C-H (sp^3) while at 3041 cm^{-1} exists vibrational band of a sp^2 (=C-H). In a range of 2000-1667 cm^{-1} there are characteristic bands of mono-substituted aromatic rings. At 1590 cm^{-1} there are vibrational modes of a double bond of the aromatic ring while at 1590 cm^{-1} exists a (C=N) double bond band of the aromatic ring. Finally, there are signals at 814

and 754 cm^{-1}, which are characteristic bands of C-H folding (Fig. 31).[51]
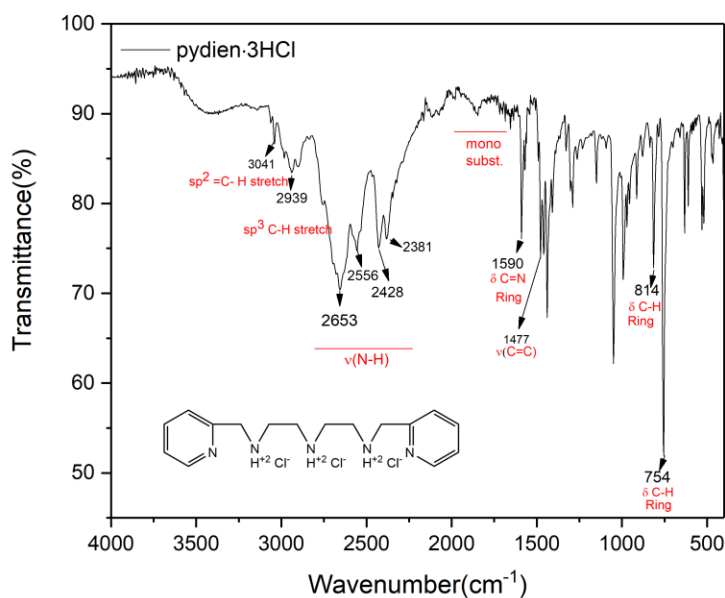
Figure 31. IR spectra L$_2$·3HCl.

4.1.2 Synthesis and characterization of the iron complex in ethanol

4.1.2.1 [Fe(II)L$_4$]$^{2+}$. - The reaction product is a purple solid soluble in acetonitrile, acetone slightly soluble in methanol and insoluble in ethanol, hexane, water and chloroform (according test solubility made in the laboratory). The yield of the reaction is 52% (Table 2), the compound has a melting point of approximately 200°C. According to the characteristics described in the literature[1] on this compound, the chemical formula is [Fe(C$_{24}$N$_6$H$_{30}$O)]$^{2+}$ and the counter ion used for the precipitation of the compound is [(C$_6$H$_5$)$_4$B]$^{2-}$.

4.1.2.2 IR characterization of [Fe(II)L$_4$]$^{2+}$

In the IR spectrum of the synthesized iron(III) complex, an absorption band at 3246 cm^{-1} represents vibrational mode to coordinated N-H. A signal at 3050 cm^{-1} corresponds vibrational signals of the double bonds (C=C) in aromatic rings, while at 2998 cm^{-1} there is a C-H vibrational signal of aliphatic compounds. In a range of 2000-1667 cm^{-1} belongs to the signals of mono-substituted aromatic rings and the next signal at 1654 cm^{-1} belongs to the imine (-C=N) although, that signals are not very strong in the spectrum. At 1604 cm^{-1} exists the vibrational signal of a C=N double bond in aromatic ring and the signals at 1543, 1477 and 1438 cm^{-1} are characteristic vibrational bands of pyridine while signals at 1578,

29

1459 and 1427 cm^{-1} are vibrational bands to phenyls of tetra phenyl borate. The signals at 846 and 767 cm^{-1} are the aromatic ring to pyridine in mono substitution while the 732,700 and 611 cm^{-1} signals belong to the phenyls group. Finally, at 1088 cm^{-1} exists a weak vibrational signal corresponding to an ether group (Fig. 32). Most of the signals are not intense in our synthesized product because impurities or raw reagents did not reacted must be present in the final product, but the peaks coincide with those reported in the literature.[1,51] To conclude, the most important signal in the IR spectrum is at 1654 cm^{-1} where there is a C=N double bond that confirms that the ligand coordinated with iron(III).
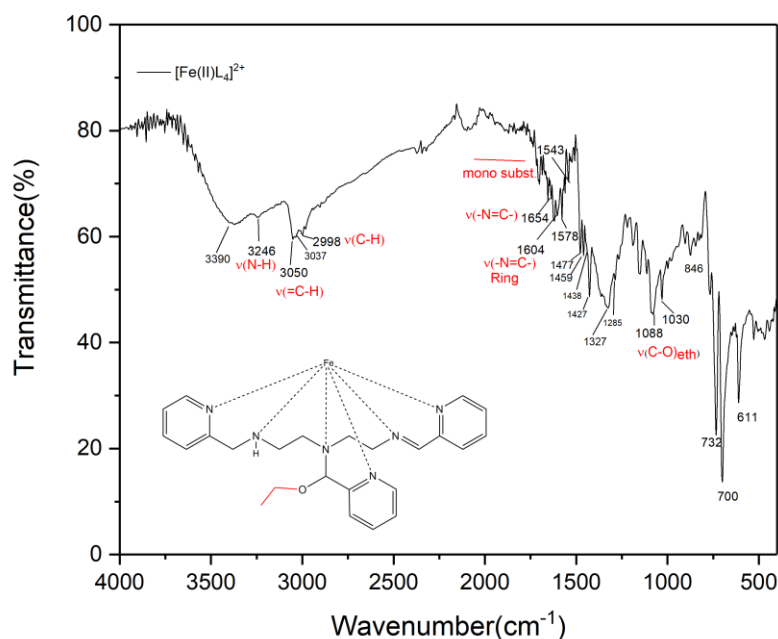
Figure 32. IR Spectra of [Fe(II)L₄]²⁺.

4.1.2.3 Electron absorption spectroscopy

In Fig. 33a there is a Uv-vis spectrum of the iron complex. In this case it would be a strong field d^6 LS species with octahedral geometry. This is possible to know by means of the diffuse reflectance spectrum. Assignation of absorption bands in 571, 400, 276, 262 and 251 nm was made with the use of Tanabe-Sugano diagram for a d^6 species, form those analysis we determined the electronic transitions of $^1A^{2g}$ (^{1}F) ← $^1A_{1g}$, $^1A_{2g}$ (^{1}I) ← $^1A_{1g}$, ^1E_g ← $^1A_{1g}$, $^1T_{2g}$ ← $^1A_{1g}$ and $^1T_{1g}$ ← $^1A_{1g}$ for the wavelengths above (Annex 2). On the other hand, in the liquid Uv-vis spectrum (Fig. 33b) there are two signals at 577 and 396 nm in visible region corresponding to the low energetic signals found in solid state spectrum. Interestingly, it is

not possible to observe the signals below 325 nm because they are masked with the charge transfer signals (area or zone of electron transfer between metal atoms and ligands).[50,52] Also, the differences in the wavelengths absorbed by the complex in solid and in liquid is of 4 nm, this is due to the fact that the dissolved complex has to move freely in a liquid solution while in the solid state it remains static. To conclude, the metal center of the complex is a Fe(II) LS.
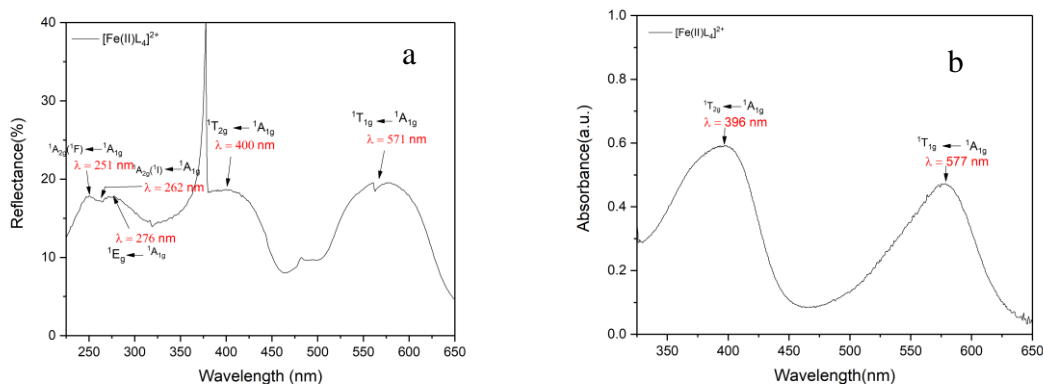
Figure 33. Uv-vis spectra of [Fe(II)L₄]²⁺ a) reflectance (solid) b) absorbance (liquid).

4.1.2.4 Magnetic Measurements

The measurement of the magnetic property of the iron complex was carried out at room temperature. The complex is diamagnetic with a value of the effective magnetic moment μ_{eff} = 0 BM (Table 1). This result is in agreement with those obtained by Uv-vis spectroscopy in which an iron(II) LS complex was assigned.

4.1.2.5 Analysis of results.

 - The synthesized iron is diamagnetic and magnetic moment is zero (μ_{eff} = 0 BM). So, this compound presents a change in the oxidation state because iron as a reagent had a 3+ oxidation state and when coordinating with the ligand the oxidation state changes. This is justified by the electron absorption spectra since the electronic transitions that are characteristic of a d^6 LS. In addition, the diffuse reflectance spectrum reveals more clearly the electronic transitions of Fe^{2+} and in the IR spectra confirms the oxidation of ligand (C=N). Which means that an oxidative dehydrogenation reaction occurred between the ligand and the metal.

4.1.3 Synthesis and characterization of the iron complex syntesized in tert-butanol

4.1.3.1 $[Fe(II)L_6]^{2+}$. - The synthesized compound is a purple solid soluble in acetone, acetonitrile slightly soluble in methanol, and insoluble in ethanol, hexane, water and chloroform. The product resulting from the reaction has a yield of 32% (Table 2) with a melting point of 200 °C, its formula is $[Fe(C_{26}N_6H_{34}O)]^{2+}$ and the counter ion used to precipitate has the following formula $[(C_6H_5)_4B]^{2-}$.

4.1.3.2 IR characterization of $[Fe(II)L_6]^{2+}$

The IR spectrum in Fig. 34 presents the most significant signals of the synthesized iron complex. In which at 3248 cm^{-1} there is a vibrational band of the N-H coordinated while at 3050 and 2983 cm^{-1} exist absorption bands correspond to the C-H vibrational signals of the aromatic rings and C-H vibrational of the aliphatic compounds respectively. The next signal at 2000-1667 cm^{-1} belongs to an overtone signal of a ring mono substituted. A weak signal at 1654 cm^{-1} corresponds to a vibrational band of imine (-N=C-) and a signal at 1604 cm^{-1} belongs to vibrational modes of double bond (N=C) of the pyridines. Other signals at 1541 and 1477 cm^{-1} belong to the pyridine ring while at 1578, 1459 and 1429 cm^{-1} are signals of the tetra phenyl borate rings. The signals at 827 and 765 cm^{-1} are characteristic signals for a mono-substituted aromatic ring to pyridine. Thus, signals at 734, 700 and 609 cm^{-1} corresponding to the aromatic phenyl rings. A signal at 1077 cm^{-1} indicates the presence of a vibrational band of the ether group in the molecule.[51] Finally, these signals in the IR spectrum coincide with the signals to the complex model. This means that the ligand is coordinated with the metal.
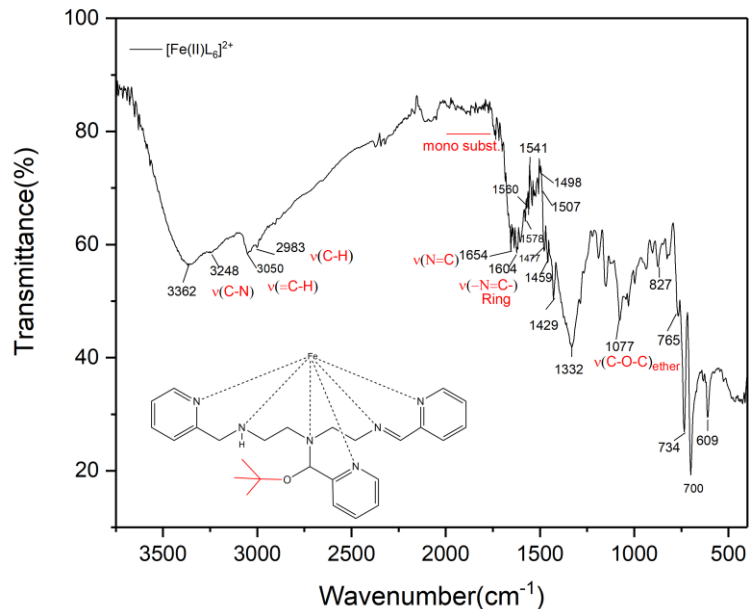
Figure 34. IR Spectra of $[Fe(II)L_6]^{2+}$.

4.1.3.3 Electron absorption spectroscopy

In Fig. 35, the Uv-vis spectrum of the iron complex is showed. In this case it would be a strong field d^6 LS species with octahedral geometry. Because the absorption bands at 579 and 380 nm are in the absorption range of d^6 LS reported in the literature.[50] However, the rest of signals do not appear in the spectrum because the signals are masked within charge transfer signals. So, according to the Tanabe-Sugano diagram there are the following the electronic transitions: $^1T_{2g} \leftarrow {}^1A_{1g}$ and $^1T_{1g} \leftarrow {}^1A_{1g}$ (Annex 2). Finally, these spectrum signals coincide with the signals to the complex model. This means that oxidative dehydrogenation reaction takes place in tert-butanol as well as ethanol.
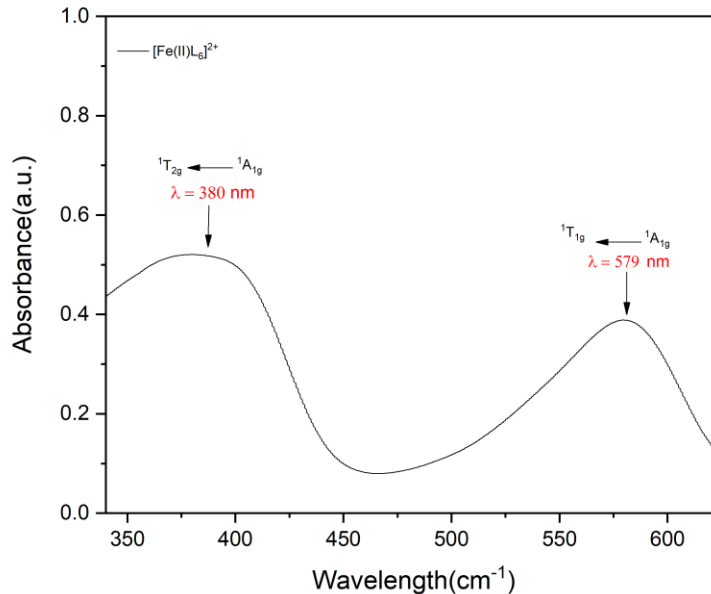
Figure 35. Uv-vis spectra of [Fe(II)L$_6$]$^{2+}$in tert-butanol.

4.1.3.4 Magnetic Measurements

The measurement of the magnetic susceptibility of the iron compound was carried out at room temperature. The complex is diamagnetic with a value of the effective magnetic moment μ_{eff} = 0 BM (Table 1).

4.1.3.5 Chemical kinetics

The study of the oxidative dehydrogenation for the reaction between the compound [Fe (DMSO)$_6$](NO$_3$)$_3$ and L$_2$·3HCl is monitored by the Uv-vis spectrophotometric in a range 300 to 500 nm during 36000 s. The spectrum shows a signal at 343.5 nm which was used to control the progress of the reaction (Fig. 36a).
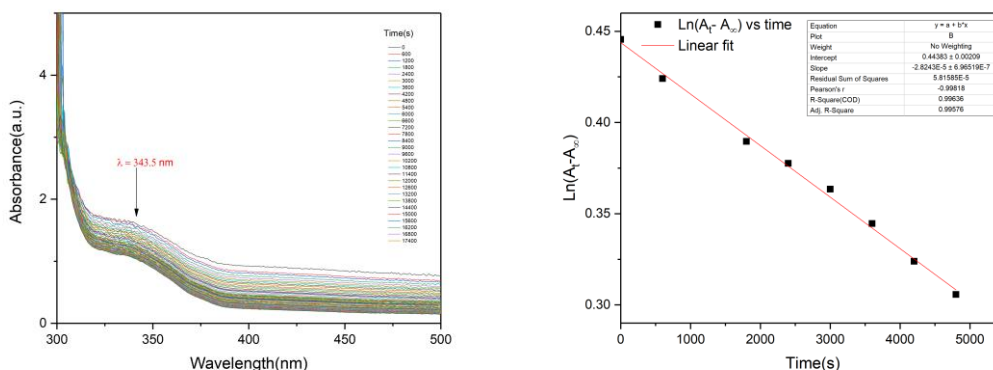
Figure 36. a) Uv-vis spectrum absorbance vs wavelength and b) Linear fit of the Ln ($A_t - A_\infty$) vs time plot the first order kinetic between [Fe(DMSO)$_6$](NO$_3$)$_3$ and L$_2$·3HCl.

The linear regression presented in Fig. 36b is adjusted to a first order equation (v = k[A]), according to the value R = 0.9964. The behavior of the chemical reaction was treated as first order reaction obtaining a value of the rate constant (k) of $2.824 \times 10^{-5}\,\text{s}^{-1}$.

4.1.3.6 Analysis of results. - The synthesized compound is diamagnetic with a magnetic moment being zero. This reflects that there is a change in the oxidation state of the metal ion from 3+ to 2+ because the metal in [Fe(DMSO)$_6$]$^{3+}$ started with Fe(III) and during the reaction ends in Fe(II). This could be clearly verified in the characterization of the complex in the Uv-vis liquid absorption spectrum and in the IR spectrum. In the case of the Uv-vis spectrum it was shown that the compound has absorption bands of a d^6 specie LS, while in the case of the IR spectrum we see an imine signal resulting from the oxidation of the ligand and consequently the reduction of the metal ion. On the other hand, in the kinetic study the reaction between L$_6$ and iron(II) follows a reaction of the first order. To conclude, these results tell us that an oxidative dehydrogenation reaction between the ligand and the metal ion was carried out with a reaction rate of the iron complex of $2.824 \times 10^{-5}\,\text{s}^{-1}$. In the Fig. 37,

there is a proposed the synthetic route of the iron complex [Fe(II)L$_6$]$^{2+}$.
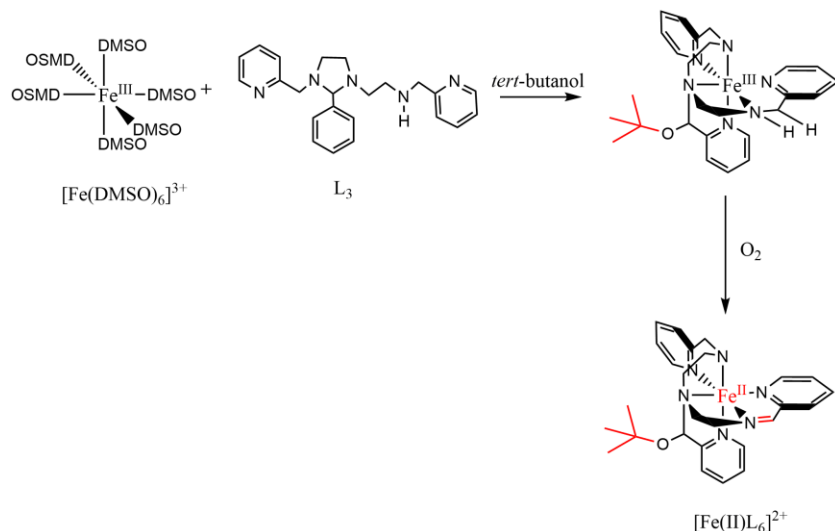
Figure 37. Formation reaction of [Fe(II)L$_6$]$^{2+}$ in air (O$_2$).

4.1.4 Synthesis and characterization of the nickel complex in tert-butanol

4.1.4.1 [Ni(II)L$_6$]$^{2+}$. - This nickel complex is a violet crystalline solid. No more data could be found because the precipitate fails to form a stable solid and re-dissolves in the same solution. Despite this adverse situation, a small crystal was obtained. The proposed formula would be [Ni(C$_{26}$N$_6$H$_{34}$O)]Cl$_2$ (Fig. 38).
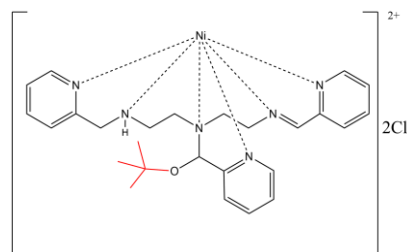
Figure 38. Proposal for the structure of the nickel complex.

4.1.4.2 Main IR characteristics of [Ni(II)L$_6$]$^{2+}$

In Fig. 39, the IR spectrum of the nickel compound there is a signal at 3255 cm^{-1} of the coordinated N-H bond and a signal at 1610 cm^{-1} is vibrational mode of C=N pyridine. The last signal at 1400 cm^{-1} would be of the pyridine rings. This spectrum belongs to the solution of crystal obtained in the reaction and shows coincidence with the spectral signals of the complex model. This means that the ligand was coordinated with the metal.
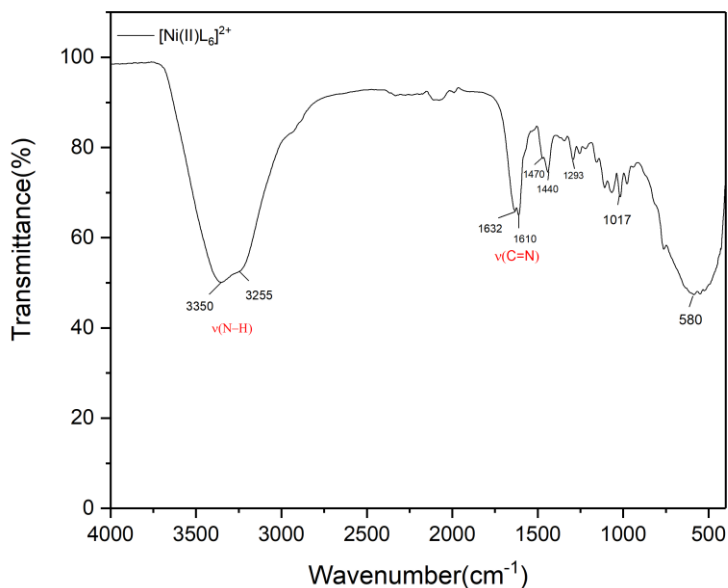
Figure 39. IR Spectra of [Ni(II)L₆]²⁺.

4.1.4.3 Electron absorption spectroscopy

For the Uv-vis spectrum (Fig. 40) of the complex dissolved in methanol shows electronic transition bands corresponding to a d^8 LS. In the spectrum there are signals at 542 and 893 nm and their electronic transition is $^3T_{1g} \leftarrow {}^3A_{2g}$ and $^3T_{2g} \leftarrow {}^3A_{2g}$ (Annex 3), respectively. However, for an element d^8 exists three signals in the spectrum. This is due to the high concentration of the complex in the solution prevents see the third signal which is possibly masked with the charge transition signals. In addition, the ligand that surrounds the metal is strong field according to spectroscopic series. This indicates that the complex is octahedral with LS.[50,53]
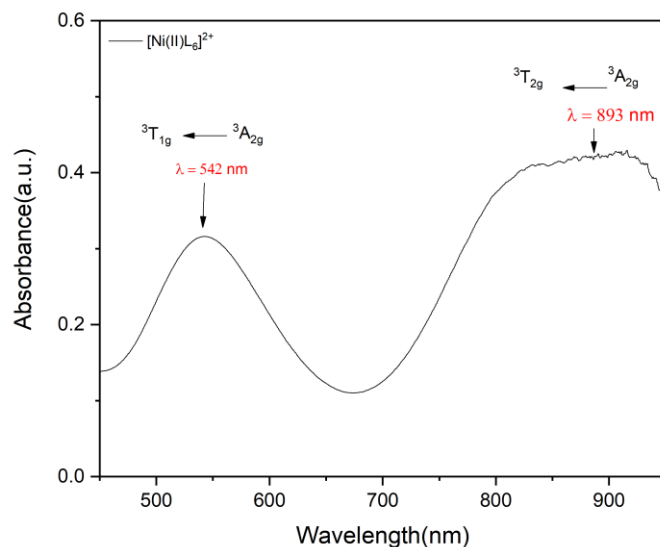
Figure 40. Uv-vis spectra of [Ni(II)L$_6$]$^{2+}$ absorbance (liquid).

4.1.4.4 Observations. - In this case, the anhydrous nickel chloride and an extra equivalent of aldehyde were used since in previous cases nickel chloride hexahydrate was used and no precipitate was obtained. With these changes a violet crystal was obtained. In addition, during the evaporation of the solvent, certain precipitates were produced which after a while re-dissolved. This is because the compound is unstable in the solid state. The Uv-vis spectrum shows the presence of an octahedral compound in the solution while the IR spectrum is not clear but the coordinated N-H signal and the presence of the bonds of the N=C double bonds of the pyridine rings appear.

The next subsection is the results and the analysis of the characterization of the nickel compound when in the synthesis process was made changes to increase its performance.

4.1.5 Characterization of the nickel complex in tert-butanol (synthesis performance improvement)

4.1.5.1 [Ni(II)L$_6$]$^{2+}$. - The nickel complex is a violet solid that is soluble in methanol, acetonitrile, DMSO, and water and insoluble in nonpolar solvents. The complex has a color change at 290 °C and melted at 338 °C. The yield of the synthesis product is 51.65% (Table 2) and the formula of the metal complex would be the following: [Ni(C$_{26}$N$_6$H$_{34}$O)]Cl$_2$ (Fig. 38).

4.1.5.2 Main IR characteristics of $[Ni(II)L_6]^{2+}$

All-important signals of the IR spectrum of the nickel compound are found in Fig. 41. A signal at 3235 cm^{-1} corresponds to the vibrational signal of coordinated N-H. There are signals at 2911 cm^{-1} and 3067 cm^{-1} vibrational bands of aliphatic compounds and aromatic rings respectively. Some signals or overtones at a region of 2000-1667 cm^{-1} show vibrational modes of a ring mono-substituted. A signal of weak intensity at 1654 cm^{-1} belongs to vibrational modes of imine while a signal at 1604 cm^{-1} is the vibrational band of pyridines. Another important signals at 1541, 1477 and 1440 cm^{-1} are vibrational modes to pyridine ring. The 859 and 760 cm^{-1} signal belongs to the pyridine substitution bands. The signal at 1082 cm^{-1} represents to an vibrational band of ether group because it is in the range of the ether groups 1300-1000 cm^{-1} according to the literature.[51,54] To conclude, these signals coincide with spectrum signals IR of the model compound and confirm that the ligand coordinated to the metal.
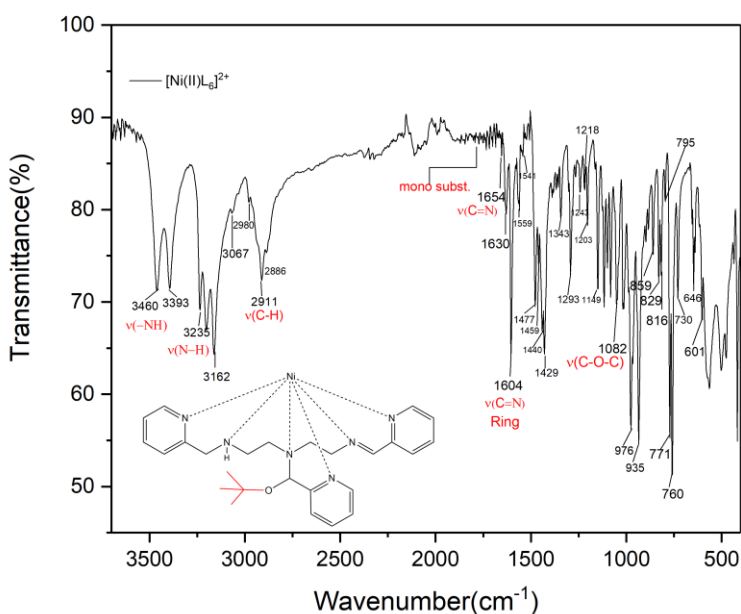
Figure 41. IR spectra of $[Ni(II)L_6]^{2+}$.

4.1.5.3 Electron absorption spectroscopy

In the Uv-vis reflectance spectrum of the nickel compound (Fig. 42a) there are three important signals: 339, 549 and 850 cm^{-1} with their respective electronic transitions $^3T_{1g}$ (^3P)

$\leftarrow$ $^3A_{2g}$, $^3T_{1g} \leftarrow$ $^3A_{2g}$ and $^3T_{2g} \leftarrow$ $^3A_{2g}$ (Annex 3). Those signals describe the behavior of a weak field high spin d^8. In this case it is a nickel complex of octahedral geometry. On the other hand, in the Uv-vis spectrum of the nickel complex dissolved in methanol shows two signals at 546 and 870 cm^{-1} (Fig. 42b) with their respective electronic transitions $^3T_{1g} \leftarrow$ $^3A_{2g}$ and $^3T_{2g} \leftarrow$ $^3A_{2g}$, respectively.[50] In this sense, in a Uv-vis spectral analysis of the compound $NiCl_2 \cdot 6H_2O$ dissolved in water result in $[Ni(H_2O)_6]^{2+}$, Dolores[55] mentions that the complex is a d^8 species HS with an octahedral geometry because the spectrum presents three signals, one in the infrared (no visible), at 722 nm and other in range 350-500 nm with the following electronic transitions: $^3T_{2g} \leftarrow$ $^3A_{2g}$, $^3T_{1g}$ (F) $\leftarrow$ $^3A_{2g}$ and $^3T_{1g}$ (P) $\leftarrow$ $^3A_{2g}$. That spectral signals of the synthesized complex was compared with the compound dissolved in water (reference[56]), in both cases there are three signals but they differ in the absorption signals. It means that the metallic center changed of ligands but no changed of oxidation state. According to the spectrum showed for the nickel complex synthesized has almost the same signals reported in the literature[57] with the following signals 355, 545 and 881nm. Then, the nickel (II) complex synthesized is a high-spin d^8 with a distorted octahedral geometry.
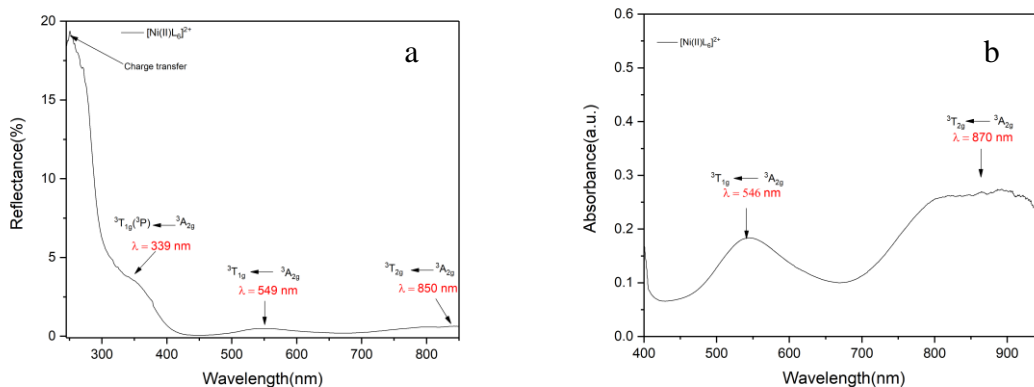
Figure 42. Uv-vis spectra of [Ni(II)L₆]²⁺ a) reflectance (solid).b) absorbance (liquid).

4.1.5.4 Magnetic Measurements

The magnetic susceptibility measurement for the nickel complex was performed at room temperature. The nickel complex is paramagnetic with a magnetic moment of $\mu_{eff} = 2.95$ BM (Table 1). According to the literature[58], this result is in the range of 2.9-3.3 BM which is characteristic for octahedral nickel(II) complexes.

4.1.5.5 Chemical kinetics

The chemical kinetics of the reaction of nickel chloride and L$_2$·3HCl in tert-butanol in equimolar amounts was measured in a Uv-vis spectrophotometer. The reaction progress was tracked at 260.5 nm in a range of 200-500 nm. The reaction time was 20400 seconds at room temperature (Fig. 43a).
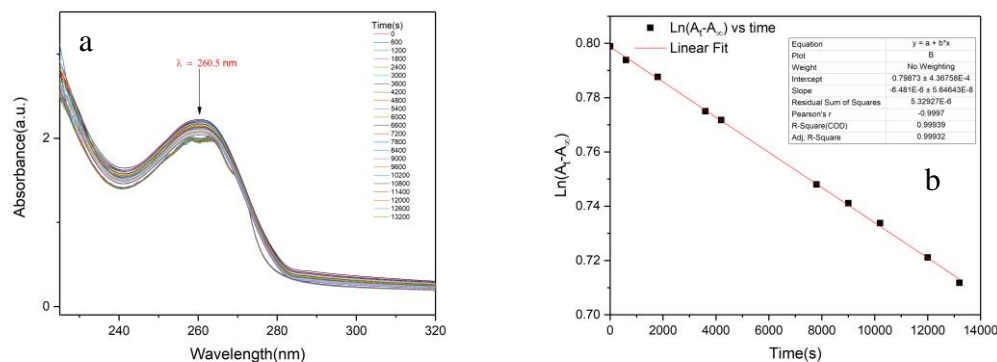
Figure 43. a) Uv-vis spectrum absorbance vs wavelength and b) Plot of Ln (A$_t$-A$_\infty$) vs time for the reaction [Ni(II)L$_6$]$^{2+}$at maxim absorbance at 260.5 nm.

To know the order of the reaction, below we have a graph that describes the linear regression between absorbance vs. time. According to the behavior of linear regression, the first order equation (v = k[A]) is the one that fits the data extracted from the Uv-vis spectrum. The reaction constant (k) is 6.4801x10-6 s^{-1} (Fig. 43b).

4.1.5.6 Analysis of results. - The nickel complex is a violet paramagnetic solid with a magnetic moment (μ_{eff}) 2.95 BM, which is characteristic for octahedral complex of nickel (II). It was also found in the diffuse reflectance Uv-vis spectrum and Uv-vis spectrum of complex dissolved in methanol with electronic transitions of an octahedral d^8 complex HS, which confirms that we have a complex of Ni(II). However, in the IR spectrum there is a weak signal at 1654 cm^{-1} corresponding to the vibration of the imines. This small signal suggest that there was oxidation of the ligand when it coordinated with the metal, but the change in the oxidation state of the metal was not observed. To clear up this doubt in Fig. 44, there is a proposal for reaction pathway to explain the formation of the double bond and the oxidation state of the metal ion 2+. From **step 1** to **2** the base extracts the more acidic hydrogen that is bound to the nitrogen of the complex then one of the free electrons attacks the metal ion reducing it from Ni^{2+} to Ni$^+$. From **step 2** to **3** the oxygen oxidizes the metal

ion (Ni^+ to Ni^{2+}) and a proton remains on the nitrogen. From **step 3** to **4**, as the radical on the nitrogen is unstable, it attacks the metal ion reducing it from Ni^{2+} to Ni^+ while the nitrogen remains defective in protons, another base takes the hydrogen and allows the formation of the double bond. From **step 4** to **5** again the oxygen attacks the metal ion oxidizing it from Ni^+ to Ni^{2+}. This metal oxidation step happens because the redox potential of Ni^+ must be less than the redox potential of oxygen. If we compare this with the iron model compound we can see that it ends with Fe^{2+} this is because the redox potential of Fe^{2+} in that complex is higher than the oxygen redox potential.[1] Also, In the case of the kinetic study of the reaction, the spectral result of the nickel complex shows that the reaction order is first order with a rate constant of 6.5055×10^{-6} s^{-1}, which is lower than the reaction rate of the complex of iron.
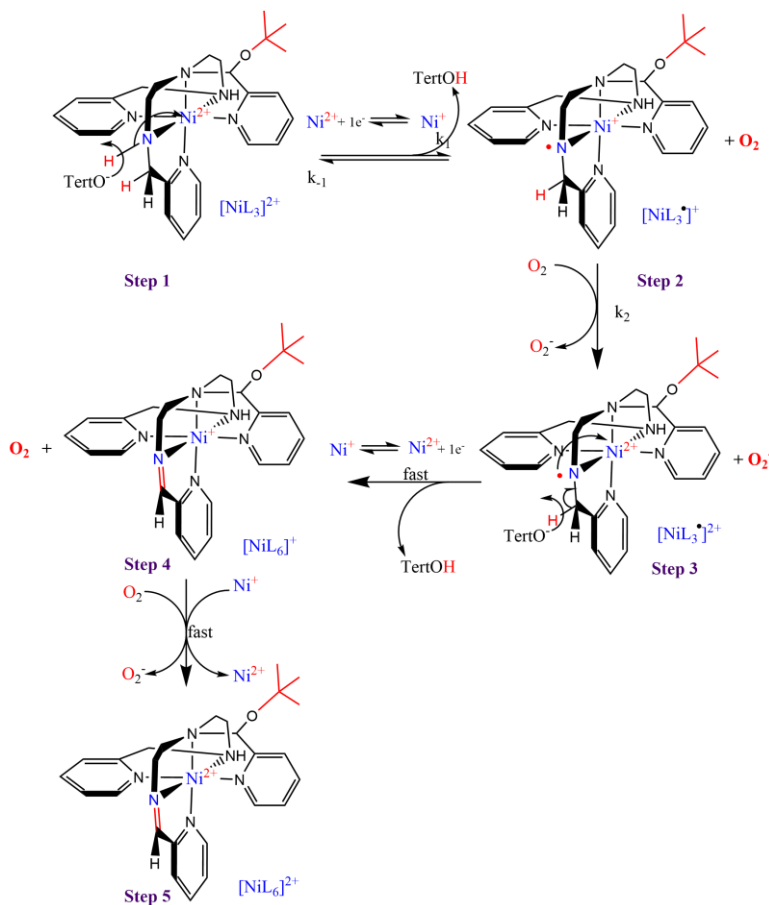
Figure 44. Proposal for an OD reaction mechanism of the Nickel(II) complex.

4.1.7 Synthesis and characterization of the copper complex in tert-butanol

4.1.7.1 $[Cu(II)L_6]^{2+}$. - The copper complex is blue at the moment we have the product final with solvent and the evaporation of the solvent is slow. However, we managed to perform some characterizations on the solid compound.

4.1.7.2 Main IR characteristics of $[Cu(II)L_6]^{2+}$

From the analysis of the IR spectrum of the blue solid, a signal at 3490 cm^{-1} assigned to the N-H coordinate vibrational band and a signal at 3317 cm^{-1} shows the stretching vibration of OH group. That signal of OH appears in the spectrum because the copper complex was not completely dry. The signals at 3020 and 2967 cm^{-1} are characteristic vibrational bands of the aromatic and aliphatic groups, respectively. The vibrational modes in range 2000-1667 cm^{-1} represent the overtones of the aromatic compounds in the mono substitution. A weak signal at 1654 cm^{-1} belongs to vibrational modes of imine (C=N) and the next signal at 1606 cm^{-1} are characteristic bands of pyridines. The 1571, 1474 cm^{-1} signals are the C=C signals of pyridines. The signal at 1345 cm^{-1} represents the vibrational folding bands of the CH$_3$ and CH$_2$ groups. The signal at 838 and 771 cm^{-1} are the mono substitution patterns on the aromatic rings of pyridine. At 1075 cm^{-1}, the signal of an ether since it is in the range of 1300-1000 cm^{-1} reported in the literature (Fig. 45).[51,59]
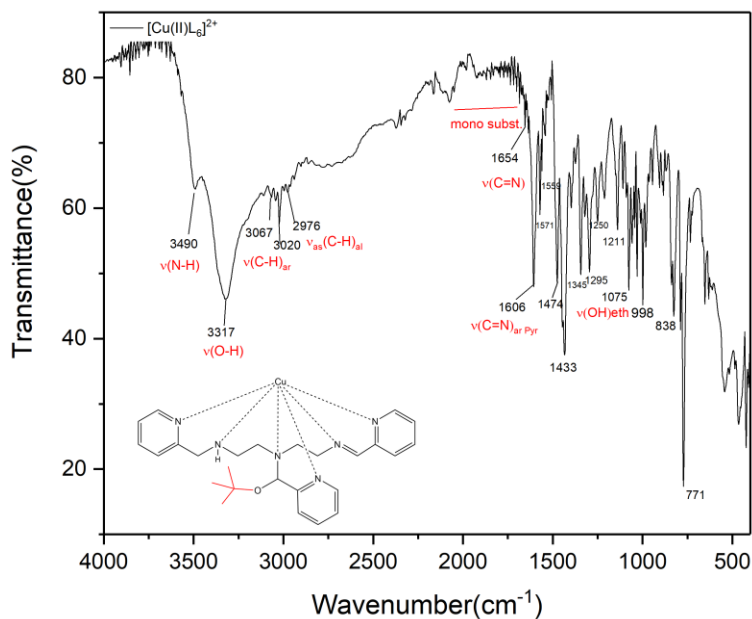
Figure 45. IR spectra of [Cu(II)L₆]²⁺.

4.1.7.3 Electron absorption spectroscopy

The Uv-vis absorption electron spectrum dissolved in DMSO (Fig. 46a) shows absorption bands for the electron transition in the region expected for a low spin d^9. In this case, there are two signals, one at 485 cm^{-1} ($^2E_g \leftarrow {}^2B_{1g}$)[47] and the other at 675 cm^{-1} ($^2B_{2g} \leftarrow {}^2B_{1g}$). The signal is wide in a range of 600-900 cm^{-1} and presents a distortion at 845 cm^{-1}, such distortion is assigned to Janh Teller effect that commonly occurs in octahedral complexes. On the other hand, in Fig. 46b the Uv-vis spectrum of CuCl$_2$ dissolved shows a signal at 816 nm, which is in the absorption range (600-900 nm) for d^9 species octahedral with an electronic transition of $^2T_{2g} \leftarrow {}^2E_g$. According to the spectral characteristics previously described on the copper complex, which coincides with the literature and the raw material. This make sure that the synthesized complex is octahedral LS.[53]
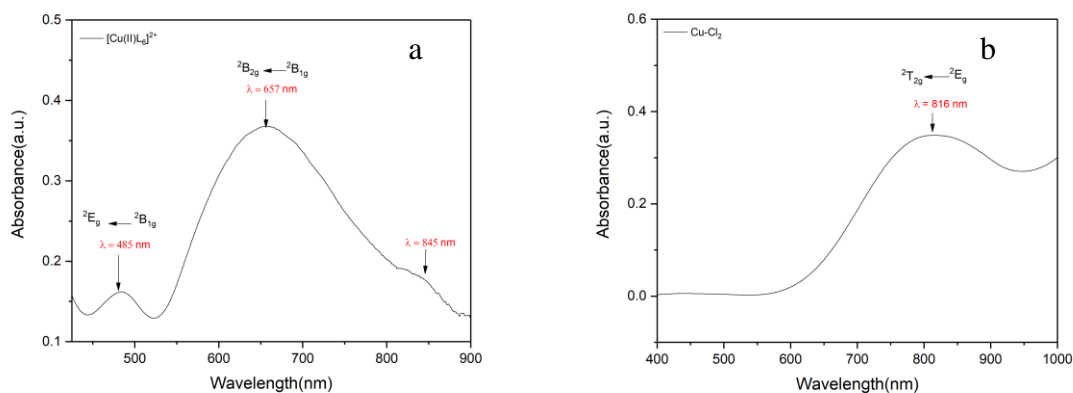
Figure 46. Uv-vis spectra of a) [Cu(II)L₆]²⁺ in DMSO absorbance and b) CuCl₂ dissolve in water.

4.1.7.4 Chemical kinetics

The chemical reaction between $CuCl_2$ with $L_2 \cdot 3HCl$ was performed in stoichiometric quantities and the monitoring of the chemical reaction by means of the Uv-vis spectrophotometer was in a range of 300-500 nm. In the spectrum there are two important signals, the first close to 300 nm represents the charge transfer and at 345.5 nm describes the progress of the reaction (Fig. 47a).
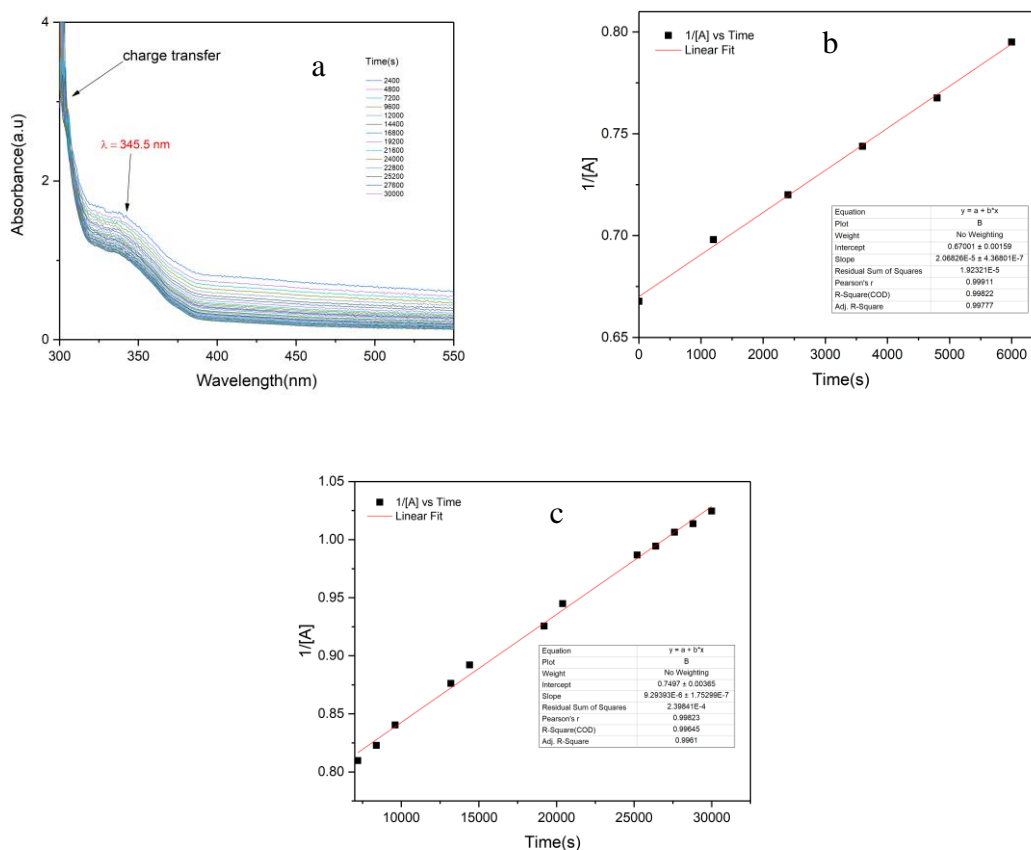
Figure 47. a) Uv-vis spectrum absorbance vs wavelength, b) Plot of 1/[A] vs time for the initial reaction and b) Plot of 1/[A] vs time for the final reaction.

The chemical kinetics of the copper complex is described by the second order equation ($v = k[A]^2$) and allows proposing that the reaction occurred in two steps: in the first step, the coordination between the ligand and the metal occurred with a rate constant (k_1) of $2.068 \times 10^{-5}\,M^{-1}s^{-1}$ (Fig. 47b, 48) while in the second step there is a redox reaction with the oxidation of the amine ligand ($-2e^-$, $-2H^+$) and the reduction of the metal (Cu) with a rate constant (k_2) of $9.29 \times 10^{-6}\,M^{-1}s^{-1}$ (Fig. 47c, 48).
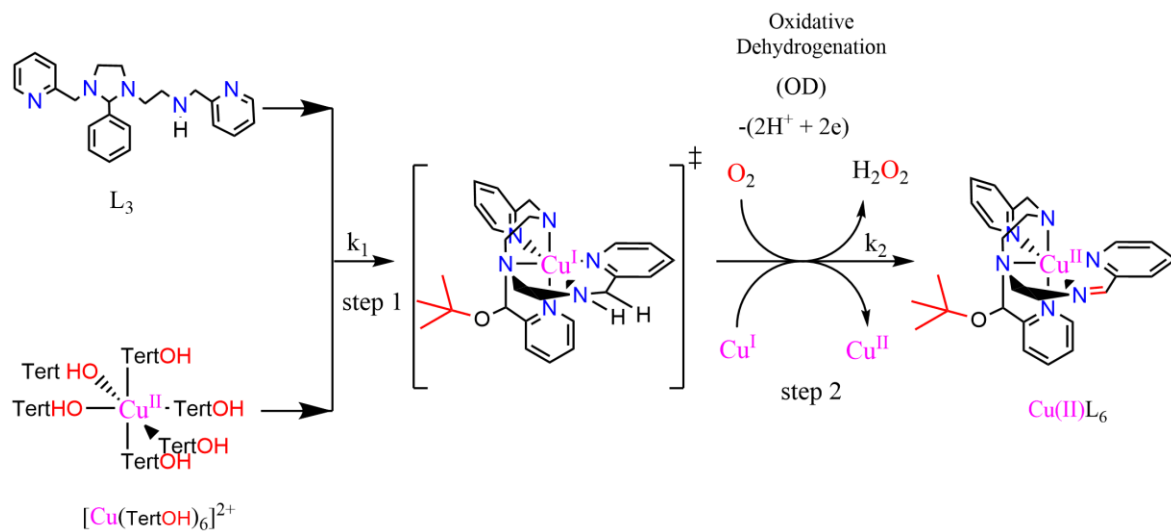
Figure 48. Scheme of formation of the copper complex in two reaction steps. Step 1 coordination of ligand and metal, step 2 redox reaction.

4.1.7.5 Analysis of results. - In the synthesis of the copper complex the formation of the precipitate takes a week while the evaporation of the solvent is slow. So, a small sample was used for characterization in IR and Uv-vis. In the kinetic study of the copper complex, it shows that the reaction has a two-step reaction path. The first step is the coordination and the second step is the redox reaction between the metal and the ligand. Where $k_2 < k_1$ and whose value shows that the redox reaction step is the determining step of the reaction because it is low. On the other hand, despite the conditions mentioned above, it was possible to measure the Uv-vis in liquid that shows an electronic transition characteristic of octahedral complexes d^9 while in the IR spectrum there are a weak signal at 1654 cm^{-1} correspond to vibrational mode of the imine group. Both results do not coincide since in the Uv-vis spectrum shows that there is no change in the oxidation state of the metal but in the IR spectrum shows the formation of a double bond (C=N), which is the result by a change in the oxidation state of the metal. To clarify this doubt two reaction steps is not enough to explain the reaction mechanism of the copper complex, so in Fig. 49 a reaction path for the formation of the double bond and the oxidation of the metal is proposed. From **step 1** to **2** the base traps the more acidic hydrogen and leaves a highly reactive electron that attacks the metal center of the complex and reduces it from Cu^{2+} to Cu^+. From **step 2** to **3** the oxygen oxidizes the metal ion going from Cu^+ to Cu^{2+} and the radical remains on the nitrogen. From **step 3** to **4** the highly reactive radical attacks the metal and reduces it from Cu^{2+} to Cu^+

47

meanwhile another base removes another hydrogen from the ligand and allows the formation of the double bond (C=N). From **step 4** to **5** again the oxygen attacks the metal to oxidize it from Cu^+ to Cu^{2+}. This happens because the redox potential must be less than the oxygen redox potential, this happens to complex of iron (II).[1] Another explanation that strength this criteria is that the complex of copper(I) in an atmosphere without oxygen there is not reaction while the complex in air copper is easily oxidized by the oxygen of the air to copper(II), so it promotes the formation of double bond (C=N).[60] This reaction is known as oxidative dehydrogenation reaction.
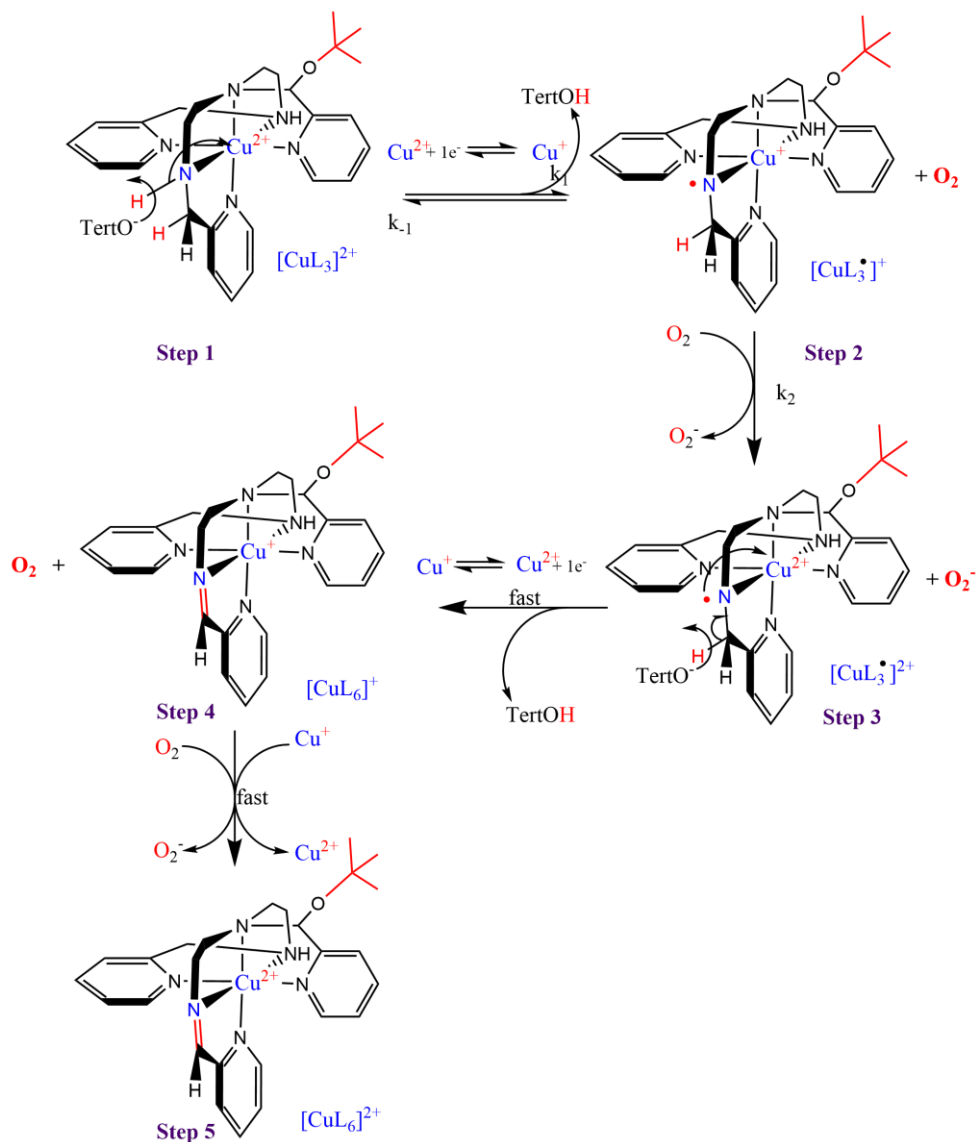
Figure 49. Proposal for an OD reaction mechanism of the Copper(II) complex.

4.2 SYNTHESIS AND CHARACTERIZATION OF HMTA WITH COPPER AND NICKEL

4.2.1 Main IR characteristics of raw materials for copper

4.2.1.1 Main IR characteristics of HMTA

In this section the HMTA ligand is discussed. The coordination between HMTA metal salts can be form several complexes and represent important applications in the medicine, military and others. This heterocyclic compound has a chair configuration and can form a mono, bi, tri, or tetra dentate ligand. The HMTA configuration allows it to bind different metal ions.[61] In some cases it can be act as a multiple function ligand due to its N atoms interact with ionic metals of the transition metals and form coordination complexes. However, this interaction can be a bridging and no act as an agent chelating. For instances, with thiocyanate ligands it has been reported that only mono and bidentate complexes are formed. This is attributed to HMTA trying to maintain its chair configuration by forming an uncoordinated ligand.[62]

For the IR spectrum of HMTA there are bands mainly between 400 to 1600 cm^{-1} and 2870 to 2940 cm^{-1}. Thus, the signals at 2870, 2920 and 2941 cm^{-1} belong to stretching vibrations of the CH group while signals at 1455 and 1367 cm^{-1} are vibrational bands symmetric and asymmetric of CH group. At 806 cm^{-1} there is vibrational stretching of the CH group, while the signal at 1231 cm^{-1} is characteristic of the CN group (Fig. 50).[63]
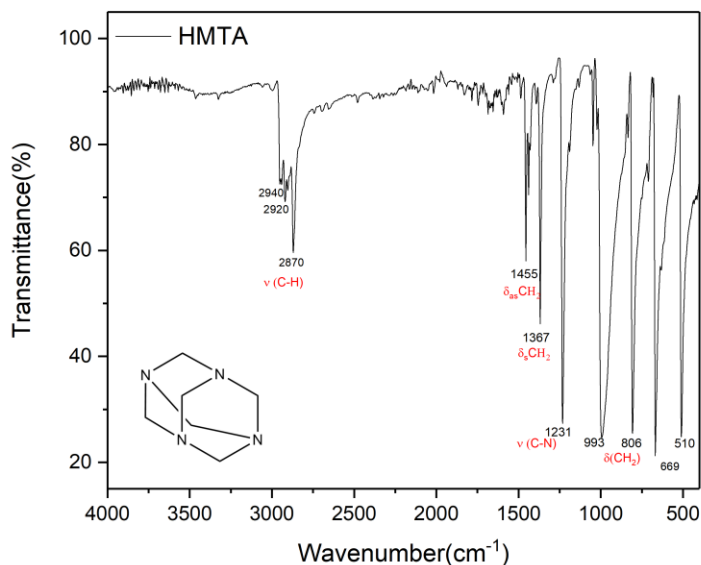
Figure 50. IR spectra of HMTA.

4.2.1.2 Main IR characteristics of $CuSO_4 \cdot 5H_2O$

The sulfate ion has a tetrahedral symmetry (T_d) and presents nine vibrational modes corresponding to Ramman spectroscopy, however the F_2 vibrational modes belong to the active infrared. The vibrational modes are represented by symmetric stretching ν_1 (A_1). The vibrational bending modes are assigned to ν_2 (E) and ν_4 (F_2). The vibrational antisymmetric stretch modes is represented by ν_3 (F_2) (Fig. 51). The characteristic ranges for the vibrational modes are ν_2 around 449 cm^{-1}, ν_4 corresponds between 610-650 cm^{-1}, ν_1 is in a wavelength range of 970-995 cm^{-1} and ν_3 is between 1100-1160 cm^{-1}.[64]
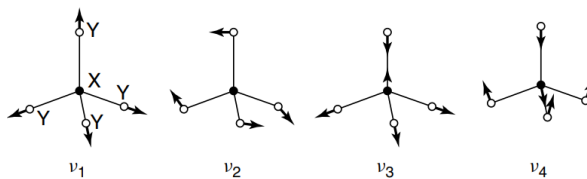
Figure 51. Vibrational modes of a tetrahedral molecule. [65]

The compound copper sulfate pentahydrate as a raw material shows significant signals in the IR spectrum. The signals above at 3000 cm^{-1} explain the presence of water in the crystalline structure of the compound, so the signal is at 3099 cm^{-1}. This represents the stretching vibration of the O-H group while at 1664 cm^{-1} there is a vibrational bending mode of O-H.

On the other hand, at 1062 cm^{-1} there is a vibrational stretching of the S-O group and 432 cm^{-1}, there is the vibrational bending of the S-O group. Finally, at 862 cm^{-1} exists the vibrational modes of the metal ion Cu-OH (Fig. 52).
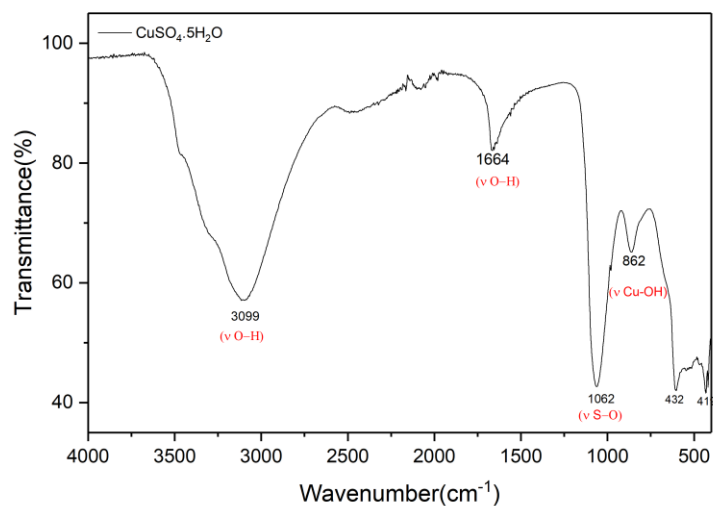
Figure 52. IR spectra of pure copper sulphate pentahydrate.

4.2.1.3 Electron absorption spectroscopy

The starting reagent (CuSO$_4$·5H$_2$O) has a broad signal at 814 nm. In this sense, an octahedral copper (II) complex is a d^9 species with a broad absorption band in the range of 900-600 nm and according to Tanabe Sugano's diagram (Annex 4), a d^9 species has an electronic transition of $^2T_{2g} \leftarrow {}^2E_g$. When comparing both spectra and they coincide. So the complex is an octahedral species d^9 (Fig. 53).
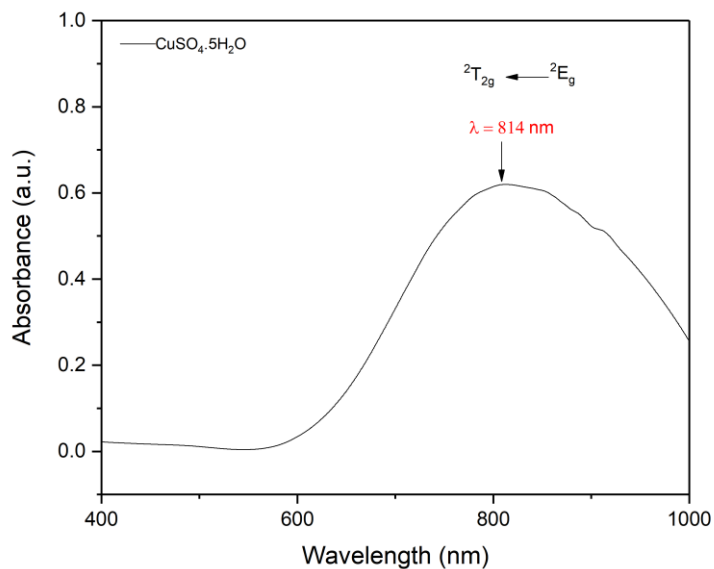
Figure 53. Uv-vis spectrum of the compound CuSO₄·5H2O.

4.2.2 Synthesis and characterization of Cu(II)-HMTA

4.2.2.1 Cu(II)-HMTA. - The color of the complex is green while HMTA and copper sulfate pentahydrate are white and blue, respectively (Table 2). This color difference between the complex and the starting reagents indicates that the reaction between the reagents produced another compound. The synthesized complex has a melting point of 230 °C, which is different from the starting reagents HMTA 280 °C and copper sulfate pentahydrate 110 °C (Table 2). The complex is soluble in water, poorly soluble in methanol, insoluble in DMSO, ethanol, and nonpolar solvents. The yield of the reaction is 91.5%. According to the results obtained in section 4.2.2.2, 4.2.2.3 and 4.2.2.5 there is a suggestion in chemical formula and structure: $[Cu(C_6H_{12}N_4)(H_2O)(EtOH)_2]SO_4$ (Fig. 54).
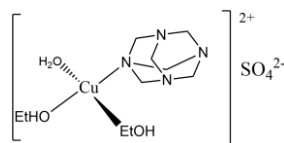
Figure 54. Proposal of chemical structure of the copper(II) complex.

4.2.2.2 Main IR characteristics of Cu-HMTA

Based on the data from the literature (See section 4.2.1.2), the synthesized compound presents peculiar characteristics about the vibrational modes v_3 and v_4 related to the SO_4^{2-}

ion. Signal ν_3 appears at 1058 cm^{-1} of the synthesized compound. Which decreases in intensity compared to the IR spectrum of copper sulfate pentahydrate 1060 cm^{-1}. The ν_4 signal is at 650 cm^{-1}in the synthesized compound while the literature mentions that at 610-650 cm^{-1} belong to sulfate ion. These vibrational modes (ν_3, ν_4) demonstrate the presence of the sulfate ion outside the coordination sphere of the synthesized compound (Fig. 55).

The characteristic broad signal at 3391-3600 cm^{-1} is vibrational mode symmetric and asymmetric of OH group. Where there is a signal at 3500-3700 cm^{-1} of overlap in a single broad. However, in the synthesized compound, these signals are observed at a low frequency. This is due to an interaction of the metal with the oxygen molecules producing very weak signals.

In the spectrum of the complex there is a band at 1653 cm^{-1} belonging to the vibrational mode of stretching of the water molecules. This signal is weak and shifted at the shorter wavelength compared to 1664 cm^{-1} for copper sulfate because there are no strong hydrogen bonding interactions with the sulfate ion molecules and HMTA. The complex has weak vibrational bands at 682, 693 and 732 cm^{-1}. Whose values are representative for the interaction between the metal and the water molecule ν(M-OH$_2$).[66]

The HMTA molecule presents characteristic C-N signals in bands 511, 672, 1009, 1238 cm^{-1}, which to confirm Cu-N(HMTA) is coordinated. The interactions of HMTA with the metal generate changes in the symmetry of HMTA that goes from T$_d$ to C$_{3v}$ or C$_{2v}$ (Fig. 50).[66]

So the main bands of 1009 cm^{-1} →1015 + 1000 + 995 + 975 + 970 cm^{-1}; 1238 cm^{-1} →1255 + 1248 + 1235 + 1215 + 1205 cm^{-1}. The main vibrations for the C$_{3v}$ symmetry of the C-N bond are found in the 1255 cm^{-1}, 1205 cm^{-1}, 1015 cm^{-1}, 975 cm^{-1} bands.[66] These peaks are closely similar to the peaks (1259 cm^{-1}, 1200 cm^{-1}, 1017 cm^{-1}, 982 cm^{-1}) of the synthesized compound. The lack of accuracy between the peaks in the literature and synthesized compound is due to the fact that the molecule is composed of other atoms and the experimental conditions of synthesis (Fig. 55).
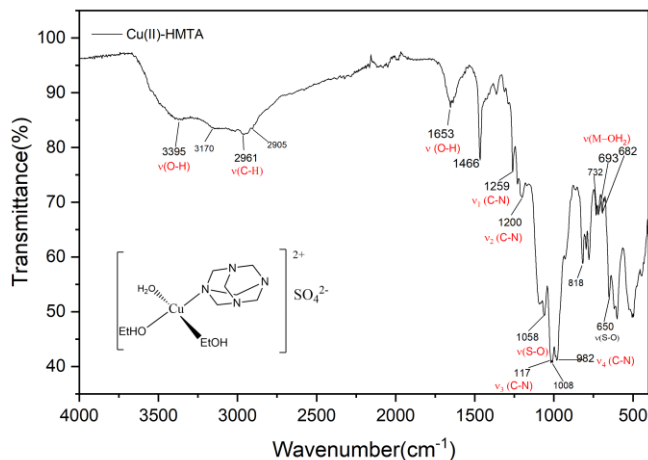
Figure 55. IR spectra of synthesis HMTA with $CuSO_4.5H_2O$.

4.2.2.3 Electron absorption spectroscopy

In the Uv-vis spectrum of reflectance diffuse (Fig. 56) of the synthesized product shows a maximum absorption band at 540 nm (Table 4) while the signal Uv-vis of the copper salt (reagent reference) is at 814 nm (Fig. 53). This means that the Cu^{2+} suffered a change in geometry or oxidation state. In this case, the literature mentions that: a copper compound can be octahedral or tetrahedral under a signal between 600-900 nm and for copper complexes with a square plane geometry the absorption range is 500-600 nm. In addition, the octahedral and tetrahedral copper complexes present distortions on the bands known as the Jhan Teller effect.[53] Therefore the synthesized complex is a d^9 of square plane geometry with an electronic transition $^2T_2 \leftarrow {}^2E$ (Annex 4).
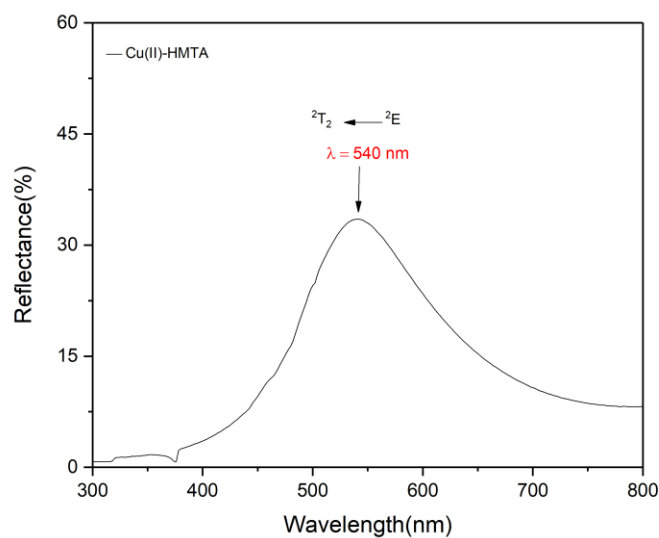
Figure 56. Uv-vis spectrum of Cu(II)-HMTA.

4.2.2.4 Changes of pH in synthesis of HMTA with Cu(II)

4.2.2.4.1 Main IR characteristics

In the IR spectrum (Fig. 57) shows the influence of pH on the synthesis of the copper complex. All the signals described in section 4.2.2.2 remain in the same absorption bands but a signal at 2115 cm^{-1} appears a new signal corresponding to the vibrational modes of a triple bond characteristic of nitriles. On the other hand, all absorption bands decrease with the increase in the concentration of OH$^-$ ions in the solution. Therefore, the increase in pH allows the formation of new bonds.
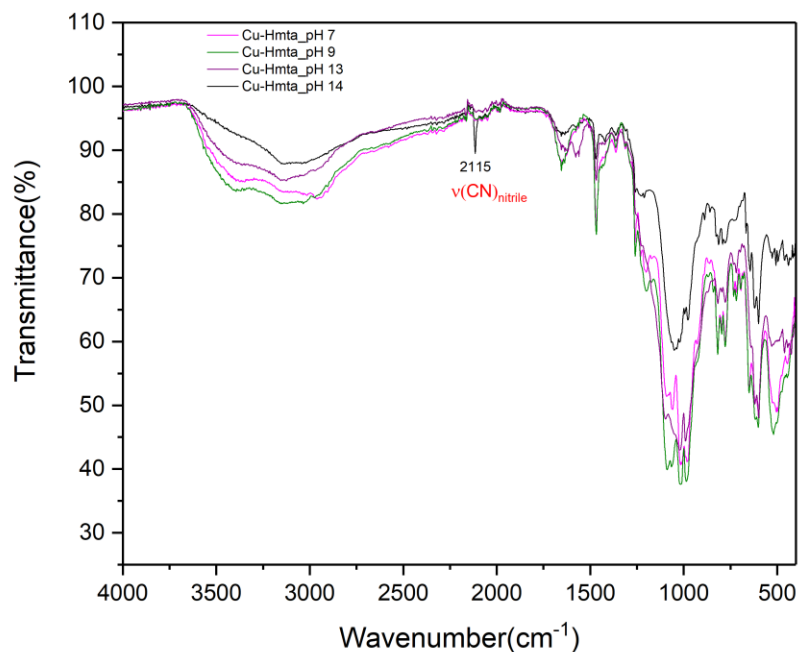
Figure 57. IR spectrum of the copper compound synthesized at different pH levels.

4.2.2.4.2 Electron absorption spectroscopy

As mentioned before, the amounts used to increase the pH of the sodium ethoxide solution were 0.032 g, 0.065 g, 0.08 g and > 0.08 g for pH 9, 13, 14 and > 14 respectively. The spectrum obtained is shown in the Fig. 58. The band observed is due to the complex formed with the metal ion Cu^{2+} and the respective ligands. The spectrum shows the formation of a square-plane structure around the metal ion, hypothetically, it would have 3 molecules of water and one of HMTA. Taking into account that the compound is a d^9 we could say that the complex has an electronic transition $^2T_2 \leftarrow {}^2E$. In the Fig. 58 the spectral signals increase until the concentration reaches pH 13 from here the spectral signals decrease drastically for pH 14 and pH > 14 with variations of 2 to 4 nm in the absorption bands. Finally, changes in the oxidation state of the metal or in the geometry of the compound are not visible, but at pH levels > 14 the metal ion disappears, that is, the OH^- concentration is so strong that it decomposes the metal complex of copper.
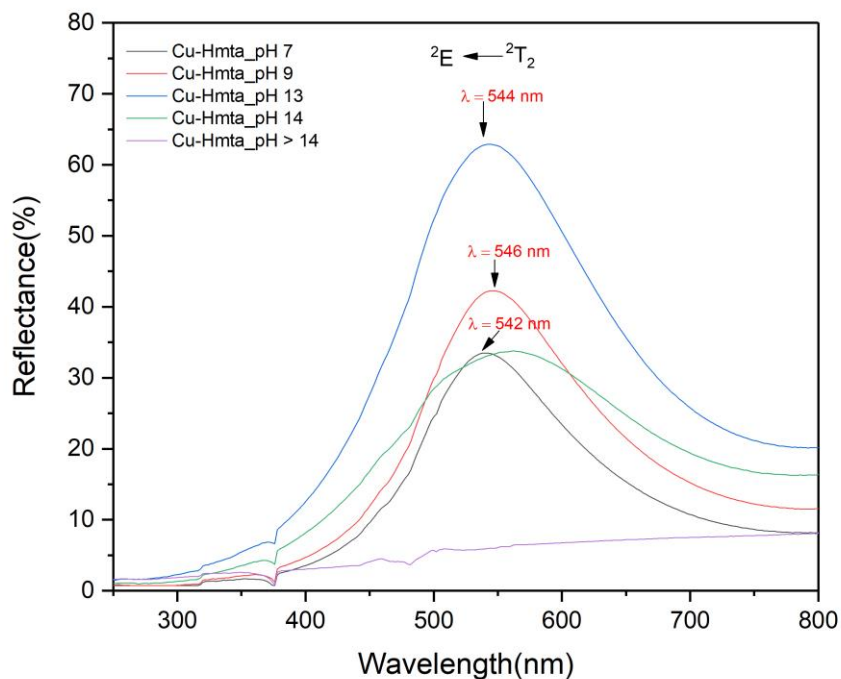
Figure 58. Uv-vis spectrum of the synthesized copper complex at different pH values.

4.2.2.5 Magnetic Measurements

The measurement of the magnetic susceptibility was made a room temperature and the synthesized complexes are paramagnetic with a value of the effective magnetic moment (μ_{eff}) of 2.169, 1.847, 2.141, 1.309 BM for pH 7, 9, 13, 14, respectively (Table 1). The magnetic properties of the complexes vary at each pH value but remain in the range of the μ_{eff} values reported in the literature.[67]

4.2.2.6 Chemical kinetics

The chemical kinetics the dissolution in ethanol in equimolar amounts between copper sulfate pentahydrate and HMTA was followed by Uv-vis spectrophotometry in a range of 200-550 nm for 29400 seconds (Fig. 59a). The spectrum shows two peaks: one at 200 nm corresponding to charge transfer and the other at 284 nm assigned to the progress of the reaction. Also, the isosbestic point was found at 324 nm.
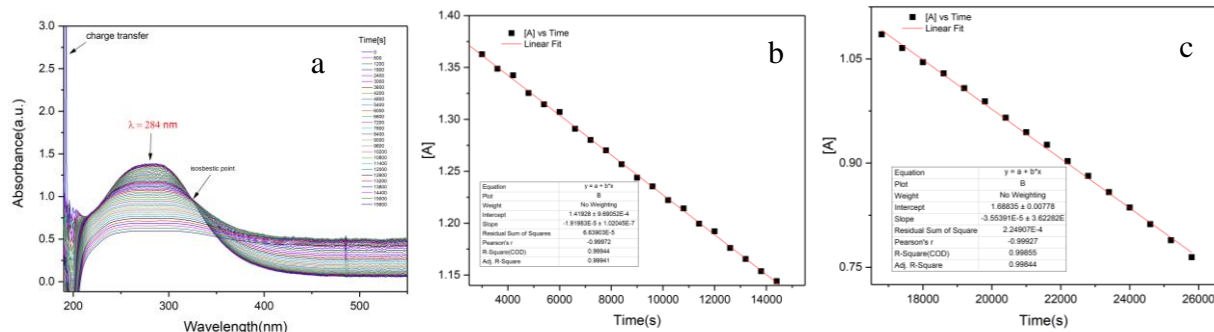
Figure 59. a) Uv-vis spectrum absorbance vs wavelength, b) Plot of [A] vs time for the initial state of reaction and c) Plot of [A] vs time for the final state of reaction, $[Cu(II)L_6]^{2+}$.

To know the order of the reaction (v = k), a linear regression was performed between [A] vs time and it was determined that the reaction is zero order. On the other hand, it was found that the reaction has two stages throughout the reaction and each one has its own rate constant. In the first stage (Fig. 59b) the rate constant (k_1) is 1.9198×10^{-5} $M^{-1}s^{-1}$ and in the second stage (Fig. 59c) the rate constant (k_2) is 3.555×10^{-5} $M^{-1}s^{-1}$. The values R for the linear fit of the graph b and c are 0.999 and 0.998, respectively. In Fig. 60, there is a proposed the two-step reaction mechanism for the formation of the copper (II) complex.
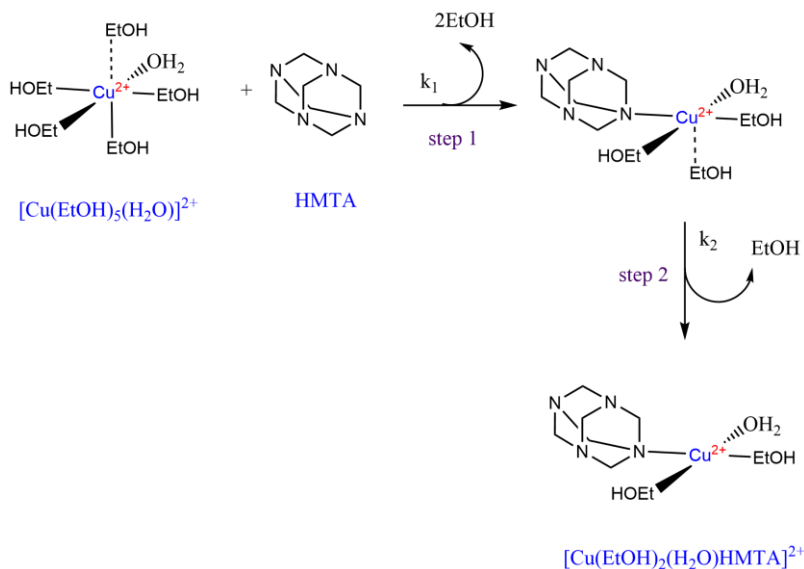
Figure 60. Mechanistic proposal for the formation of the copper complex.

4.2.2.7 Analysis of results. - The copper complex is a paramagnetic green solid with an

58

effective magnetic moment of 2.169 BM. According to the Uv-vis spectrum of diffuse reflectance, the complex is a kind of square plane geometry. This is because the signal appears in the range of 500-600 nm and does not present distortions (Jahn Teller effect) in the signal. In the Uv-vis spectrum it does not show change in the oxidation state of the metal, instead it can only be known that there is a change in the geometry of the complex since the starting material or copper salt is octahedral and when coordinating with the ligand it ends with another geometry. This was also appreciated in the kinetic study of the complex where there are two reaction rate constants (k_1, k_2) which represent the change of the metal coordination sphere and the slow or determining step of the reaction is in k_1. In the IR spectrum, only coordination signals of the metal and the ligand could be seen. In this case, the purpose was not achieved because OD reaction was not happened. On the other hand, due to interest of this project in building systems that oxidize HMTA, a pH study was made because at high pH is known that the dehydrogenation reaction is favored.[43] Then, synthesize of copper complexes at pH 9, 13, 14 and > 14 was made with the following results: there are changes in the magnetic properties of the complexes and a variation in their physical characteristics. In the analysis of the IR spectrum, each increase the pH of the solution, the spectral intensity of the compound decreases until at pH 14 a characteristic signal of a triple bond of nitriles appeared. However, in the Uv-vis spectrum, no changes are observed in the oxidation state of the metal. So to understand the behavior of the ligand and the metal at basic pH in the Fig. 61, a mechanism reaction for the formation of nitrile is proposed. From step 1 to 2 the hydrogen from the carbon is trapped by the base. From step 2 to 3 there is the formation of the double bond (C=N). From step 3 to 4 there is the reduction of the metal ion by the electrons of the nitrogen. From step 4 to 5 the hydrogen is trapped by the bases. From step 5 to 6 there is the formation of the triple bond. From step 6 to 7 there is the oxidation of the metal due to the presence of oxygen in the reaction.
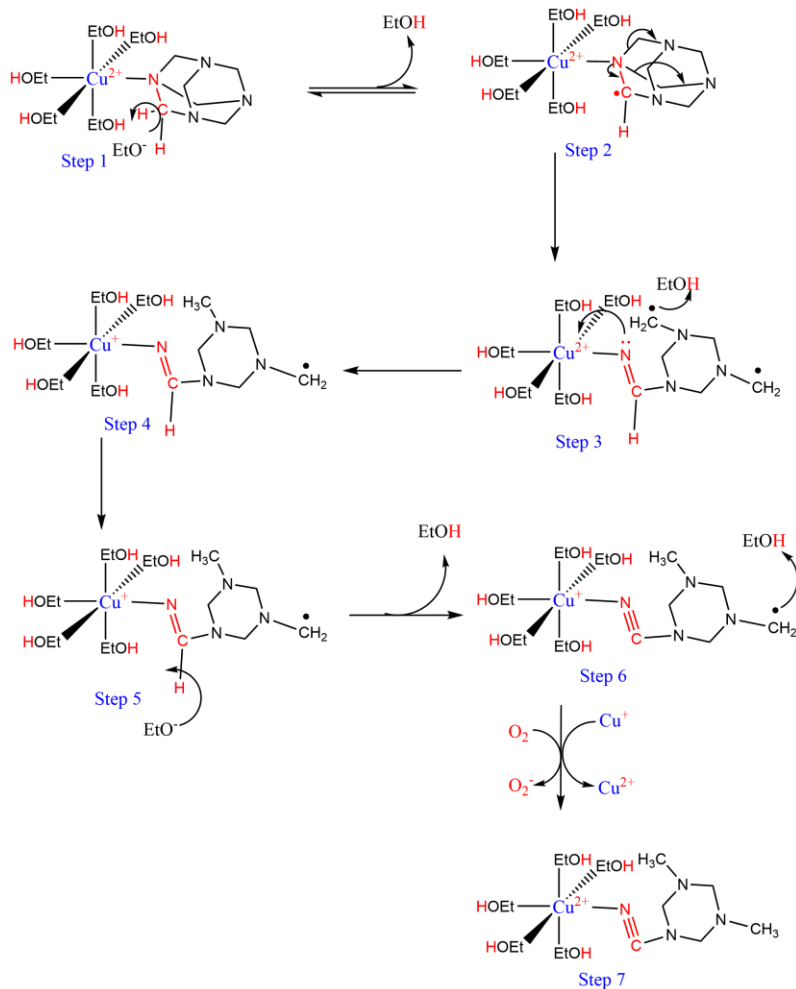
Figure 61. Proposal reaction mechanism for the formation of nitriles.

4.2.3 Main IR characteristics of raw materials for nickel

4.2.3.1 Main IR characteristics of $NiCl_2 \cdot 6H_2O$

In the IR spectrum of the $NiCl_2 \cdot 6H_2O$ molecule (Fig. 62) there is a band at 3507 cm^{-1} belongs to a weak formation of metallic hydrates between the water molecules and the metal. The characteristic signals at 3153 and 3391 cm^{-1} are vibrational bands of nickel salts have very high intensity. At 2070 cm^{-1} a very characteristic band of water molecules representing their vibrational and deformational modes. A band at 1615 cm^{-1} represents scissor-like vibrational modes with a broad absorption for molecules of water. According to the literature, there is a signal at the range 750-100 cm^{-1} that shows stretch between metal and halogen but in compound synthesized there are small bands superimposed on each other in that range. A report on the synthesis of $NiCl_2$ nanoparticles shows that a band at 723 cm^{-1} for the interaction of Ni-Cl. With this background we could affirm that the band at 797 cm^{-1} belongs

60

to the Ni-Cl interaction (Fig. 62).[52,68-70]
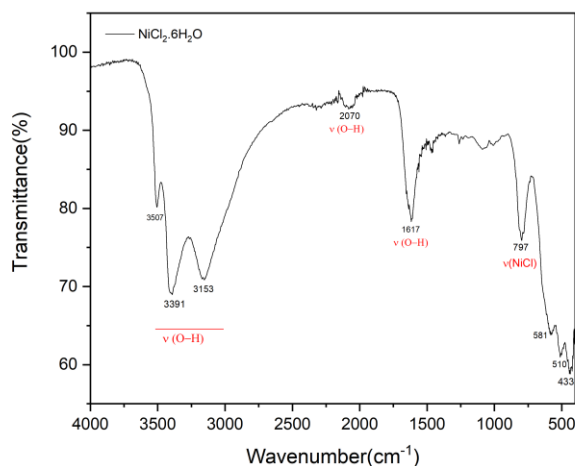
Figure 62. IR spectra of $NiCl_2 \cdot 6H_2O$.

4.2.4 Synthesis and characterization of Ni(II)-HMTA

4.2.4.1 Ni(II)-HMTA. - The synthesized nickel complex is green in color very different from the color of the initial reagents such as nickel chloride hexahydrate and HMTA, which are light green and white respectively. The nickel complex has a melting point 200 °C which is different from the initial compounds (Table 2). This complex is soluble in water and poorly soluble in some polar solvents such as methanol, 2-butanol, butanol, ethanol and insoluble in apolar solvents. According to the results obtained in sections 4.2.4.2, 4.2.4.3 and 4.2.4.5 we can suggest the following chemical formula and structure: $[Ni(C_6H_{12}N_4)(H_2O)_5]Cl_2$ (Fig. 63).
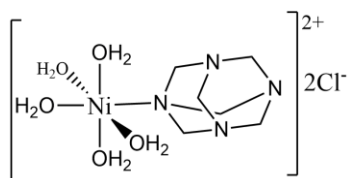
Figure 63. Proposal of chemical structure of the Nickel (II) complex.

4.2.4.2 Main IR characteristics of Ni(II)-HMTA

The IR spectrum of the synthesized compound shows a narrowing in the signals greater than 3000 cm^{-1} compared to the spectrum of $NiCl_2 \cdot 6H_2O$. The two signals at 3354 and 3170 cm^{-1} are characteristic for nickel salts. Likewise, there is an apparent overlap between the CH_3 signals from HMTA with the signal from the nickel salt and a signal at 2968 cm^{-1} of medium

61

intensity in the stretch area of the CH_3 groups appears. At 2070 cm^{-1} there are the deformational and vibrational signals of the water molecules in the synthesized compound. A high intensity signal at 1617 cm^{-1} belonging to the scissor-like mode of movement of water molecules (see section 4.2.3.1). Also, in this spectrum some important HMTA signals appear at 1462 cm^{-1} CH_2 stretch, at 1231 cm^{-1} the low intensity of the CN stretch mode and at 805 cm^{-1} a CH_2 stretch (see section 4.2.1.1). In this last signal Ni-Cl is not clear because there is an overlap of bands and meaning that there is no interaction between them, this is, the chloride is in the second coordination sphere. A signal at 680 cm^{-1} presents a vibrational band between metal and oxygen (Fig. 64).[66]
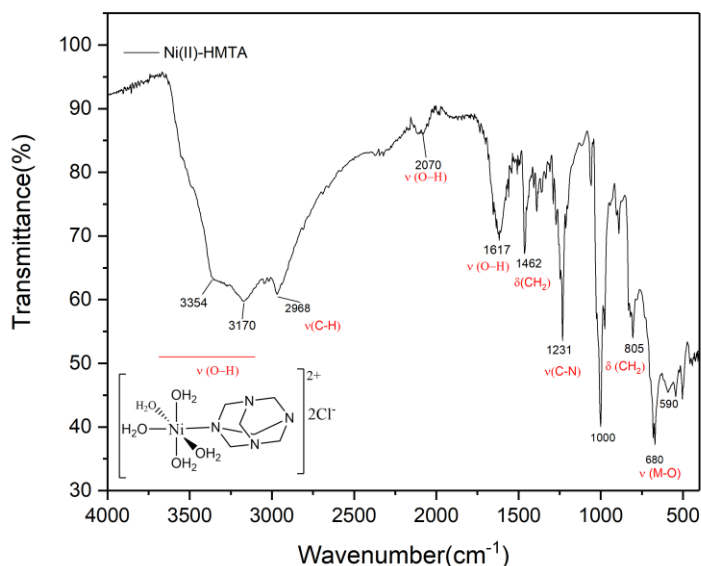
Figure 64. IR spectra of synthesize product Ni(II)-HMTA.

4.2.4.3 Electron absorption spectroscopy

In the Fig. 65 two absorption bands at 568 nm, 364 nm and apparently a third signal higher than 800 nm but the last signal is in the infrared and that signal do not appear. These signals coincide with the signals reported in the literature[53,69,71] (Table 4). So the spectrum would have 3 absorption bands. Which are characteristic of a specie d^8 with geometry octahedral and electronic transitions for the first, second and third signals are found in Tanabe Sugano diagram (Annex 3) $^4T_{2g}$ (F) $\leftarrow$ $^4A_{2g}$ (F), $^4T_{1g}$ (F) $\leftarrow$ $^4A_{2g}$ (F) and $^4T_{1g}$ (F) $\leftarrow$ $^4A_{2g}$ (P). This means that it is a Ni(II) d^8 of octahedral geometry.
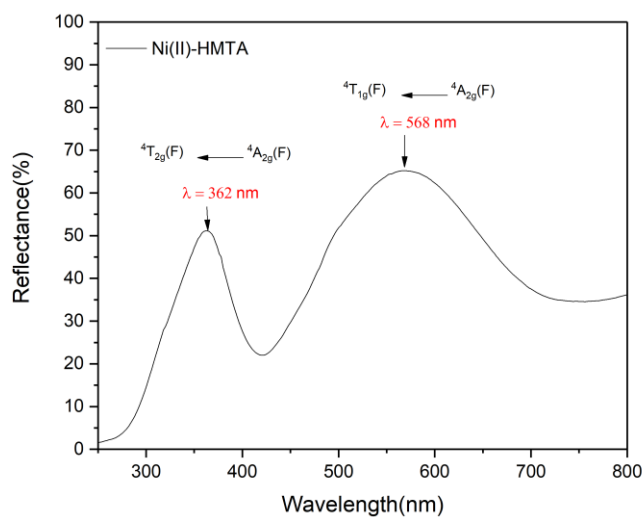
Figure 65. Uv-vis spectrum of Ni(II)-HMTA.

4.2.4.4 Changes of pH in synthesis of HMTA with Ni(II)

4.2.4.4.1 Main IR characteristics

In the IR spectrum (Fig. 66) shows the influence of pH on the synthesis of the nickel complex. All the signals described in section 4.2.3.1 remain in the same absorption bands but two signals appear, one at 2115 cm^{-1} and the other at 1375 cm^{-1} when the pH of the solution is higher than 14. The signal at 2115 cm^{-1} belongs to the vibrational bands of nitriles while the other signal is not easy to identify because it is in the area of the fingerprint. On the other hand, the absorption bands decrease while increase in the concentration of OH^- ions in the solution. Therefore, the increase in pH favors the formation of new signals in any range of the IR spectrum but affects in other cases.
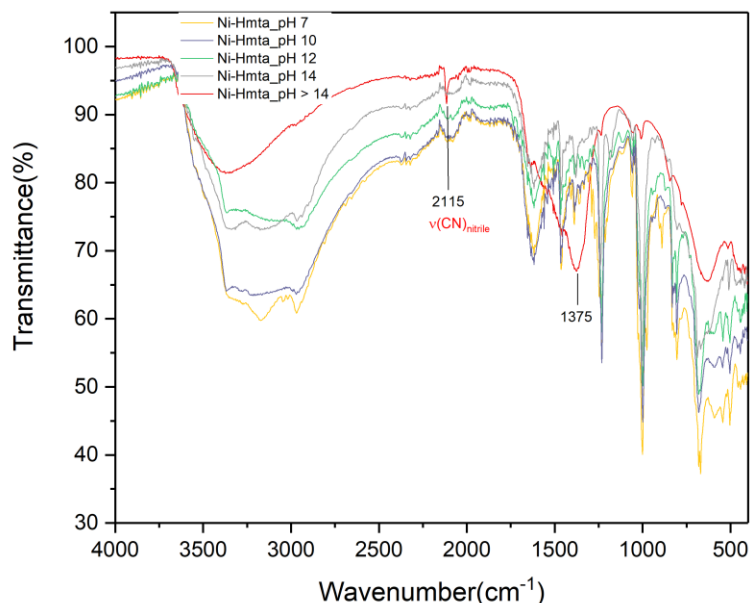
Figure 66. IR spectrum of the nickel compound synthesized at different pH levels.

4.2.4.4.2 Electron absorption spectroscopy

For this experimental process the following amounts of sodium ethoxide 0.036, 0.054, 0.07 and 0.09 g were used to increase the pH of the solution from 7 to 10, 12, 14 and > 14, respectively. The spectrum in Fig. 67 shows the absorption signals described above (see section 4.2.4.3) of the complex formed between the metal ion Ni^{2+} and the respective ligands. The spectrum shows that the complex maintains its octahedral geometry at all pH levels. Taking into account that the compound is a d^8, the complex has an electronic transition $^4T_{2g}$ (F) $\leftarrow$ $^4A_{2g}$ (F), $^4T_{1g}$ (F) $\leftarrow$ $^4A_{2g}$ (F) and $^4T_{1g}$ (F) $\leftarrow$ $^4A_{2g}$ (P) (Annex 3). In the Fig. 83 shows the first change from pH 7 to 10 with an increase in the spectral signal until the concentration of ethoxide in the solution is increased but decreases the spectral signals until the absorption signals disappear around 360 nm for pH values over 12 and there is a slight change in the absorption bands in a range of 4 to 6 nm. To conclude, at pH levels > 12 some signals disappear for the high concentration of OH⁻, it decomposes and changes the nickel complex.
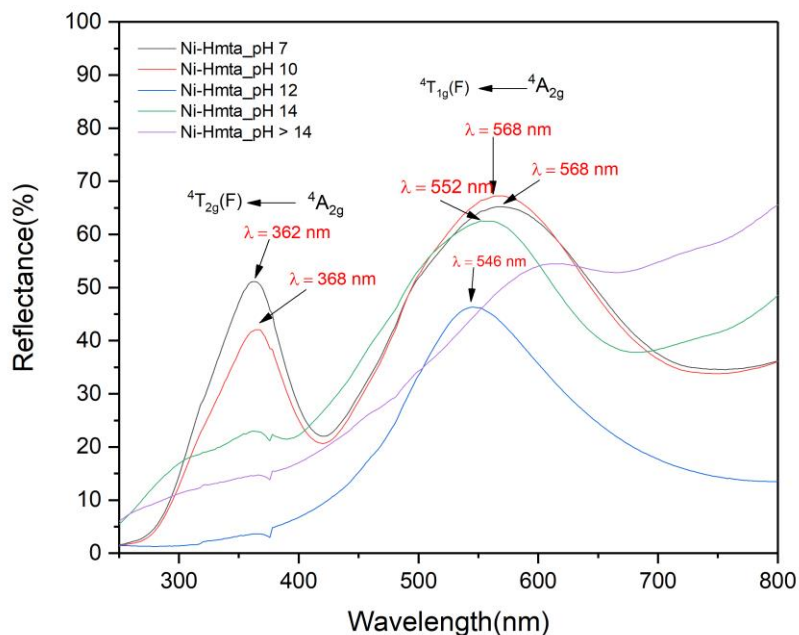
Figure 67. Uv-vis spectrum of the synthesized nickel complex at different pH levels.

4.2.4.5 Magnetic measurements

The magnetic susceptibility measurement was carried out at room temperature and the value of the effective magnetic moment (μ_{eff}) are 4.475, 3.898, 3.9107, 3.562 BM for pH 7, 10, 14, > 14 (Table 1).

4.2.4.6 Chemical kinetic

The kinetics of the reaction between nickel chloride hexahydrate was followed by Uv-vis spectrophotometry in a range of 225-475 nm for 69600 seconds (Fig. 68a). The spectrum presents two peaks 282 nm and 426 nm. The signal 282 nm is used to measure the progress of the reaction.
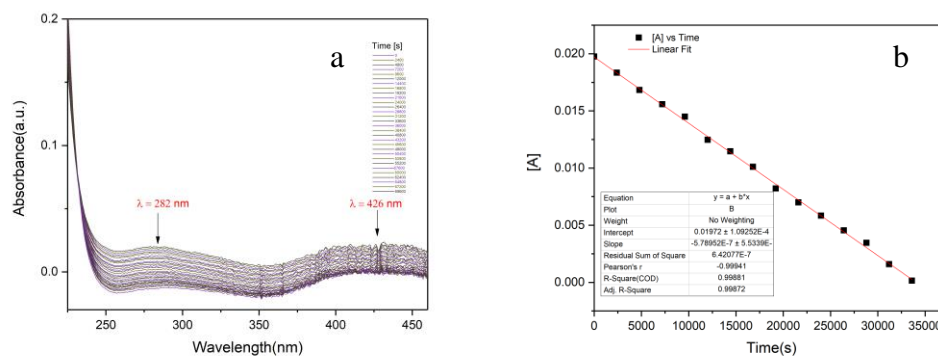
Figure 68. a) Uv-vis spectrum absorbance vs wavelength and b) Plot of [A] vs time for the reaction Ni(II)L₆.

In Fig. 68b shows the linear regression of the absorbance *vs* time of the reaction kinetics with the value of R = 0.998. According to linear regression the order of the reaction is zero (v = k). That value of the slope represents the rate constant (k) is 5.795×10^{-7} Ms^{-1}.

4.2.4.7 Analysis of results. - The nickel complex is a greenish-yellow solid with an effective magnetic moment of 4.47 BM, which reflects a paramagnetic behavior. According to this result, the complex would have a metal center Ni^{+2}. This result is also reached with diffuse reflectance Uv-vis spectral analysis, whose spectrum shows the characteristic absorption bands of a d^8 species and the geometry of the complex would be octahedral. In the Uv-vis spectrum, no signs of change in the oxidation state of the metal are observed because the absorption signals of the complex are similar to those of a d^8 species and in the kinetic study of the reaction it shows that the reaction rate of the nickel complex is slow with $k = 5.795 \times 10^{-7}$ Ms^{-1}. On the other hand, in the IR spectrum, only the coordination of the ligand with the metal is observed. With these results were unable to obtain an OD reaction but the coordination of the ligand was successful. Due to purpose of this project for finding an oxidation system of the HMTA ligand and the synthesis of the nickel complex at basic pH levels was tested because at high pH levels the OD reaction is favored. The nickel complexes synthesized at pH 10, 12, 14, > 14 showed a change in the magnetic behavior and in the physical characteristics of the complexes. Reviewing the IR spectrum at pH > 14 appears a signal at 2115 cm^{-1} belongs to nitrile groups with low intensity, which shows that the increase in the concentration of Hydronium ions in the solution trap the hydrogens of the ligand and allow the formation of triple bonds, while in the Uv-vis spectrum again do not appear change in the oxidation state of the metal. To understand this phenomenon, a mechanistic proposal

for the formation of nitrile is presented in the Fig. 69.
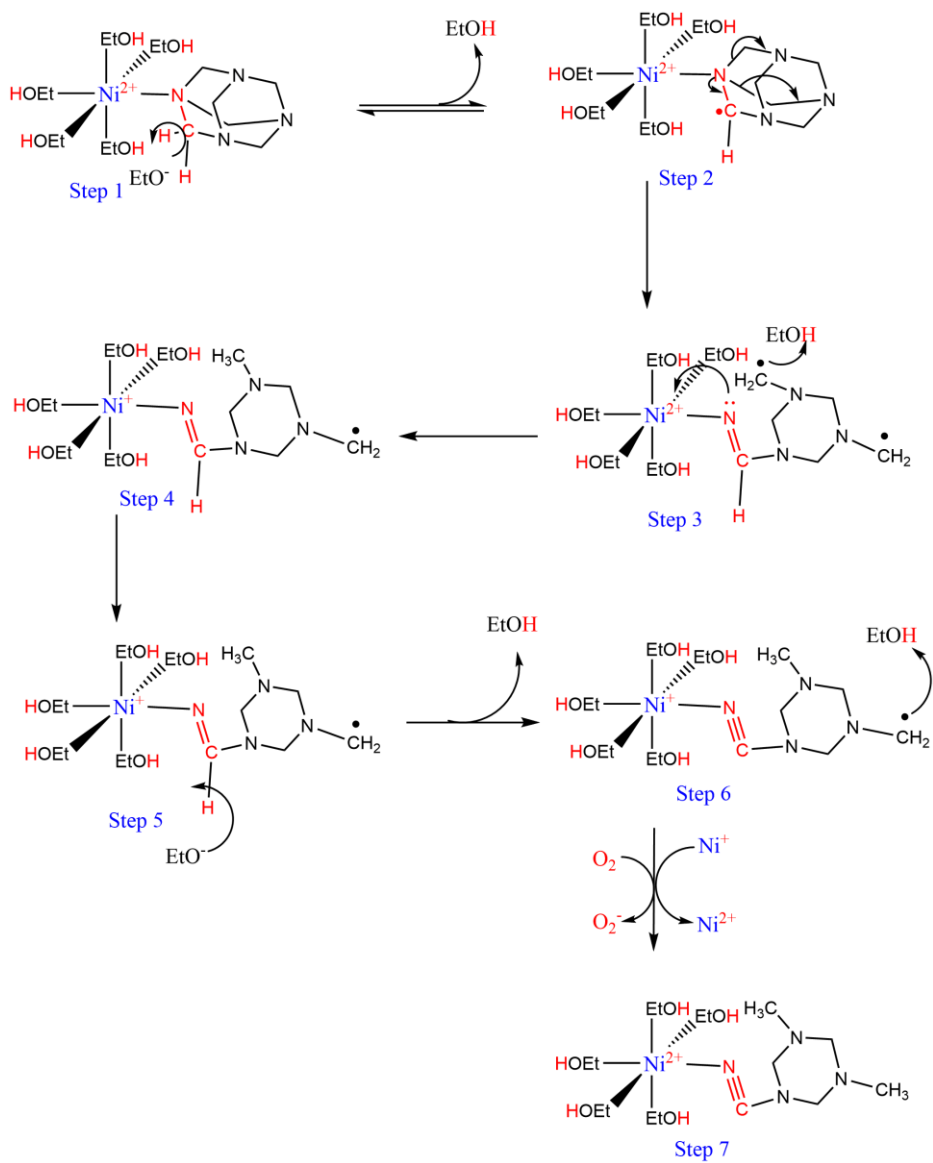
Figure 69. Proposed OD reaction mechanism for the formation of nitriles.

5.0 CONCLUSIONS

- The reaction between Fe(III) and the polyamine ligand $L_2 \cdot 3HCl$ in ethanol leads to the formation of the $[Fe(II)L_4]^{2+}$ complex via OD. This was proven because in the Uv-vis spectrum the reduction of the metal $3+$ to $2+$ is clearly observed and in the IR spectrum the oxidation of the ligand was determined, that is, the formation of the double bond (C=N).

- The formation of the $[Fe(II)L_6]^{2+}$ complex in tert-butanol also follows the synthesis path of oxidative dehydrogenation because the ligand undergoes oxidation when coordinating with the metal and consequently the metal is reduced.

- The formation of the $[Ni(II)L_6]^{2+}$ complex also follows an intramolecular redox reaction (OD reaction). The reduction of the metal is not observed in the Uv-vis spectrum but the IR spectrum shows the formation of a double bond in the final product. On the other hand, it is known that the oxygen in the air could carry out the oxidation of Ni(I) to Ni(II). This phenomenon occurs because the redox potential of the Ni(I) complex must be less than the redox potential of oxygen.

- In the case of the synthesis of the $[Cu(II)L_6]^{2+}$ complex, the reduction of the metal in the Uv-vis spectrum cannot be seen either, but it has been found in the literature that the oxygen in the air participates in the oxidation of the Cu(I) ion to Cu(II). Therefore the synthesis of the copper complex also undergoes an oxidative dehydrogenation reaction.

- On the evaluation of the reactivity of copper and nickel with HMTA, it has been seen that at pH 7 conditions, only the coordination of the ligand with the metal was observed, however, increasing the pH value of the synthesis favors the oxidative dehydrogenation reaction towards the formation of nitriles. This was verified with the IR spectrum of the complexes.

- The kinetic study of the iron, copper and nickel complexes have allowed us to know the speed of the complexes. In this case, copper complexes react faster than nickel complexes and it has been shown that copper complexes can be described in 2 steps.

PERSPECTIVES AND SUGGESTIONS

Considering the compounds obtained, it is necessary to carry out other more in-depth characterization tests (NMR, XPS, EPR, X-ray, etc.) to reaffirm the proposed conclusions on the structure and chemical equation. Analyzes and procedures of the synthesized compounds will be used to improve the performance of the complexes. Also, for the proposed mechanisms it is necessary to perform electrochemical studies to determine the redox potentials of the copper and nickel compounds.

6.0 BIBLIOGRAPHY

(1)   Ugalde-Saldívar, M.; Sosa-Torres, M. E.; Ortiz-Frade, L.; Bernès, S.; Höpfl, H. Novel Iron(II) Complexes with Hexadentate Nitrogen Ligands Obtained via Intramolecular Redox Reactions. *Dalt. Trans.* **2001**, 3099–3107. https://doi.org/10.1039/b100915j.

(2)   Lawrance, G. *Introduction to Coordination Chemistry*, First.; Australia, 2010. https://doi.org/10.1002/9780470687123.

(3)   Miessler, G.; Tarr, D. *Inorganic Chemistry*, Third.; 2004.

(4)   Flora, S.; Pachauri, V. Chelation in Metal Intoxication. *International Journal of Environmental Research and Public Health*. July 2010, pp 2745–2788. https://doi.org/10.3390/ijerph7072745.

(5)   Conry, R. Copper: Inorganic & Coordination Chemistry. *Encycl. Inorg. Chem.* **2006**, 1–18. https://doi.org/10.1002/0470862106.ia052.

(6)   Sánchez, G.; Fuentes, D.; Bello, H. *Copper Nanoparticles as Potential Antimicrobial Agent in Disinfecting Root Canals. A Systematic Review*; 2016; Vol. 10.

(7)   Bencini, A.; Lippolis, V. Metal-Based Optical Chemosensors for CN− Detection. *Environ. Sci. Pollut. Res.* **2016**, *23* (24), 24451–24475. https://doi.org/10.1007/s11356-016-7419-1.

(8)   Modec, B.; Podjed, N.; Lah, N. Beyond the Simple Copper(II) Coordination Chemistry with Quinaldinate and Secondary Amines. *Molecules* **2020**, *25* (7). https://doi.org/10.3390/molecules25071573.

(9)   Keinan, S.; Avnir, D. Continuous Symmetry Analysis of Tetrahedral/Planar Distortions. Copper Chlorides and Other AB4 Species. *Inorg. Chem.* **2001**, *40* (2), 318–323. https://doi.org/10.1021/ic000681z.

(10) Kamau, P.; Jordan, R. B. Complex Formation Constants for the Aqueous Copper(I) - Acetonitrile System by a Simple General Method. *Inorg. Chem.* **2001**, *40* (16), 3879–3883. https://doi.org/10.1021/ic001447b.

(11) Keown, W.; Brannon, G.; Daniel, S. High-Valent Copper in Biomimetic and Biological Oxidations. *J. Biol. Inorg. Chem.* **2017**, 1–29. https://doi.org/10.1007/s00775-016-1420-5.

(12) Synthesis and Structure of Copper Complexes of a N6O4 Macrocyclic Ligand and Catalytic Application in Alcohol Oxidation - Buscar con Google https://www.google.com/search?q=Synthesis+and+Structure+of+Copper+Complexe s+of+a+N6O4+Macrocyclic+Ligand+and+Catalytic+Application+in+Alcohol+Oxid ation&oq=Synthesis+and+Structure+of+Copper+Complexes+of+a+N6O4+Macrocy clic+Ligand+and+Catalytic+Application+in+Alcohol+Oxidation&aqs=chrome..69i5 7j69i61l2.1036j0j7&sourceid=chrome&ie=UTF-8 (accessed Jul 16, 2020).

(13) Raha, S.; Mallick, R.; Basak, S.; Duttaroy, A. K. Is Copper Beneficial for COVID-19 Patients? *Med. Hypotheses* **2020**, *142*, 109814. https://doi.org/10.1016/j.mehy.2020.109814.

(14) Gawande, M. B.; Goswami, A.; Felpin, F. X.; Asefa, T.; Huang, X.; Silva, R.; Zou, X.; Zboril, R.; Varma, R. S. Cu and Cu-Based Nanoparticles: Synthesis and Applications in Catalysis. *Chemical Reviews*. American Chemical Society March 23, 2016, pp 3722–3811. https://doi.org/10.1021/acs.chemrev.5b00482.

(15) Collinson, S. R.; Schröder, M. Nickel: Inorganic & Coordination Chemistry. In *Encyclopedia of Inorganic and Bioinorganic Chemistry*; John Wiley & Sons, Ltd, 2011. https://doi.org/10.1002/9781119951438.eibc0140.

(16) Lascelles, K.; Morgan, L. G.; Nicholls, D.; Beyersmann, D. Nickel Compounds. In *Ullmann's Encyclopedia of Industrial Chemistry*; Wiley-VCH Verlag GmbH & Co. KGaA, 2005. https://doi.org/10.1002/14356007.a17_235.pub2.

(17) Clares, M. P.; Acosta-Rueda, L.; Castillo, C. E.; Blasco, S.; Jiménez, H. R.; García-

España, E.; Basallote, M. G. Iron(II) Complexes with Scorpiand-Like Macrocyclic Polyamines: Kinetico-Mechanistic Aspects of Complex Formation and Oxidative Dehydrogenation of Coordinated Amines. *Inorg. Chem.* **2017**, *56* (8), 4400–4412. https://doi.org/10.1021/acs.inorgchem.6b03070.

(18)   Richard Keene, F. Metal-Ion Promotion of the Oxidative Dehydrogenation of Coordinated Amines and Alcohols. *Coord. Chem. Rev.* **1999**, *187* (1), 121–149. https://doi.org/10.1016/S0010-8545(99)00034-X.

(19)   Curtis, N. Two Isomeric Cyclic Tetra-Amines and Dehydro-Derivatives with One to Four Imine Donor Groups. *Chem. Commun.* **1966**, *881* (23), 881–883. https://doi.org/10.1039/C19660000881.

(20)   Curtis, N. Some Acetato-Amine Complexes of Nickel(II), Copper(II), and Zinc(II). *J. Chem. Soc. A Inorganic, Phys. Theor.* **1968**, No. ii, 1579–1584. https://doi.org/10.1039/J19680001579.

(21)   Toma, H.; Stadler, E. Oxidative Dehydrogenation of an Iron-Tetraazacyclotetradecatriene Complex. *Inorganica Chim. Acta* **1986**, *19*, 49–53. https://doi.org/10.1016/S0020-1693(00)81330-4.

(22)   Saucedo-Vázquez, J. P.; Kroneck, P. M. H.; Sosa-Torres, M. E. The Role of Molecular Oxygen in the Iron(III)-Promoted Oxidative Dehydrogenation of Amines. *pubs.rsc.org* **2015**, *44*, 5510. https://doi.org/10.1039/c4dt03606a.

(23)   Raleigh, C. J.; Martell, A. E. Oxidative Dehydrogenation of Coordinated l,9-Bis(2-Pyridyl)-2,5,8-Triazanonane through Formation of a Cobalt Dioxygen Complex Intermediate. *Inorg. Chem.* **1985**, *24* (2), 142–148. https://doi.org/10.1021/ic00196a005.

(24)   Majouga, A.; Beloglazkina, E.; Yudina, A.; Mironov, A.; Zyk, N. Oxidative Dehydrogenation of 5-(Pyridine-2-Yl-Methyl)-2-Thioxo-4- Imidazolidinones in Complexation Reaction with Copper(II) Chloride. *Inorg. Chem. Commun.* **2015**, *51*, 114–117. https://doi.org/10.1016/j.inoche.2014.11.021.

(25) Kimura, E. Evolution of Macrocyclic Polyamines From Molecular Science to Supramolecular ScienceEvolution of Macrocyclic Polyamines From Molecular Science to Supramolecular Science. *Bull. Japan Soc. Coord. Chem.* **2012**, *59* (0), 26–47. https://doi.org/10.4019/bjscc.59.26.

(26) Inorganic and Bio-Inorganic Chemistry - Volume II - Google Libros https://books.google.com.ec/books?id=Oqq2CwAAQBAJ&pg=PA163&dq=oxidativ e+dehydrogenation+of+macrocycles&hl=es&sa=X&ved=2ahUKEwiWjPLLtN_tAh WCuVkKHTwlAzIQ6AEwA3oECAEQAg#v=onepage&q=oxidative dehydrogenation of macrocycles&f=false (accessed Dec 22, 2020).

(27) Inorganic and Bio-Inorganic Chemistry - Volume II - Google Libros https://books.google.com.ec/books?id=Oqq2CwAAQBAJ&pg=PA163&dq=oxidativ e+dehydrogenation+of+macrocycles&hl=es&sa=X&ved=2ahUKEwiWjPLLtN_tAh WCuVk#v=onepage&q=oxidative dehydrogenation of macrocycles&f=false (accessed Mar 27, 2021).

(28) Reeves, W. P. Organic Chemistry (Wade, L.G.Jr.). *J. Chem. Educ.* **1988**, *65* (6). https://doi.org/10.1021/ed065pa169.1.

(29) Layer, R. W. The Chemistry of Imines. *Chem. Rev.* **1963**, *63* (5). https://doi.org/10.1021/cr60225a003.

(30) Gloe, K. *Macrocyclic Chemistry: Current Trends and Future Perspectives*; 2005. https://doi.org/10.1007/1-4020-3687-6.

(31) Sánchez, T. Fármacos Que Contienen Grupo Nitrilo. Aplicaciones Biológicas, UNIVERSIDAD COMPLUTENSE TRABAJO, 2014.

(32) Kannan, M.; Muthaiah, S. Extending the Chemistry of Hexamethylenetetramine in Ruthenium-Catalyzed Amine Oxidation. *Organometallics* **2019**, *38* (19). https://doi.org/10.1021/acs.organomet.9b00399.

(33) Yamazaki, S.; Yamazaki, Y. Nickel-Catalyzed Dehydrogenation of Amines to Nitriles. *Bull. Chem. Soc. Jpn.* **1990**, *63* (1), 301–303.

https://doi.org/10.1246/bcsj.63.301.

(34) Bernskoetter, W. H.; Brookhart, M. Kinetics and Mechanism of Iridium-Catalyzed Dehydrogenation of Primary Amines to Nitriles. *Organometallics* **2008**, *27* (9), 2036–2045. https://doi.org/10.1021/om701148t.

(35) Zhang, Y.; Zhao, X.; Zhang, H.; Yan, X.; Zhao, J. Conversion of Benzyl Alcohol to Benzonitrile over a Cu10.3/SiO2 Catalyst. *Appl. Catal. A Gen.* **2016**, *522*, 45–53. https://doi.org/10.1016/j.apcata.2016.04.031.

(36) Wang, Y.; Furukawa, S.; Zhang, Z.; Torrente-Murciano, L.; Khan, S. A.; Yan, N. Oxidant Free Conversion of Alcohols to Nitriles over Ni-Based Catalysts. *Catal. Sci. Technol.* **2019**, *9* (1), 86–96. https://doi.org/10.1039/c8cy01799a.

(37) Wang, H. H.; Lv, L. B.; Zhang, S. N.; Su, H.; Zhai, G. Y.; Lei, W. W.; Li, X. H.; Chen, J. S. Synergy of Fe-N4 and Non-Coordinated Boron Atoms for Highly Selective Oxidation of Amine into Nitrile. *Nano Res.* **2020**, *13* (8), 2079–2084. https://doi.org/10.1007/s12274-020-2810-0.

(38) Copper Nanoparticles from Copper Aluminum Hydrotalcite: An Efficient Catalyst for Acceptor- and Oxidant-Free Dehydrogenation of Amines and Alcohols - Damodara - 2014 - Advanced Synthesis & Catalysis - Wiley Online Library https://onlinelibrary.wiley.com/doi/abs/10.1002/adsc.201300453 (accessed Mar 21, 2021).

(39) Hu, Y.; Jin, S.; Zhang, Z.; Zhang, L. One-Step Synthesis of Nitriles by the Dehydrogenation–Amination of Fatty Primary Alcohols over Cu/m-ZrO2. *Catal. Commun. J.* **2014**, 45–49. https://doi.org/10.1016/j.catcom.2014.05.010.

(40) Busca, G. Metal Catalysts for Hydrogenations and Dehydrogenations. In *Heterogeneous Catalytic Materials*; Elsevier, 2014; pp 297–343. https://doi.org/10.1016/b978-0-444-59524-9.00009-2.

(41) Langford, C. H.; Chung, F. M. On the Mechanism of Complex Formation and Solvent-Exchange Reactions of Iron(3+) in Dimethyl Sulfoxide. *J. Am. Chem. Soc.*

1968, *90* (16), 4485–4486. https://doi.org/10.1021/ja01018a067.

(42)   Mattson, B.; Anderson, M. *Microscale Gas Chemistry.*; USA, 2017.

(43)   Gangwal, V. R.; Van Der Schaaf, J.; Kuster, B. F. M.; Schouten, J. C. Influence of PH on Noble Metal Catalysed Alcohol Oxidation: Reaction Kinetics and Modelling. *J. Catal.* **2005**, *229* (2), 389–403. https://doi.org/10.1016/j.jcat.2004.11.021.

(44)   Jeong, Y.; Kim, I.; Kang, J. Y.; Jeong, H.; Park, J. K.; Park, J. H.; Jung, J. C. Alcohol-Assisted Low Temperature Methanol Synthesis from Syngas over Cu/ZnO Catalysts: Effect of PH Value in the Co-Precipitation Step. *J. Mol. Catal. A Chem.* **2015**, *400*, 132–138. https://doi.org/10.1016/j.molcata.2015.01.008.

(45)   Xia, K.; Lang, W. Z.; Li, P. P.; Long, L. L.; Yan, X.; Guo, Y. J. The Influences of Mg/Al Molar Ratio on the Properties of PtIn/Mg(Al)O-x Catalysts for Propane Dehydrogenation Reaction. *Chem. Eng. J.* **2016**, *284*, 1068–1079. https://doi.org/10.1016/j.cej.2015.09.046.

(46)   Xia, K.; Lang, W. Z.; Li, P. P.; Yan, X.; Guo, Y. J. The Properties and Catalytic Performance of PtIn/Mg(Al)O Catalysts for the Propane Dehydrogenation Reaction: Effects of PH Value in Preparing Mg(Al)O Supports by the Co-Precipitation Method. *J. Catal.* **2016**, *338*, 104–114. https://doi.org/10.1016/j.jcat.2016.02.028.

(47)   Huheey, J.; Keiter, E.; Keiter, R. Inorganic Chemistry: Principles of Structure and Reactivity (Huheey, James E.). *Journal of Chemical Education*. 1993, p 465. https://doi.org/10.1021/ed050pa379.1.

(48)   Solano-Peralta, A.; Saucedo-Vázquez, J. P.; Escudero, R.; Höpfl, H.; El-Mkami, H.; Smith, G. M.; Sosa-Torres, M. E. Magnetic and High-Frequency EPR Studies of an Octahedral Fe(III) Compound with Unusual Zero-Field Splitting Parameters. *Dalt. Trans.* **2009**, No. 9, 1668–1674. https://doi.org/10.1039/b814225d.

(49)   Colthup, N.; Daly, L.; Wiberley, S. *Introduction to Infrared and Raman Spectroscopy*, 2nd editio.; New York, 2012.

(50)   Spectral Methods in Transition Metal Complexes - K. Sridharan - Google Libros
        https://books.google.com.ec/books?id=pihBCwAAQBAJ&printsec=frontcover&dq=
        spectrum+of+bands+Uv-vis+for+the+transition+metals&hl=es-
        419&sa=X&ved=2ahUKEwjLoKG36brvAhUrq1kKHWdSAUUQ6AEwAnoECAM
        QAg#v=onepage&q=spectrum of bands Uv-vis for the transition metals&f=false
        (accessed Mar 18, 2021).

(51)   Guthrie, R. D. Introduction to Spectroscopy (Pavia, Donald; Lampman, Gary M.;
        Kriz, George S., Jr.). *J. Chem. Educ.* **1979**, *56* (10), A323.
        https://doi.org/10.1021/ed056pa323.2.

(52)   Nakamoto, K. Infrared and Raman Spectra of Inorganic and Coordination
        Compounds. In *Handbook of Vibrational Spectroscopy*; John Wiley & Sons, Ltd,
        2006. https://doi.org/10.1002/0470027320.s4104.

(53)   sutton, D.; espectros electronicos de los metales... - Google Académico
        https://scholar.google.es/scholar?hl=es&as_sdt=0%2C5&q=sutton%2C+D.%3B+es
        pectros+electronicos+de+los+metales+de+transicion%2C+Ed+Reverte%2C+S.A.%
        2C1975&btnG= (accessed Mar 18, 2021).

(54)   Synthesis and structural studies of N- and P-donor ligands in Chromium(III)
        complexes https://repository.up.ac.za/handle/2263/28960 (accessed Mar 18, 2021).

(55)   Quisahuano, D. REMOVAL OF POTENTIALLY TOXIC METALS BY USING
        LOW COST BIO-ADSORBENTS PREPARED FROM AGRICULTURAL
        WASTE, Yachay Tech University, Ibarra-Ecuador, 2019.

(56)   Zhang, N.; Brugger, J.; Etschmann, B.; Ngothai, Y.; Zeng, D. Thermodynamic
        Modeling of Poorly Complexing Metals in Concentrated Electrolyte Solutions: An
        X-Ray Absorption and UV-Vis Spectroscopic Study of Ni(II) in the NiCl2-MgCl2-
        H2O System. *PLoS One* **2015**, *10* (4). https://doi.org/10.1371/journal.pone.0119805.

(57)   Tak, H.; Lee, H.; Kang, J.; Cho, J. A High-Spin Nickel(II) Borohydride Complex in
        Dehalogenation. *Inorg. Chem. Front.* **2016**, *3* (1), 157–163.

https://doi.org/10.1039/c5qi00206k.

(58)   Lever, A. B. P. The Magnetic Moments of Some Tetragonal Nickel Complexes.
        Inorg. Chem. **1965**, *4* (5), 763–764. https://doi.org/10.1021/ic50027a041.

(59)   Sarmiento-Pavía, P. D.; Flores-Álamo, M.; Solano-Peralta, A.; Kroneck, P. M. H.;
        Sosa-Torres, M. E. Copper (II)-Mediated Oxidative Dehydrogenation of Amine
        Ligands. *Inorganica Chim. Acta* **2018**, *481* (II), 189–196.
        https://doi.org/10.1016/j.ica.2017.10.019.

(60)   Dey, S.; Maity, S.; Pal, K.; Jana, K.; Sinha, C. The Oxidative Dehydrogenation of a
        Coumarinyl Scaffold with Copper Ion and Metal Ion Detection in Human Liver
        Cancer Cells (HepG2). *Dalt. Trans.* **2019**, *48* (48), 17818–17830.
        https://doi.org/10.1039/c9dt03870a.

(61)   Ahuja, I. S.; Singh, R.; Yadava, C. L. Hexamethylenetetramine Complexes with
        Manganese(II), Cobalt(II), Nickel(II), Copper(II), Zinc(II) and Cadmium(II)
        Thiocyanates. *Spectrochim. Acta Part A Mol. Spectrosc.* **1981**, *37* (6), 407–414.
        https://doi.org/10.1016/0584-8539(81)80112-2.

(62)   Afanasiev, P.; Chouzier, S.; Czeri, T.; Pilet, G.; Pichon, C.; Roy, M.; Vrinat, M.
        Nickel and Cobalt Hexamethylentetramine Complexes (NO3)
        2Me(H2O)6(HMTA)2·4H 2O (Me = Co2+, Ni2+): New Molecular Precursors for
        the Preparation of Metal Dispersions. *Inorg. Chem.* **2008**, *47* (7), 2303–2311.
        https://doi.org/10.1021/ic7013013.

(63)   Ezzayani, K.; Khélifa, A. Ben; Loiseau, F.; Nasri, H.; Khelifa, A. Ben; Saint-Aman,
        E.; Loiseau, F. Complex of Hexamethylenetetramine with Magnesium-
        Tetraphenylporphyrin: Synthesis, Structure, Spectroscopic Characterizations and
        Electrochemical Properties. *J. Mol. Struct.* **2017**, 412–418.
        https://doi.org/10.1016/j.molstruc.2017.02.054.

(64)   Ben Mabrouk, K.; Kauffmann, T. H.; Aroui, H.; Fontana, M. D. Raman Study of
        Cation Effect on Sulfate Vibration Modes in Solid State and in Aqueous Solutions.

J. Raman Spectrosc. **2013**, *44* (11), 1603–1608. https://doi.org/10.1002/jrs.4374.

(65) Stuart, B. Infrared Spectroscopy. In *Kirk-Othmer Encyclopedia of Chemical Technology*; John Wiley & Sons, Inc.: Hoboken, NJ, USA, 2005. https://doi.org/10.1002/0471238961.0914061810151405.a01.pub2.

(66) Thermogravimetric and Antimicrobial Properties of... - Google Académico https://scholar.google.es/scholar?hl=es&as_sdt=0%2C5&q=Thermogravimetric+and +Antimicrobial+Properties+of+Some+Divalent+Metal+Complexes+of+Hexamethyl enetetramine&btnG= (accessed Mar 5, 2021).

(67) Ranjan, R.; Sinha, N.; Kumar, S.; Chandra, C. M.; Sharma, S. Abnormal Magnetic Moment and Zero Field Splitting of Some Nickel (II) Complexes. *IRA-International J. Appl. Sci. (ISSN 2455-4499)* **2017**, *7* (1), 34. https://doi.org/10.21013/jas.v7.n1.p3.

(68) Rahmani, Z.; Ghamamy, S. Synthesis and Characterization of Nickel (II) Chloride Nanoparticles with the Study of Their Thermal Behavior. *Int. J. Nano Dimens.* **2014**, *6* (4), 401–407.

(69) Wang, H.; Jia, Y.; Wang, X.; Yao, Y.; Jing, Y. Physical-Chemical Properties of Nickel Analogs Ionic Liquid Based on Choline Chloride. *J. Therm. Anal. Calorim.* **2014**, *115* (2), 1779–1785. https://doi.org/10.1007/s10973-013-3398-3.

(70) Netskina, O. V.; Pochtar, A. A.; Komova, O. V.; Simagina, V. I. Solid-State NaBH4 Composites as Hydrogen Generation Material: Effect of Thermal Treatment of a Catalyst Precursor on the Hydrogen Generation Rate. *Catalysts* **2020**, *10* (2). https://doi.org/10.3390/catal10020201.

(71) Vecoven, A.; Rahman, D. R.; Apblett, A. W. Green Process for Preparation of Nickel Hydroxide Films and Membranes. *J. Mater. Eng. Perform.* **2020**, *29* (9), 5602–5608. https://doi.org/10.1007/s11665-020-05100-5.

(72) Atkins, P. W.; Overton, T. L.; Rourke, J. P.; Weller, M. T. *Shriver and Atkins' Inorganic Chemistry, Fifth Edition*; 2010.

(73) Physical Inorganic Chemistry: Principles, Methods, and Models - Google Libros https://books.google.com.ec/books?id=VaAgihZusxwC&pg=PA5&dq=tanabe+suga no+diagram+d9&hl=es-419&sa=X&ved=2ahUKEwiqoKS-4brwAhVHc98KHdA3CosQ6AEwAXoECAAQAg#v=onepage&q=tanabe sugano diagram d9&f=false (accessed May 8, 2021).

7.0 ANNEXES

7.1 Calculations of the yield, magnetic susceptibility and effective moment of the synthesized complexes.

7.1.1 Yield of complex synthesis [Fe(DMSO)$_3$](NO$_3$)$_3$

According to the synthesis described in section 3.3.1 for calculating the yield of the reaction between 1 g (0.00247 mol) Fe(NO$_3$)$_3$·9H$_2$O with 30 mL (0.422 mol) DMSO is necessary to know the limiting reactant. So, one mol of Fe(NO$_3$)$_3$·9H$_2$O produce one mol of final product, this mean that Fe(NO$_3$)$_3$·9H$_2$O is limiting reagent (equation 1).

$$Fe(NO_3)_3 \cdot 9H_2O + 6\ DMSO \rightarrow [Fe(DMSO)_3](NO_3)_3 + 9H_2O \tag{1}$$
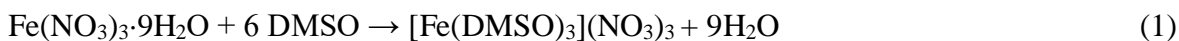
$$1\ g_{Fe(NO_3)_3 \cdot 9H_2O} * \frac{1\ mol_{Fe(NO_3)_3 \cdot 9H_2O}}{403.99\ g_{Fe(NO_3)_3 \cdot 9H_2O}} * \frac{1\ mol_{[Fe(DMSO)_3](NO_3)_3}}{1\ mol_{Fe(NO_3)_3 \cdot 9H_2O}}$$

$$* \frac{710.66\ g_{[Fe(DMSO)_3](NO_3)_3}}{1\ mol_{[Fe(DMSO)_3](NO_3)_3}} = 1.759\ g_{[Fe(DMSO)_3](NO_3)_3}$$

The mass produced in reaction is 1.495 g

$$yield = \frac{Expeimental}{Theoretical} * 100\% = \frac{1.495}{1.759} * 100\% = 85\%$$

7.1.2 Magnetic susceptibility and effective magnetic moment for the [Fe(DMSO)$_3$](NO$_3$)$_3$

Data:

R = 71, R$_o$= -7, m$_o$= 0.143 g, m = 0.151 g, L = 2 cm, C = 0.976

$$X_g = \frac{C * l * (R - R_o)}{(m - m_o)x10^9}$$

X$_g$ = 1.879x10^{-5}cm^3/g

X$_M$= X$_g$ * PM (molecular Wight)

X$_M$= 1.0295x10^{-5} cm^3/g *710.66g/mol

X$_M$ = 0.013345 cm^3/mol

X$_{Pascal}$ = X$_M$ − X$_{diam}$x10^{-6}

X$_{Pascal}$ = 0.013345 cm^3/mol + 361.78 x10^{-6} cm^3/mol

X$_{Pascal}$ = 0.0137 cm^3/mol

$$\mu_{eff} = 2.828\sqrt{X_{Pascal} * 298.15}$$

$$\mu_{eff} = 2.828\sqrt{0.01370 * 298.15}$$

$\mu_{eff} = 5.73$ BM

7.2 Data tables for magnetic susceptibility

Table 1. Data of magnetic properties of final product.

Compound	m_o(g)	m_f(g)	R_o	R	L (cm)	C	χ_g	μ_{eff}(BM)	Magnetic behavior
$[Fe(DMSO)_6](NO_3)_3$	0.143	0.151	-7	71	2	0.976	1.879E-05	5.730	paramagnetic
$[Fe(II)L_4]^{2+}$	0.119	0.136	-5	-5	1.800	0.986	0	0	diamagnetic
$[Fe(II)L_6]^{2+}$	0.145	0.152	-6	-6	2	0.970	0	0	
$[Ni(II)L_6]^{2+}$	0.142	0.149	-6	14	2	0.970	5.731E-06	2.950	paramagnetic
Cu(II)-HMTA pH 7	0.832	0.930	-34	179	2	0.979	4.269E-06	2.169	
Cu(II)-HMTA pH 9	0.831	0.951	-34	215	2	0.975	4.046E-06	1.847	
Cu(II)-HMTA pH 13	0.827	0.954	-34	285	2	0.975	4.913E-06	2.141	
Cu(II)-HMTA pH 14	0.830	0.965	-34	71	2	0.975	1.514E-06	1.309	
Ni(II)-HMTA pH 7	0.827	0.915	-34	994	2	0.979	2.280E-05	4.475	
Ni(II)-HMTA pH 10	0.832	0.977	-34	1392	2	0.975	1.912E-05	3.898	
Ni(II)-HMTA pH 14	0.827	1.000	-34	1676	2	0.975	1.925E-05	3.910	
Ni(II)-HMTA pH > 14	0.830	0.917	-34	675	2	0.975	1.587E-05	3.562	

7.3 Data table for Characteristic of the compounds synthesized and reagent

Table 2. Physical characteristics of the synthesized compound and raw materials.

Compound	Color	Melting Point(°C)	yield(%)
$[Fe(DMSO)_6](NO_3)_3$	Greenish yellow	219	85
pydien	White	205	20
$[Fe(II)L_4]^{2+}$	Purple	200	52
$[Fe(II)L_6]^{2+}$	Purple	200	32
$[Ni(II)L_6]^{2+}$	Violet	290(change color), 338(l)	51.650
$[Cu(C_6H_{12}N_4)(H_2O)_3]SO_4$	Green	230	91.500
$[Ni(C_6H_{12}N_4)(H_2O)_5]Cl_2$	Greenish yellow	180	79

7.4 Data table for Characteristic physics of compounds Ni and Cu with HMTA in changes pH

*Table 3. Physical characteristics of the synthesized compound in diferent levels of pH.*

Compound	Color	Melting Point(°C)
Cu(II)-HMTA pH 9	Green	213
Cu(II)-HMTA pH 13	More deep green	225
Cu(II)-HMTA pH 14	Blacker green	243
Ni(II)-HMTA pH 10	Greenish-yellow	180
Ni(II)-HMTA pH 14	Light green	250
Ni(II)-HMTA pH > 14	Whitish brown	260

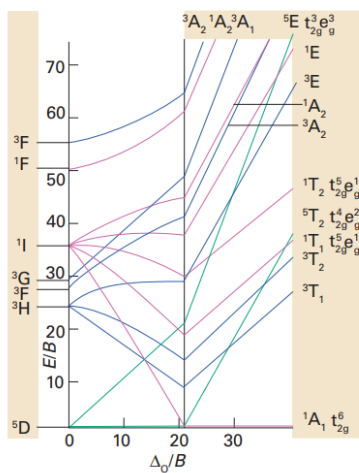## 7.5 Data table for absorption Uv-vis in synthesis complex with HMTA

Table 4. Signals of absorption Uv-vis of raw and synthesized product.

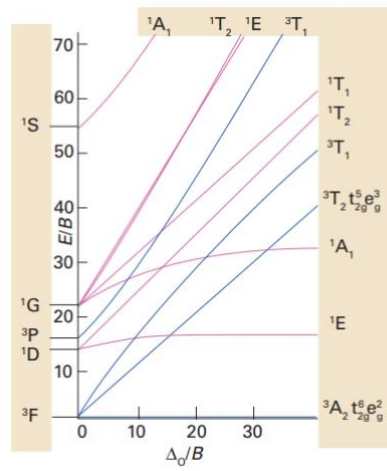| Compound	Maximum absorption(nm)
$NiCl_2 \cdot 6H_2O$	330-500, 540-720, 900-1200
$[Ni(C_6H_{12}N_4)(H_2O)_5]Cl_2$	364, 568
$CuSO_4 \cdot 5H_2O$	814
$[Cu(C_6H_{12}N_4)(H_2O)_3]SO_4$	540

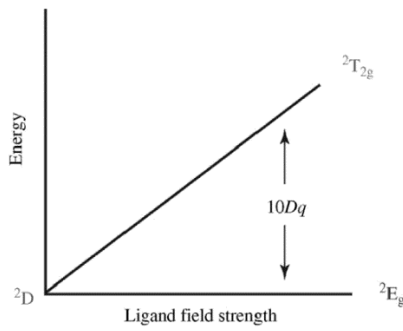## 7.6 Tanabe Sugano Diagrams
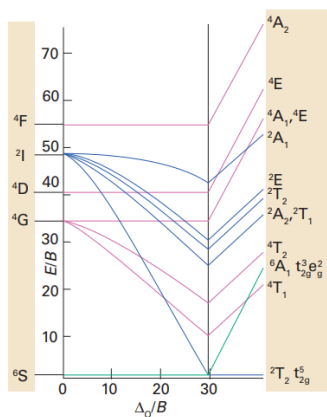
Annex 1. Diagram for a d^5 specie.[72]

Annex 2. Diagram for a d^6 element.[72]

Annex 3. Diagram for a d^8 element.[72]

Annex 4. Diagram for a d^9 element.[73]